INFORMATION TO USERS

This manuscript has been reproduced from the microfilm master. UMI films the text directly from the original or copy submitted. Thus, some thesis and dissertation copies are in typewriter face, while others may be from any type of computer printer.

The quality of this reproduction is dependent upon the quality of the copy submitted. Broken or indistinct print, colored or poor quality illustrations and photographs, print bleedthrough, substandard margins, and improper alignment can adversely affect reproduction.

In the unlikely event that the author did not send UMI a complete manuscript and there are missing pages, these will be noted. Also, if unauthorized copyright material had to be removed, a note will indicate the deletion.

Oversize materials (e.g., maps, drawings, charts) are reproduced by sectioning the original, beginning at the upper left-hand corner and continuing from left to right in equal sections with small overlaps. Each original is also photographed in one exposure and is included in reduced form at the back of the book.

Photographs included in the original manuscript have been reproduced xerographically in this copy. Higher quality 6" x 9" black and white photographic prints are available for any photographs or illustrations appearing in this copy for an additional charge. Contact UMI directly to order.

UMI

University Microfilms International
A Bell & Howell Information Company
300 North Zeeb Road. Ann Arbor. MI 48106-1346 USA
313/761-4700 800/521-0600

Order Number 9510645

The mechanism of action of dihydrofolate reductase revealed by nonresonance Raman difference spectroscopy

Chen, Yong-Qing, Ph.D.

City University of New York, 1994

U·M·I
300 N. Zeeb Rd.
Ann Arbor, MI 48106

The Mechanism of Action of Dihydrofolate Reductase Revealed by Nonresonance Raman Difference Spectroscopy

by

Yong Qing Chen

A dissertation submitted to the Graduate Faculty in Physics in partial fulfillment of the requirements for the degree of Doctor of Philosophy.
The City University of New York

1994

This manuscript has been read and accepted for the Graduate Faculty in Physics in the satisfaction of the dissertation requirement for the degree of Doctor of Philosophy.

September 1, 1994
Date

Robert Callender
Chair of Examining Committee

September 14, 1994
Date

Edward T. Newman
Executive Officer

Thomas C. Stuben

Ronald L. Burke
Supervisory Committee

The City University of New York

ABSTRACT

The Mechanism of Action of Dihydrofolate Reductase
Revealed by
Nonresonance Raman Difference Spectroscopy

by
Yong Qing Chen

Advisor: Professor Robert H. Callender

We have studied the interactions of dihydrofolate reductase (DHFR) with NADP coenzymes, folate substrates and inhibitors using nonresonance difference Raman spectroscopy.

A 35 cm^{-1} upshift observed in the rocking motion the carboxamide -NH_2 group of NADPH upon binding to *E. coli* DHFR (ecDHFR) indicates that this group forms strong hydrogen bonds in the active site. These interactions appear to be responsible for holding the nicotinamide ring in close contact with protein groups, causing a 44 cm^{-1} upshift of the C4-D stretch frequency of $NADPD_B$ bound to the binary complex. Two C4-D stretch bands were observed for $NADPD_A$ or $NADPD_B$ bound in the ternary complex with methotrexate (MTX), suggesting two environments for the nicotinamide ring.

We have observed three forms of biopterin or folate in the ecDHFR ternary complex with $NADP^+$, a slightly polarized keto form with C4=O stretch at 1693 cm^{-1}, a highly polarized keto form with C4$\underline{\bullet\bullet}$O stretch at 1653 cm^{-1}, and an enolate form with C4-O^- stretch at 1341 cm^{-1}.

We have measured the Raman difference spectrum between ecDHFR and the Asp-27 to serine mutant (D27S), and found no evidence for Asp-27 having an elevated pK_a of 6.5. Instead, we have found the pK_a of N5 of dihydrofolate in the ecDHFR ternary complex with $NADP^+$ is elevated to 6.5 from 2.6 in solution. This value is found to be no lower than 5 in human DHFR ternary complex with 1,4,5,6-tetrahydronicotinamide adenine dinucleotide phosphate (H_2NADPH). In contrast, the pK_a of N5 is less than 4.0 in the ecDHFR ternary complex with H_2NADPH, the D27S ternary complex with $NADP^+$, or the binary complex with either ecDHFR or human DHFR.

We have also found that MTX can be reduced to 5,8-dihydro-MTX in the ecDHFR ternary complex with NADPH. Irradiation of laser light with wavelength below 568.2 nm will greatly increase the reaction equilibrium constant. The reduced MTX is slowly oxidized back to MTX, probably by reacting with protein side chains or oxygen in solution.

ACKNOWLEDGMENT

I would like to express my sincere gratitude to Professor Robert H. Callender for his guidance and patience during the course of this thesis work. I would like to thank Professor Joseph Kraut at University of California, San Diego for his direction and valuable suggestions. I would also like to thank Dr. Raymond L. Blakley at St. Jude Children's Research Hospital and Dr. H. T. A. Cheung at University of Sydney, Australia for their generous support. I thank Dr. Vincente Reyes and Dr. Janet Grimsley for their help in preparing the protein samples.

I would like to thank Professor Marilyn Gunner for her many helpful suggestions. I thank Profs. Thomas Strekas, Ronald Birke, Joel Gersten, David Calhoun, Steven Meshnick and Valeria Balogh-Nair for their guidance.

Special thanks go to Dr. Hua Deng for his valuable advice and fruitful discussions. I would like to thank Drs. Danny Manor, Jie Zheng, Gezhi Weng, Jeroen Van Beek, Rodolf Gilmanshin, Larry Senak and Chungxiang Chen for their help in many ways. I also thank Dongguang Xiao, Liewen Huang, Zhongmo Ju, Zunhai Dong and Mrs. Naomi Hellmann for their generous help.

Finally, I would like to thank my wife, Qun Wei, for her support and patience during the course of this work. I also thank my mother, my family, and my teachers for their help throughout my school years.

Table of Contents

LIST OF TABLES

LIST OF FIGURES

LIST OF ABBREVIATIONS

APADP+	3-acetylpyridine adenine dinucleotide phosphate
APAD(P)H	3-acetylpyridine adenine dinucleotide (phosphate), reduced form
ATPR	2'-phospho-adenosine-5'-diphosphoribose
biopterin	2-amino-6-(1,2-dihydroxypropyl)-4(3H)-pteridinone
DHF	dihydrofolate; 7,8-dihydropteroyl-*L*-glutamic acid
H_2biopterin	7,8-dihydrobiopterin
DHFR	dihydrofolate reductase
ecDHFR	*Escherichia coli* dihydrofolate reductase
DMSO	dimethyl sulfoxide
MTX	4-amino-1-methylfolic acid
NAD(P)H	nicotinamide adenine dinucleotide (phosphate), reduced form
H_2NADPH	1,4,5,6-tetrahydro-nicotinamide adenine dinucleotide phosphate
$NADPD_A$	*pro-R*-[4-^{2}H]NADPH
$NADPD_B$	*pro-S*-[4-^{2}H]NADPH
$NAD(P)^+$	nicotinamide adenine dinucleotide (phosphate)
[4-D]$NADP^+$	[4-^{2}H]nicotinamide adenine dinucleotide (phosphate)
THF	5,6,7,8-tetrahydrofolate
TMP	trimethoprim

Chapter 1

INTRODUCTION

Dihydrofolate reductase (DHFR; 5,6,7,8-tetrahydrofolate: $NADP^+$ oxidoreductase, EC 1.5.1.3.) is a widely occurring enzyme that catalyzes the NADP-dependent reduction of 7,8-dihydrofolate (DHF) to 5,6,7,8-tetrahydrofolate (THF) by transferring a hydride ion from the C4 position of the nicotinamide ring to C6 of the pteridine ring:

$$DHF + NADPH + H^+ \longrightarrow THF + NADP^+$$

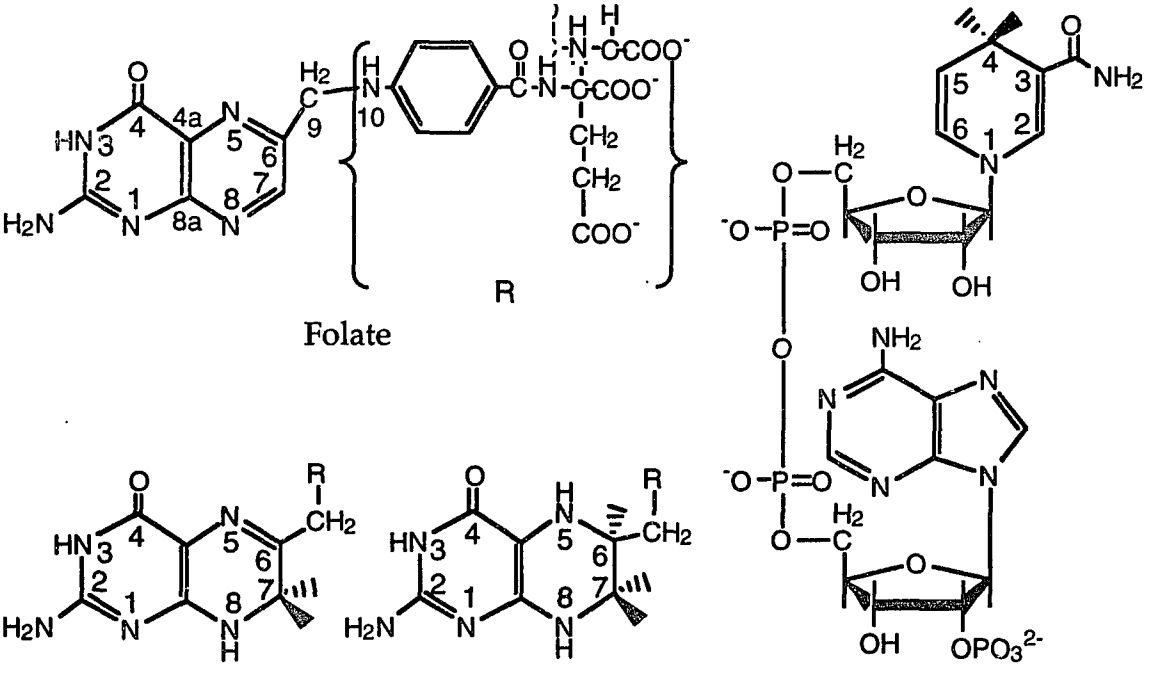

Figure 1.1 Structure formulas for folate, DHF, THF and NADPH. The pteridine and nicotinamide rings are numbered as indicated.

Figure 1.1 shows structural formulas for folate, DHF, THF and NADPH. In the structure of folic acid, 6-methylpterin is linked through the amino group of *p*-aminobenzoic acid (PABA) to form pteroic acid, which is linked in turn via an amide to glutamate, to form pterolymonoglutamate. Naturally occurring folates may differ from this compound in the number of glutamate residues per molecule of the folate vitamin, which ranges from three to eight or more. These residues are linked to one another, not by the familiar peptide bond, but rather by a modified peptide bond involving the α-amino group and the γ-carboxyl group. A typical representative of these folate polyglutamates is shown below (Mathews & van Holde, 1990).

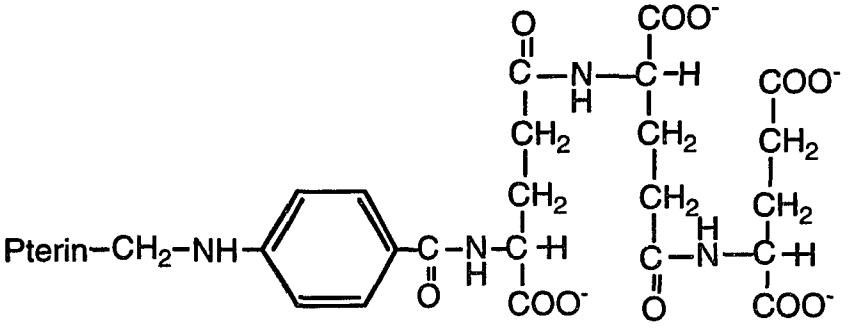

Pteroyl-γ-triglutamate

Folate is converted to the active form tetrahydrofolate by two successive reductions of the pyrazine part of the pteridine ring, which are catalyzed by DHFR. The activity of this NADPH-specific enzyme was first detected in crude preparations of pigeon liver by EGreenberg (1954), and the enzyme was partially purified from chicken liver by Futterman (1957) and by EZakrzewski and Nichol (1958). Osborn and Huennekens (1958) further purified chicken DHFR 100-fold, defined the enzyme-catalyzed reaction, and reported the first definitive enzymological characterization.

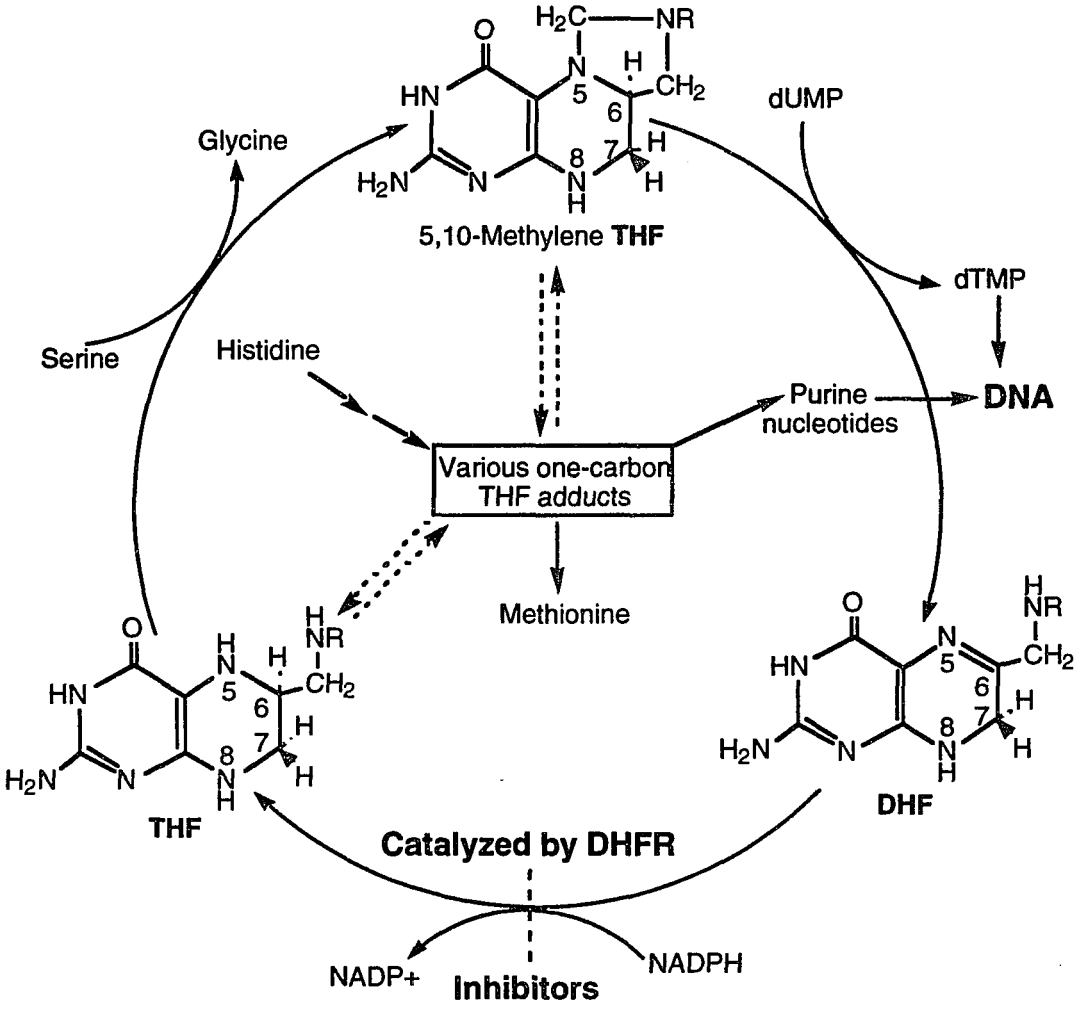

Figure 1.2 Metabolic reactions involving dihydrofolate, tetrahydrofolate and its derivatives (R=benzoyl-*L*-glutamate). The reduction of DHF to THF catalyzed by DHFR is a key step in thymidylate synthesis which is essential for DNA synthesis, so DHFR is of particular interest as a target for inhibitors in cancer chemotherapy.

Tetrahydrofolate can carry single-carbon groups on N5 or N10, or bridged between them. These derivative forms are involved in the metabolism of serine, glycine, methionine, and histidine, among the amino acids, and in the biosynthesis of purine nucleotides and the methyl group of thymine (Figure 1.2). These reactions occur in almost every type of living cell throughout the biological

world. In particular, because the fully reduced tetrahydrofolate must be regenerated for thymidylate synthesis, DHFR plays a vital role in the metabolism of proliferating cells. The inhibition of DHFR, in a line of rapidly multiplying cells, therefore leads to a deficiency of the components of nucleic acids and proteins to eventual cessation of DNA synthesis and hence to cell death. DHFR inhibitors are used in the control of a number of disease processes including various tumors and bacterial infections. Understanding of inhibitor binding at molecular level is of potential value in the design of drugs having greater inhibitory potential and improved selectivity towards the appropriate organism. Examples are methotrexate, trimethoprim (TMP) (Figure 1.3), and pyrimethamine (Hitcings & Baccanari, 1984; Jolivet et al., 1983; Roth & Cheng, 1982). A significant early finding was that some of these DHFR inhibitors showed a marked species selectivity, that is, they inhibit DHFR from some species much more strongly than others. For example, the binding of TMP to human DHFR is 30,000 times weaker than to *E. coli* DHFR (Margosiak et al., 1993). This latter property renders TMP a useful antibiotic in the treatment of bacterial infections.

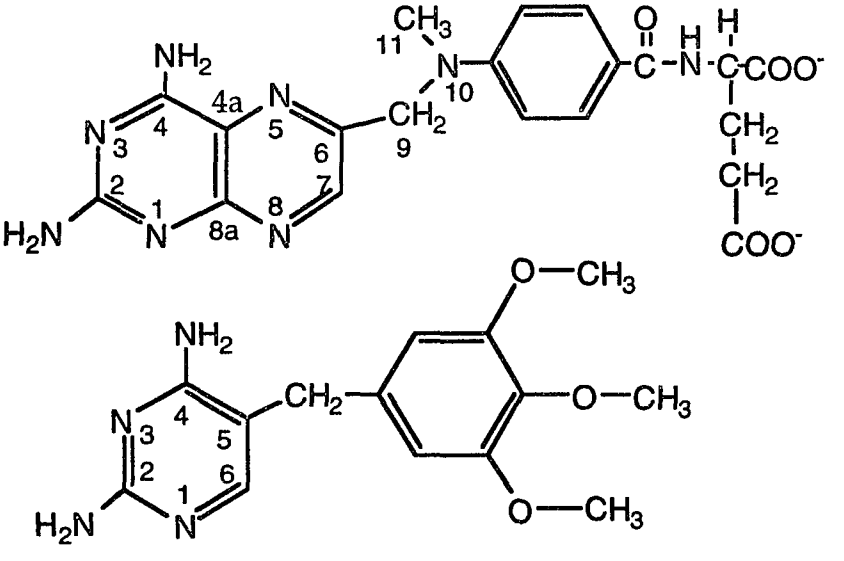

Figure 1.3 Covalent structures and atom numbering for methotrexate (top) and trimethoprim (bottom).

Because of DHFR's biological and pharmacological importance, and the availability of large quantities of enzymes from various species with the help of MTX-bound affinity chromatography, DHFR has been the subject of extensive structural and biochemical studies. A variety of techniques have been applied, such as ultraviolet absorption spectroscopy (Hood & Roberts, 1978; Poe et al., 1974), resonant Raman spectroscopy (Ozaki et al., 1981; Saperstein et al., 1978), NMR (Blakley et al., 1993; Cheung et al., 1993; Cheung et al., 1992; Cocco et al., 1981), X-ray crystallographic methods (Bolin et al., 1982; Bystroff et al., 1990; Filman et al., 1982; McTigue et al., 1992), and a wealth of information about this enzyme has been obtained.

However, some key issues regarding to the catalytic pathway of DHFR remain to be uncovered. For example, how does the N5 of pteridine ring get protonated? What is the role of the active site carboxyl side chain? Kinetic data have shown that the catalysis is controlled by a group with pK_a of 6.5. What is responsible for this pK_a?

Vibrational spectroscopy is well know for its sensitive ability to report on the properties of molecules inside proteins. The conformations of molecule may be probed and the ionization states of polar groups are easily determined. It also provides a wealth of information on protein-ligand interactions, like hydrogen bonding which perturbs a molecule's electronic distribution, and results in modified vibrational force constants and vibrational frequency shifts. Thus, the changes observed in the vibrational spectra of a bound ligand are a direct measure of how a protein acts upon it. Our group has succeeded previously in obtaining the non-resonance Raman spectrum of a small molecule bound to a protein by difference spectroscopy (for review, see Callender & Deng, 1994). The changes in the bound spectrum relative to the solution one yield a lot of

information about the protein-ligand interactions. This method can provide complementary information to X-ray and NMR techniques, and it also has certain advantages. For example, it has minimal or no damage to the sample, and the sample preparation for Raman spectroscopy is simple and the data collection is fast. A reasonable good quality Raman spectrum may be obtained within half an hour. This is extremely helpful when the sample is not very stable, such as the ternary complex of DHFR•$NADP^+$•DHF which will be discussed in Chapter 6.

We report here the results obtained by classical Raman difference technique on the studies of coenzymes, substrates and inhibitors bound to *E. coli* DHFR.

Chapter 2

DIFFERENCE RAMAN SPECTROSCOPY

2.1 Raman Scattering

The Raman effect is a molecular light-scattering phenomenon in which a change in frequency of the light occurs, and the amount of shift corresponds to a vibrational normal mode frequency of the molecule. A Raman spectrum can thus provide detailed information on the vibrational motions of atoms in molecules.

Figure 2.1 shows some of the possible consequences of a photon-molecule interactions. Raman scattering is depicted as a two-photon process. The first step in this process (indicated by the upward-pointing arrows) is the combination of a photon and a molecule to raise the molecule to a higher energy state of extremely short lifetime, which may or may not correspond to a quantized energy state of the molecule depending on the energy of the incident photon. In the normal Raman scattering, the molecule is brought to a virtual energy state; in the resonance Raman scattering, the molecule is brought to a real electronic excited state; and in the pre-resonance Raman scattering, the molecule is brought near but not to the excited state. The second step, indicated by the downward-pointing arrows, involves the release of a photon after a very short time interval ($<10^{-13}$ second). This photon has either higher energy (anti-Stokes process) or lower energy (Stokes process) than the incoming light, and the difference in light frequency corresponds directly to the ground state vibrational frequency of the molecule, which lies in the range of 10-4000 cm^{-1}. In the

Rayleigh scattering process, the frequency of scattered light is the same as that of incident light, and there is no change in the molecule's vibrational energy.

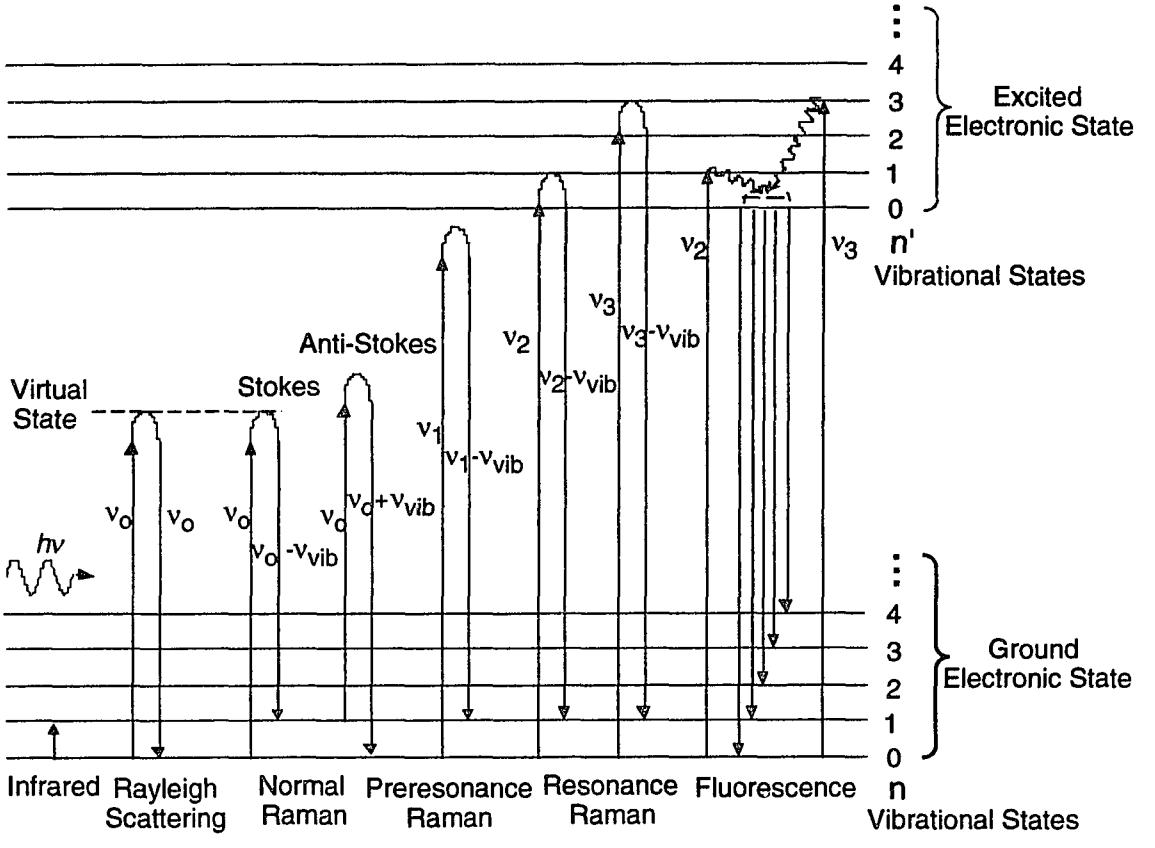

Figure 2.1 The energy diagram of photon-molecule interactions. In infrared process, the molecule absorbs a photon with an energy ν_{vib}; in normal Raman (NR), the molecule is elevated to a virtual state by a photon and then releases another photon with an energy difference ν_{vib} (Raman shift); in resonance Raman (RR), the molecule is elevated to a electronic excited state by a photon and then releases another photon with an energy difference ν_{vib}, and the band intensities are usually orders of magnitude greater.

Since the intensity of Stokes line is several orders higher than that of anti-Stokes line, the feeble anti-Stokes scattering is usually ignored in conventional Raman spectroscopy and only the Stokes spectrum is recorded. The positions of Raman peaks are properties solely of the electronic ground state of a molecule,

but the intensities are functions of both ground- and excited-state electronic structures. For normal or nonresonance conditions, Raman intensities are proportional to fourth power of the scattered light frequency. However, as preresonance and resonance Raman conditions are approached, the intensity of scattering increases much more dramatically, and can be orders of magnitude greater that those in normal Raman spectra. One drawback for resonance Raman is that the fluorescence normally increases, too. It is sometimes found that fluorescence from either the sample itself or some impurities is so overwhelming that the signal to noise ratio for resonance Raman spectrum is much worse than that of normal Raman spectrum.

The Raman spectrum of a typical biological molecule contains many peaks, and is usually very complicated. It is very hard to understand and interpret Raman spectra of these molecules by normal mode calculations, which attempt to solve the equations of motion for all the atoms in the molecule using normal coordinates. For most compounds, some characteristic vibrational frequencies are found to be correlated with certain chemical functional groups. These vibrational modes are called group frequencies. The existence of group frequencies is attributable to the fact that the force constant for a given chemical bond is, to a degree, transferable from one molecule to another. For a group frequency concept to apply to a part of a molecule, the motion in a given normal mode must be essentially localized with that group. Group frequencies find their maximum utility when they give rise to intense features, when they occur in a spectral region that is free from other intense features, and when small variations in the group frequency can be correlated with conformational and environmental changes. The vibrations of S-H, or C-H, or O-H, or N-H moieties within molecules are prime examples of the group frequency concept. The N-H and O-H group frequencies have been used with great effect to study hydrogen

bonding. The protein amide I (which arises from peptide C=O stretch) and amide III (which is mostly due to peptide N-H bending) vibrational modes are correlated to the secondary structure of the peptide backbone. We will use mainly the concept of group frequencies to interpret our Raman results.

2.2 Instrumentation

Figure 2.2 shows the typical instrumental set-up of our Raman experiment. A laser beam is introduced through the sample. The scattered light is collected at 90 degrees and focused on the entrance slit of a spectrometer. The gratings in the spectrometer disperse the incoming light into a spectrum of frequencies. This spectrum is transformed into electronic signal by a detector, and then sent to a computer for analysis.

The laser sources available in our laboratory are a 4-Watt argon ion laser from Spectra Physics (model 165), a 5-Watt INNOVA 400 k3 krypton ion laser and a 10-Watt INNOVA-200 argon ion laser (Coherent Radiation Inc.). The sample holder can hold a double or a triple split cuvette specially designed for measuring several spectra under the same conditions, and each sample space of the split cell has a dimension of 2.5x2.5mm. The cuvette is set on a computer controlled stage which can be moved to within 1 μm accuracy. Raman spectra are measured by a Triplemate spectrometer (Spex Industries), equipped with a solid state detector system (model DIDA-1000 water cooled photodiode array and a model ST-100 detector controller; Princeton Instruments), or a charge coupled detector (CCD) system (CCD model LN/CCD-1152UV liquid nitrogen cooled and a model ST-135 detector controller; Princeton Instruments). Data are acquired, stored and analyzed on a Macintosh computer (Apple, Cupertino CA). Spectral lines are calibrated against known Raman lines of toluene and are

accurate to within ±2 cm^{-1}. The spectral resolution of the instruments is typically set to 6 cm^{-1} full width at half maximum.

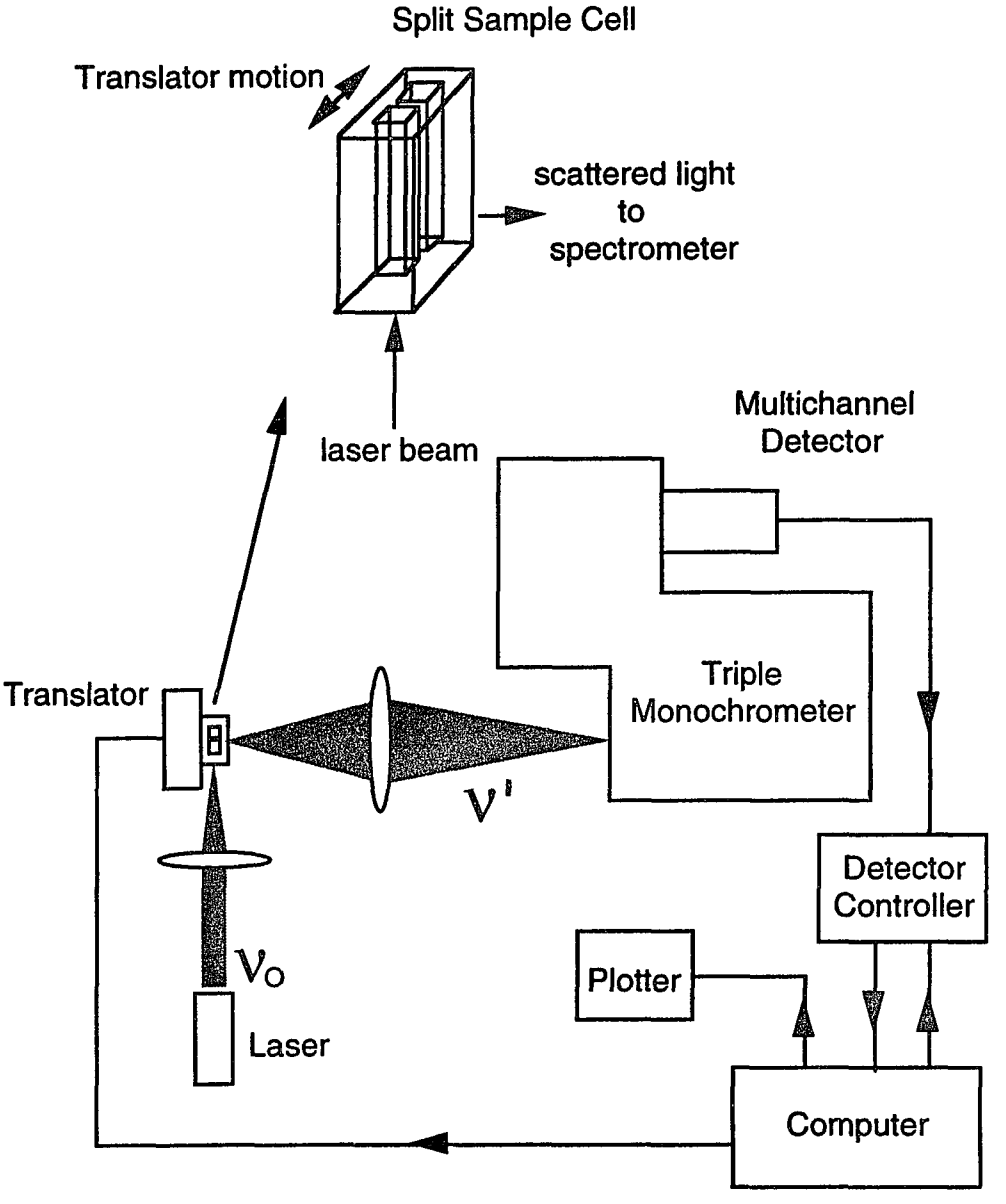

Figure 2.2 A schematic drawing of the instrumental set up for Raman measurement. The monochromatic light emitted from a laser source is introduced through the sample. The scattered light is focused on the entrance slid of a triplemate monochrometer. The spectrometer disperses the incident light into a frequency spectrum and focuses it on to a detector. The spectrum was converted into electrical signals by a charge coupled device, and transferred to a computer for analysis.

2.3 Difference Raman Spectroscopy

To study protein-ligand interactions we intend to measure the Raman spectrum of bound ligand or other small protein molecular moieties. An important experimental constraint, however, in the use of vibrational spectroscopy has been that the signals from this part of the complex are difficult to isolate. Because of the smaller number of modes of the ligand compared to that of the protein, signals from the former are generally overwhelmed by background vibration bands form the protein itself. This difficulty has been largely overcome in recent years using Raman difference spectroscopy (Chen et al., 1987; Yue et al., 1989; Yue et al., 1984). The Raman spectra of protein-ligand complex as well as that of apo-protein are measured under same conditions, and the protein spectrum is numerically subtracted from the complex spectrum after the measurements. The difference spectrum thus obtained, contains the signals of bound ligand, as well as protein changes induced by ligand binding. The operation can be represented by:

Spectrum (enzyme•L) - Spectrum (enzyme)

= Spectrum (L bound in enzyme) + Spectrum (protein changes).... (1)

where L represent a cofactor, inhibitor or substrate of the enzyme.

To get accurate difference spectra and to avoid artifacts, we use a split cell (Figure 2.2) to measure several samples. The temperature and humidity in the room, where the measurements are taken, are controlled to be nearly constant. Arrangements like these are used to reduce the influences of different optical properties for the different samples and to control the environment fluctuations which may affect accuracy of forming the difference spectrum. The long term drift of the optical system can be canceled out if we take the spectra in a

sequential way and line up the spectra before adding them. A detailed procedure of the alignment is described as follows: assume sample A is a stable protein-ligand complex, sample B is another stable protein-ligand complex different from A. The spectra of A and B are measured in a $A_1B_1A_2B_2....A_nB_n$ fashion, with each run taking 10 to 20 minutes. The sets of data are then checked by the subtraction A_n-A_{n-1}, A_n-A_{n-2}, ..., A_n-A_1 and B_n-B_{n-1}, B_n-B_{n-2}, ..., B_n-B_1. All the results of the subtractions should give a flat featureless background. All the spectra taken for the same sample are then added together as A or B. To get the difference spectrum, B is subtracted from A. The disappearance of protein characteristic bands, i.e. bands from phenylanaline around 1000 cm^{-1}, methylene band around 1450 cm^{-1}, amide III band at 1200-1300 cm^{-1} region and amide I band at 1600-1700 cm^{-1} region should be taken as the criteria of the extend of the subtraction.

In general, it is possible to assign bands in the difference spectrum to the bound molecule or to protein changes, either by performing a series of measurements on binary complexes containing various analogs of the small molecule, or more elegantly, by 'editing' the difference spectrum using isotopic labeling schemes.

Figure 2.3 shows some typical results from studies of ligands bound to proteins with the difference Raman spectrometer. Figure 2.3a and b show the Raman spectra of the *E. coli* DHFR binary complex with NADPH and the apo enzyme, respectively, and Figure 2.3c shows the difference spectrum between these two by subtracting b from a. The difference spectrum contains mainly the Raman bands from NADPH bound to DHFR. The intensities for most of the bands are in the range of 1-35% of the protein Amide I band at 1666 cm^{-1}. The strongest band at 1685 cm^{-1} with a relative intensity of 35% is from nicotinamide

ring and the band at 1328 cm^{-1} with a relative intensity of 5% is from adenine ring. More will be discussed later in chapter 4.

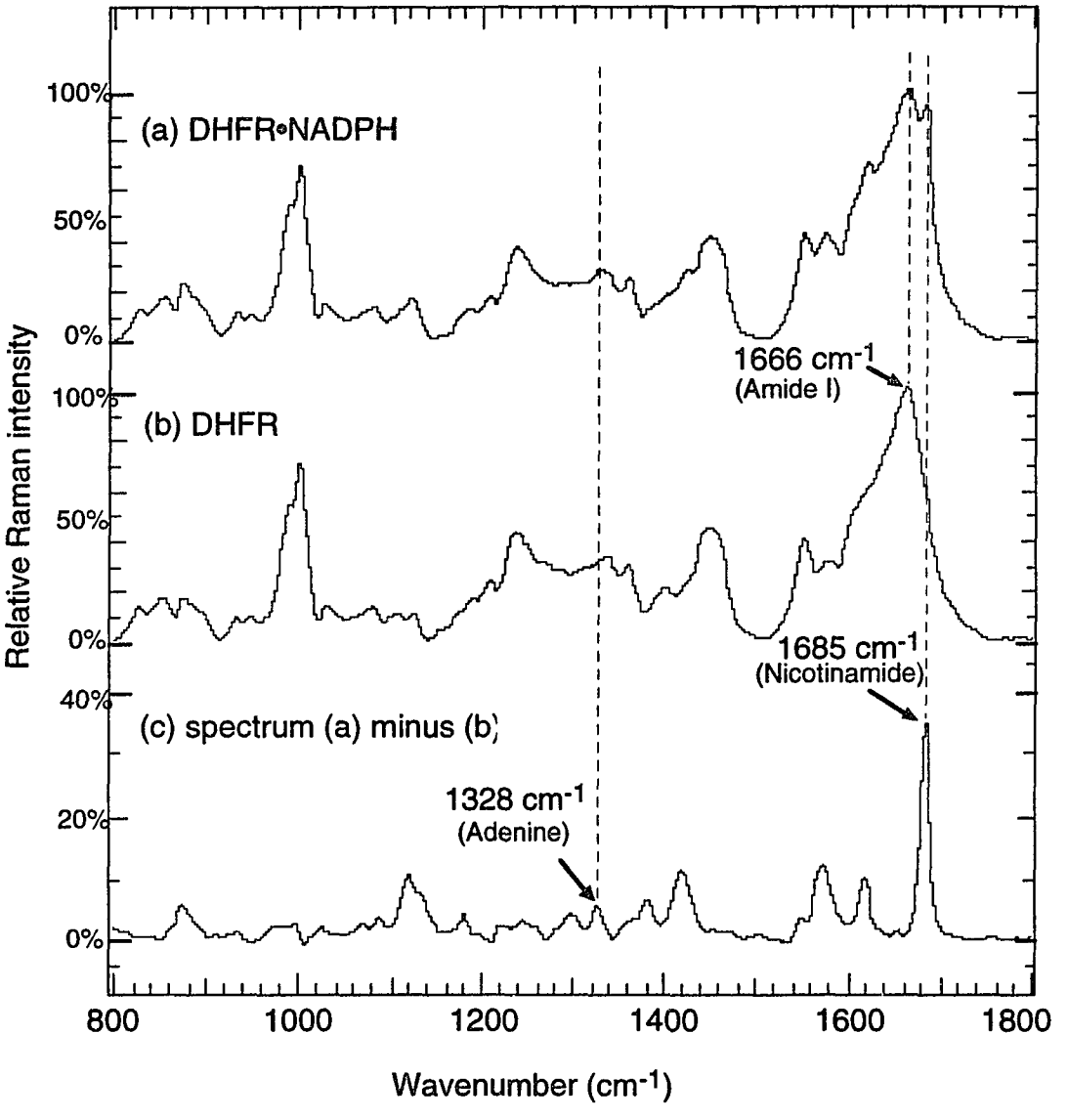

Figure 2.3 Comparison of Raman spectra of (a) DHFR•NADPH, pH 7.3; (b) apo DHFR, pH 7.3; and (c) DHFR•NADPH minus DHFR. Laser excitation: 514.5 nm, 150 mW.

Chapter 3

Sample Preparation

3.1 Dihydrofolate Reductase

Wild-type *E. coli* DHFR was purified from *E. coli* strain CV634 containing the plasmid pCV29 (wt Form I) by using a methotrexate affinity resin (purchased from Pierce). A single colony of the strain was grown at 37°C in 13 ml of LB broth (10 g/L of NaCl, 10 g/L of tryptone and 5 g/L of yeast extract) for 1 hr, and add ampicillin and trimethoprim to the culture to final concentrations of 200 μg/mL each and let grow for about 6 hr. The amplified bacteria culture was added to 12 L of LB medium with 80 μg/L of ampicillin and 25 μg/L of trimethoprim and let grow for 24 hr at 37°C. The cells were spun down, and then resuspended in 200 ml of opening buffer containing 40 mM Tris, 1 mM EDTA and 0.3 mM DTE, pH 8. All further operations were performed at 4°C. 28 mg lysozyme was added and the cells was opened by sonication with Branson sonifier 450. 40 ml of 5% Brij 58 was added and let stand on ice for 20-30 min. The cell debris was removed by centrifuging, and streptomycin sulfate was added gradually to the extract to a final concentration of 1.5% (w/v). The precipitate was removed by centrifuging and the supernatant solution was dialyzed in a buffer of 50 mM potassium phosphate, 1 mM EDTA and 0.5 mM DTE, pH 6.0. The sample was then loaded to a methotrexate affinity column, and washed with 50 mM potassium phosphate buffer containing 1 mM EDTA and 0.5 mM DTE, pH 6.0 until no absorption at 280 nm is detected for the effluent. The column was then washed with 2 L of phosphate buffer containing 1 M KCl, and

the enzyme was eluted with 1 mM folate at pH 9.0. The first 40 fractions were checked on polyacrylamide gel, and those containing the enzyme were combined and dialyzed in 10 mM Tris, 1 mM EDTA and 0.5 mM DTE, pH 7.2. The enzyme was further purified by DEAE-sephacel column using non-linear gradient of KCl from 0.0 to 0.5 M in 10 mM Tris, 1 mM EDTA and 0.5 mM DTE, pH 7.2. The peak fractions with OD_{280}/OD_{260} = 1.9 was saved. The typical yield was 100-300 mg of purified DHFR.

The Asp27 to Ser mutant D27S from *E. coli* was provided by Dr. Joseph Kraut of University California, San Diego and was prepared by Dr. Janet Grimsley as described (Villafranca et al., 1983).

Human DHFR was provided by Dr. Raymond L. Blakley of St. Jude children's Research Hospital.

3.2 Coenzymes and Analogs

NADH, NADPH, NAD^+ and $NADP^+$ was obtained from Boehringer Mannheim Co. ATPR and $APADP^+$ were purchased from Sigma Chemical Co.

H_2NADPH was prepared by the following modification of the procedure of Biellmann and Jung (1971). Five milligrams of 5% palladium on charcoal was added to a solution of 10 mg of NADPH dissolved in 4 mL of H_2O, pH 8, and the resulting mixture was put on ice and hydrogenated by bubbling hydrogen gas. The reaction was stopped just when the absorption at 340 nm was no longer detectable. The mixture was then washed through Centricon-30 centrifuge concentrator (Amicon, Lexington, MA) to remove the solid residue. The filtrate was lyophilized and stored in -80 °C.

pro-R-[4-^{2}H]NADPH ($NADPD_A$) was prepared enzymatically according to published prodecures (Viola et al., 1979), and *pro*-S-[4-^{2}H]NADPH ($NADPD_B$) was prepared according to the method of Deng et al. (1992).

[4-D]$NADP^+$ was prepared by the following modification of the procedure of San pietro (1954). About 40 mg of NADP+ was dissolved in 1 ml of 1 M KCN prepared in 99.5% D_2O. To this pale yellow solution was added 8 µl of 10 N NaOD (the final pH was 11.4), and the resulting solution was incubated for 3 hours at room temperature. After incubation, 5 ml of D2O containing 2 millimolar equivalent of KH_2PO_4 were added, and the HCN was removed by bubbling nitrogen through the solution. The final pH was 7. The reaction product was purified by DEAE-sephacel column using non-linear gradient of KCl from 0.0 to 0.5 M in 10 mM Tris, pH 7.0. The peak fractions with OD_{258}/OD_{231} = 2.2 was saved. The salt was removed by running the eluent from DEAE column through a Bio-gel P-2 column, and this eluent was lyophilized and stored in -80 °C. The purity of [4-D]$NADP^+$ was better than 95% as determined by the intensity of Raman band of $NADP^+$ at 1031 cm^{-1} which shifts down to 1018^{-1} for [4-D]$NADP^+$.

3.3 Substrates and Analogs

Folate, 7,8-dihydrofolate, methotrexate and trimethoprim were purchased from Sigma Chemical Co. Biopterin was purchased from Aldrich. 7,8-dihydrobiopterin (H_2biopterin) and [5-^{15}N]H_2biopterin were obtained from Dr. B. Schircks laboratory (Jona, Switzerland). [6-^{13}C]DHF was provided by Dr. Raymond Blakley and was prepared from labeled folate (Selinsky et al., 1990). [2,4a,6-]Methotrexate was provided by Dr. H. T. A. Cheung of University of Sydney, Australia.

3.4 Enzyme Binary and Ternary Complexes

The apo-enzyme concentration was determined spectrophotometrically at 280 nm using a molar extinction coefficient of 31,000 $M^{-1}cm^{-1}$. The concentrations of substrates, coenzyme and their analogs were determined with the following extinction coefficients at pH 7 (except indicated otherwise): NADPH, 6 220 $M^{-1}cm^{-1}$ at 340 nm; $NADP^+$, 17 500 $M^{-1}cm^{-1}$ at 260 nm; H_2NADPH, 15 500 $M^{-1}cm^{-1}$ at 288 nm (Biellmann & Jung, 1971); H_2folate, 28 400 cm at 282 nm (Blakley, 1969); and methotrexate, 22 100 $M^{-1}cm^{-1}$ at 302 nm (Seeger et al., 1949).

The pH of the enzyme solution was changed by washing the enzyme in a Centricon-10 centrifuge concentrator (Amicon, Lexington, MA) with the final buffer having desired pH. Typically, three cycles of diluting and concentrating were needed to reach the final pH. The final enzyme concentration was about 3-5 mM. For subtraction between the binary and the apo enzyme, the binary complex of DHFR•ligand was prepared by mixing DHFR and ligand in a molar ratio of 1:0.8. For subtraction between the ternary and binary complexes, the binary complex of DHFR•ligand1 was first prepared by mixing DHFR and ligand1 in a molar ratio of 1:1, and the ternary complex of DHFR•ligand1•ligand2 was then prepared by mixing DHFR•ligand1 and ligand2 in a molar ratio of 1:0.8.

Chapter 4

The Interactions of Coenzymes with *E. coli* DHFR

4.1 Binding of NADPH

Figure 4.1a shows the difference spectrum between the DHFR-NADPH binary complex and apo-DHFR. For comparison, the spectrum of NADPH in solution is given in panel b. The size of the difference signal was found to range from 10-40% of DHFR's 1450 cm^{-1} Raman band (which arises from δ-CH_2 motions) for the most intense coenzyme bands originating from the nicotinamide group of NADPH, to about 5% from bands arising from motions on the adenine moiety of the bound coenzyme, to about 1% for phosphate modes. The intensity of dihydronicotinamide moiety bands are substantially larger than modes from other parts of the cofactor. This is because they are preresonantly Raman enhanced since the reduced nicotinamide group absorbs near 340 nm, and this is close to that of the visible Raman excitation wavelengths used in this study (514.5 nm). Since we are able to measure Raman intensities for both the binary complex and the protein with very high signal to noise and obtain a subtraction accuracy of 0.1%, extremely good signal to noise ratios are achieved.

The difference spectrum is dominated by bands which can be associated with NADPH. However, there are changes in the protein residues that occur with the binding of the coenzyme because of residue-bound ligand interactions (for example, hydrogen bonding) and because there are changes in protein structure between the complexed and apo forms of the enzyme. Thus, the difference spectrum may contain perturbed protein bands as well. In the

previous studies of LDH (lactate dehydrogenase; Deng et al., 1989c) and LADH (liver alcohol dehydrogenase; Chen et al., 1987), a procedure was developed to identify those peaks which are due to specific portions of the coenzyme and those due to the apoprotein, which involves comparisons of the difference spectra found for NADPH and other cofactors, like $NADP^+$, and bound fragments of these, like 2'-monophosphoadenosine 5'-diphosphoribose (ATPR). These all differ substantially in bands associated with the nicotinamide head group. Also, the relative intensities of coenzyme bands compared to protein bands are generally preserved when the coenzyme binds. This and the fact that reduced nicotinamide yields comparatively more intense Raman bands, because of preresonance enhancement, makes an identification of nicotinamide bands relatively straightforward. Bands associated with other parts of the NADP cofactors and derivatives can generally be made on the basis of comparison to solution spectra, taking into account band position and intensity. We have labeled peaks as either adenine (A), nicotinamide (N), ribose (R), 2'-phosphate (P), or pyrophosphate (PP) in the data of Figure 4.1 for those peaks that are localized on these groups (Yue et al., 1986). We are able to make a somewhat more precise identification of solution bands (see Yue et al., 1986). In some cases, a band is found to be largely located on a particular moiety but its position and/or strength is somewhat dependent on a connecting group. Some of the peaks of adenine are influenced when adenosine is formed, for example. We use the nomenclature A/δR to identify such peaks. Other peaks are more equally associated with motions on both the adenine and ribose moieties, and these are labeled A/R. In some cases an observed band contains contributions from two normal modes. The peak at 1378 cm^{-1} in Figure 4.1b is an example of the sum of two bands, one located on the nicotinamide head group and one associated with adenosine. We have labeled this peak by (A/R,N) to denote this degeneracy and

similarly for the other degenerate bands. Some bands are likely associated with apoprotein, and these have been labeled by Pr. For example, the peak at 1652 cm^{-1} in panel a is not found in any of the solution spectra. Its position is, however, within the strong amide-I (peptide backbone C=O stretch) region of the DHFR spectrum. It therefore very likely arises from the perturbation of one or more backbone carbonyls that occurs when NADPH binds to DHFR. Similar difference peaks arising from perturbed amide-I C=O stretches have been observed in lactate dehydrogenase (Deng et al., 1989c). These stretch frequencies are sensitive to hydrogen bonding interactions and protein conformation. In some cases, we are unable to reasonably assign a band to a particular group; these are labeled by a "?" mark.

The Raman spectrum of NADPH in DHFR differs substantially from the spectrum of NADPH in solution. Many of the features found in Figure 4.1 are associated with the reduced nicotinamide group, and we shall concentrate on these now with a discussion of the adenine and phosphate bands to follow below. The intense broad 1546 cm^{-1} solution band (Figure 4.1b) shifts to 1572 cm^{-1} (Figure 4.1a) when NADPH binds to DHFR. The identification of the solution 1546 cm^{-1} band with the bound 1572 cm^{-1} band is strengthened by measurements with protein and protein complexes in D_2O, where, all exchangeable protons are deuterated, and shifts in bands occur. The solution 1546 cm^{-1} band shifts upward by some 10 cm^{-1} in these deuterated samples Yue et al., 1986. A smaller but similar upward shift (+ 4 cm^{-1}) of the bound 1572 cm^{-1} is observed in experiments on deuterated protein samples (data not shown). The shift of the solution 1546 cm^{-1} band to 1572 cm^{-1} in the bound spectrum is indicative (Deng et al., 1992) of a rotation of the carboxamide group from a solution *cis* conformation (with respect to the N1 nitrogen of the nicotinamide ring; cf. Fischer et al., 1988) to a *trans* conformation in the bound form. This

finding for a rotation of the carboxamide arm is in agreement with X-ray studies which show that NADP adopts the *trans* conformation in DHFR (Bystroff et al., 1990).

Most of the intensity of the solution band at 1084 cm^{-1} is associated with the nicotinamide amido group. It has been assigned to a rocking motion of the $-NH_2$ moiety (see, e.g., Yue et al., 1986). When NADPH binds to DHFR, the $-NH_2$ rocking mode shift upward 35 cm^{-1} to 1119 cm^{-1} (Figure 4.1a). This assignment is proven by experiments on samples in D_2O, where the hydrogens of the amido moiety are deuterated. The solution band shifts from 1084 cm^{-1} to 909 cm^{-1} (Yue et al., 1986) while the 1119 cm^{-1} band of bound NADPH shifts similarly to 931 cm^{-1} (data not shown). The increase of the $-NH_2$ rock observed for bound NADPH results from the formation of hydrogen bond(s) between the amido group of the coenzyme and protein that are stronger than those formed in water (see e.g., Deng et al., 1991). This will be further discussed below.

Some experiments were performed on the binding of NADH to DHFR. At a concentration as high as 5 mM DHFR and NADH, the difference spectrum of DHFR plus NADH minus that of DHFR yielded a spectrum essentially identical to the spectrum of NADH in solution (data not shown). This means that either most of the NADH is not bound to DHFR at these concentrations or that it is so loosely bound that its Raman spectrum is the same as in solution. Upon the addition of a stoichiometric amount of trimethoprim (TMP), a known inhibitor of DHFR, the Raman difference spectrum between DHFR-TMP-NADH and DHFR-TMP is dramatically different; we found it to be essentially identical to that of bound NADPH of Figure 4.1a (apart from modes introduced by the presence of the extra phosphate in NADPH, see next section). Thus, in the presence of TMP, NADH binds to DHFR like NADPH. This may be expected since all the cofactors of DHFR bind tighter to the enzyme in the presence of inhibitors like TMP.

4.2 Binding of $NADP^+$, ATPR and $APADP^+$

Figure 4.2a shows the difference spectrum of DHFR-$NADP^+$ with DHFR while that of Figure 4.3a shows the difference spectrum of DHFR-ATPR with DHFR. Most of the features of these two difference spectra can be associated with bound $NADP^+$ and bound ATPR, respectively. For comparison, the solution spectra of $NADP^+$ (Figure 4.2b) and ATPR (Figure 4.3b) are also shown. There are few bands in the $NADP^+$ spectra that arise from the oxidized nicotinamide group and none in the ATPR spectra, since it lacks the nicotinamide head group. Thus, these spectra are well suited to examine the changes that occur in the relatively weaker adenine and phosphate bands as the coenzyme binds. All the changes in the adenine and phosphate bands that are found in the bound $NADP^+$ and ATPR spectra relative to their solution counterparts are generally repeated when NADPH binds, so far as we can tell from a careful examination of the data in Figure 4.1. However, the bands in the bound spectra are at slightly different positions in some cases. For example, the adenine triplet (see below) is found at 1298, 1328, and 1368 cm^{-1} for $NADP^+$ bound to DHFR and at 1296, 1325, and 1362 cm^{-1} for NADPH bound to DHFR.

The peak at 1032 cm^{-1} in the bound (2a) and solution (2b) spectra of $NADP^+$ is an aromatic ring vibration (Bellamy, 1975). This band is assigned to the 'triangle' vibration of the C2, C4 and C6 carbons of the aromatic ring, based on isotopic labeling experiments that we have previously reported on NAD^+ (Deng et al., 1991). Neither it nor the 1620 cm^{-1} band, which is also assigned to the oxidized nicotinamide ring of $NADP^+$, are affected by binding to DHFR. Moreover, the frequency of the nicotinamide C4-D stretch of deuterated $NADP^+$ is the same for $NADP^+$ in the DHFR-$NADP^+$ binary complex as in aqueous solution, although a substantial shift (up 20 cm^{-1}) is observed for this mode in

DHFR-$NADP^+$-MTX ternary complex. The most likely explanation of this data is that the nicotinamide head group of $NADP^+$ is very loosely, or not at all, bound to DHFR as a binary complex. This is in contrast to the adenosine moiety for both NADPH and $NADP^+$, where shifts in their respective Raman spectra clearly show the result of protein interactions. These data are in general agreement with X-ray results (Bystroff et al., 1990) which show the oxidized nicotinamide ring in binary complex with DHFR to be disordered, suggesting that the group may reside in solution, while the electron density patterns for the rest of the cofactor are well defined and place the adenosine moiety in its protein binding pocket. This may be a result from there being no compensating polar groups at the nicotinamide binding pocket which could stabilize the charge on the positive $NADP^+$ (Bystroff et al., 1990).

The characteristic 'adenosine' triplet found at 1308, 1338, and 1378 cm^{-1} in solution (Figure 4.2 and 4.3, panel b) shifts downward upon binding to 1299, 1329, and 1367 cm^{-1}, respectively, (Figure 4.2 and 4.3, panel a). These bands are due to delocalized vibrations of the purine ring plus contributions from motions of the ribose group. Their delocalized nature makes for a difficult normal mode analysis although serious efforts on this problem are underway (cf. Tsuboi et al., 1987). However, these bands are sensitive to internal configurations of adenosine as well as external perturbations (Deng et al., 1991; Nishimura & Tsuboi, 1986). The observed downward shift of the triplet is like that observed when adenine analogs are transferred from water to more hydrophobic solvents (Deng et al., 1989c). While the shifts observed here are larger than previously observed, this correlation suggests the environment of adenine in DHFR is quite hydrophobic. This is in agreement qualitatively with X-ray crystallographic studies (Bystroff et al., 1990). The side chain of Leu62 forms much of a hydrophobic floor for the adenine group. On the other hand, the amide of Gln102 hydrogen bonds to

adenine's N7 and 6-NH_2 group in DHFR-coenzyme complexes forming a Hoogsteen-base-pair-like interaction, and this interaction may affect adenine's normal modes as well.

The positive peak at 973 cm^{-1} in the bound spectra of $NADP^+$ and ATPR is close to that observed in the solution spectrum of the NADP cofactors at 980 cm^{-1} at pH 8.0 (see Figures 1b, 2b, or 3b) in frequency and in intensity. This band is not present in the spectra of NAD cofactors and their fragments, like ADPR (Yue et al., 1986) or in the spectrum of NADH bound to DHFR (in ternary complex with TMP; data not shown). Moreover, model compound studies on glucose-6-phosphate show a band at this position (977 cm^{-1}) which shifts down 42 cm^{-1} upon ^{18}O labeling of the phosphate group (data not shown); this band is assigned to the P$\underline{\bullet\bullet}$O stretch of the phosphate ester. All this taken together indicates that the 980 cm^{-1} solution band of NADP cofactors may be assigned to a P$\underline{\bullet\bullet}$O stretch of dianionic phosphate of the 2'-phosphate group which shifts to 973 cm^{-1} upon binding to DHFR.

The $NADP^+$ derivative, $APADP^+$, shows a Raman band at 1710 cm^{-1} which has been assigned to the acetyl C=O stretch internal coordinate as verified by ^{18}O labeling (Deng et al., 1989a). We have used this band, and shifts in this band, as a measure of the hydrogen bonding that occurs between the coenzyme and protein in previous studies. For $APAD^+$ bound to lactate dehydrogenase and malate dehydrogenases, this band shifts downward about 10 cm^{-1} from its solution value of 1710 cm^{-1} (Deng et al., 1991; Deng et al., 1989c). No shift is observed when $APADP^+$ binds to DHFR (data not shown), indicating the poor binding of the oxidized nicotinamide headgroup to DHFR as a binary complex. In the DHFR-$APADP^+$-TMP ternary complex where the oxidized nicotinamide group is very clearly bound to the DHFR binding pocket, the C=O stretch is found at 1715 cm^{-1}, an increase of 5 cm^{-1}.

4.3 DHFR-Cofactor Interactions

In previous sections, the assignment of most of the observed bands to motions localized on one or another moiety of the bound NADP coenzyme is made. The spectral results indicate that the carboxamide group of bound NADPH adopts the *trans* conformation. This is in agreement with X-ray structural studies. Also in agreement with X-ray studies is the finding that the adenosine binding pocket of DHFR is quite hydrophobic. Although it is hard to interpret the results at the present time, the bands found between 1300-1400 cm^{-1} which are characteristic of adenosine, varies in number and position for the proteins that have been studied to date (DHFR, LDH, and MDH). This is surprising since bound adenosine lies in the so-called 'Rossmann fold', a structural motif common to these proteins. Whatever the nature of the variation of the adenosine-enzyme interaction, and we have postulated that it may be due to electrostatic effects (see Deng et al., 1991), the exact nature of how adenosine binds varies substantially across these proteins.

The $-NH_2$ rock mode of the nicotinamide ring is relatively localized and its frequency can be correlated to the strength of hydrogen bonding. Because hydrogen bonding 'stiffens' the rocking motion (Deng et al., 1991), the $-NH_2$ rock mode is expected to increase with increased hydrogen bonding. This mode is present in the Raman spectrum of NADPH at 1084 cm^{-1} in solution (Figure 4.1), and upshifts more than 35 cm^{-1} for upon binding to the enzyme, indicating that the hydrogen bond interaction between the $-NH_2$ group and DHFR is stronger than that found between it and water.

Another mode sensitive to hydrogen bonding is the carbonyl C=O stretch. The electron density that makes up the bond of a carbonyl, C=O, group is weakened when the bond is polarized by hydrogen bond formation. Both

experimental studies (Thijs & Zeegers-Huyskens, 1984) and recent theoretical calculations (Latajka & Scheiner, 1990) suggest that the frequency of a carbonyl stretch follows a Badger-Bauer like rule in that the stretching frequency is directly proportional to the strength of the hydrogen bond enthalpy between the carbonyl and its nearby proton donor. This linear relationship will probably hold only on certain localized C=O stretch mode, such as that of $APADP^+$. A number of experiments done previously in our lab on the binding of $APAD^+$ to lactate dehydrogenase and cytoplasmic and mitochondrial malate dehydrogenase all gave the shifts of -10 cm^{-1} in frequency of the carbonyl mode, which correspond to about 11 kJ/mol of favorable enthalpy relative to that in water based on the Badger-Bauer relationship found for acetophenone, which should serve as a good model for the carbonyl of $APAD^+$ (cf. Deng et al., 1991). However, the carbonyl stretch of $APADP^+$ has no shift upon binding to DHFR binary complex, but has an upshift of 5 cm^{-1} upon binding to DHFR ternary complex with TMP, correspond to an unfavorable enthalpy of 6 kJ/mol. One would expect that the pyridine headgroup might be bound less tightly in the ternary than in the binary complex. This is not true, because the headgroup looks like unbound in DHFR-$NADP^+$ or DHFR-$APADP^+$ binary complex, but is clearly bound in DHFR-TMP-$APADP^+$ or DHFR-MTX-$NADP^+$ (data will be shown later in chapter 7) ternary complex. Thus, hydrogen bonding of the amide or acetyl group to DHFR cannot account for this positive cooperativity. Other factors must be involved, such as conformational changes due to inhibitors binding and direct interactions between the pyridine ring and the inhibitors inside the binding pocket.

The positions and intensities of Raman bands of the 2'-phosphate group are very sensitive to its ionization state. The 973 cm^{-1} peak in the bound spectra (Figures 2a and 3a), assigned to the symmetric $P^{\bullet\bullet}O$ stretch of the 2'-phosphate

group, is quite close its solution counterpart at 980 cm^{-1}. Since the 2'-phosphate group is dianionic in solution, the data indicate that the cofactor binds to DHFR dianionically. This finding is the same as found previously in ^{31}P NMR experiments on *L. Casei* DHFR (Feeney et al., 1975). The 7 cm^{-1} downward shift of the P⎓O stretch mode observed when the 2'-phosphate group binds implies that the electron density between the phosphorous and oxygens of the phosphate group has decreased. We have recently derived an empirical relationship between phosphate P⎓O bond order and stretch frequency (Deng et al., 1993b). From this relationship, the P⎓O valence bond order has decreased 0.007 units from its solution value of 1.255 upon binding. This result suggests that hydrogen bonds or salt bridges are formed between the 2'-phosphate group and protein since such electrostatic interactions draw electrons from the P⎓O bond towards oxygen. The downward shift, as opposed to an upward shift, implies that the interaction is energetically favorable (see above and, cf., Joesten & Schaad, 1974). We thus conclude that DHFR forms stronger hydrogen bonds (i.e. binds tighter) with the 2'-phosphate group than does water, consistent with selective binding of the NADPH to DHFR compared to NADH. In DHFR, a number of polar groups interact with the 2'-phosphate group of bound NADP coenzymes as determined from crystallographic studies (Bystroff et al., 1990). Close enough to form hydrogen bonds are the γ-hydroxyls of serines 63 and 64, Ser64(N), Wat204, the 3'-hydroxyl of the adenosine ribose group, and the side chain of Arg44. Arg44 is a conserved basic side chain among known DHFRs and is likely to provide the strongest interaction with the 2'-phosphate group considering its positive charge.

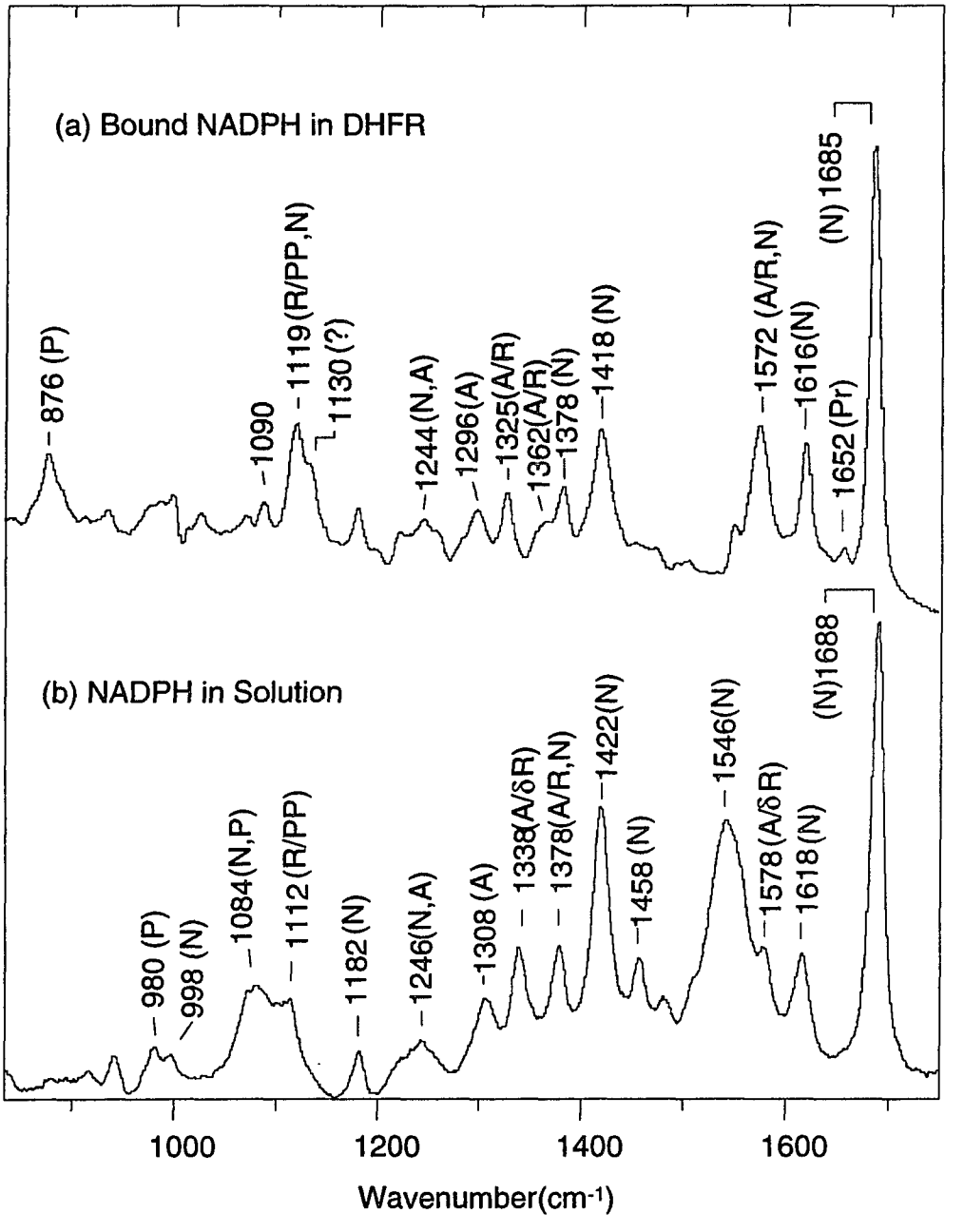

Figure 4.1 **(a)** Difference Raman spectrum of bound NADPH in DHFR at 4°C in 10 mM Tris and 0.5 M NaCl, pH 8.0 (Molar ratio in mM, DHFR:NADPH = 5:4.5) and **(b)** Raman spectrum of NADPH in solution at 4°C, pH 8.0 (100 mM). The Raman peaks are assigned as arising from adenine (A), nicotinamide (N), ribose (R), 2'-phosphate on adenine ribose (P), pyrophosphate (PP), protein (Pr) and unknown (?). Laser excitation: 514.5 nm, 150 mW.

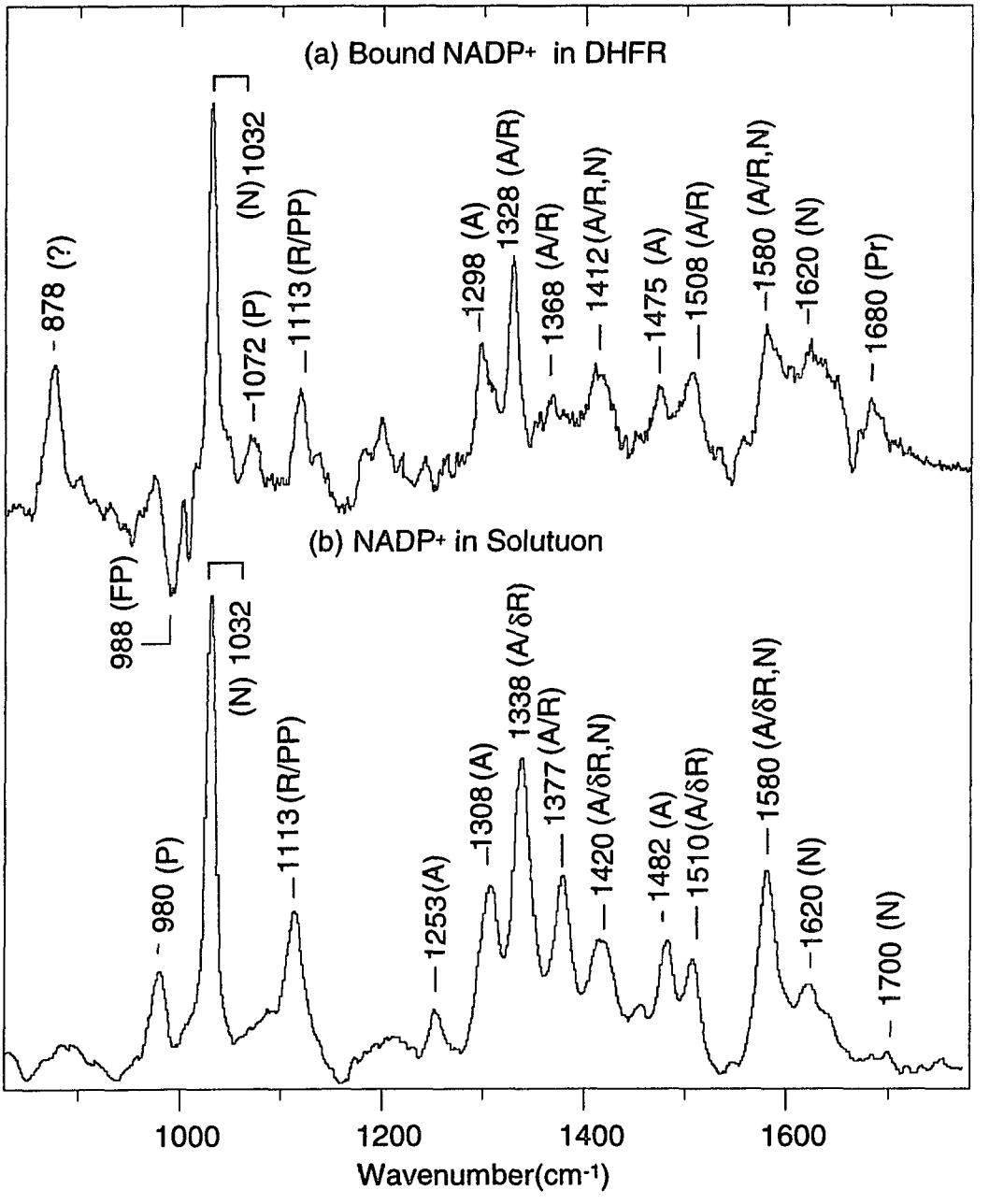

Figure 4.2 **(a)** Difference Raman spectrum of bound $NADP^+$ in DHFR at 4°C in 10 mM Tris and 0.5 M NaCl, pH 8.0 (Molar ratio in mM, DHFR:$NADP^+$ = 5:4.5) and **(b)** Raman spectrum of $NADP^+$ in solution at 4°C, pH 7.5 (100 mM). See text and Figure 4.1 for the labelling scheme. The negative peak at 988 cm^{-1} (FP) is thought to arise from phosphate in the buffer bound to apo-enzyme; it disappears upon extensive dialysis in Tris buffer. Laser excitation: 514.5 nm, 150 mW.

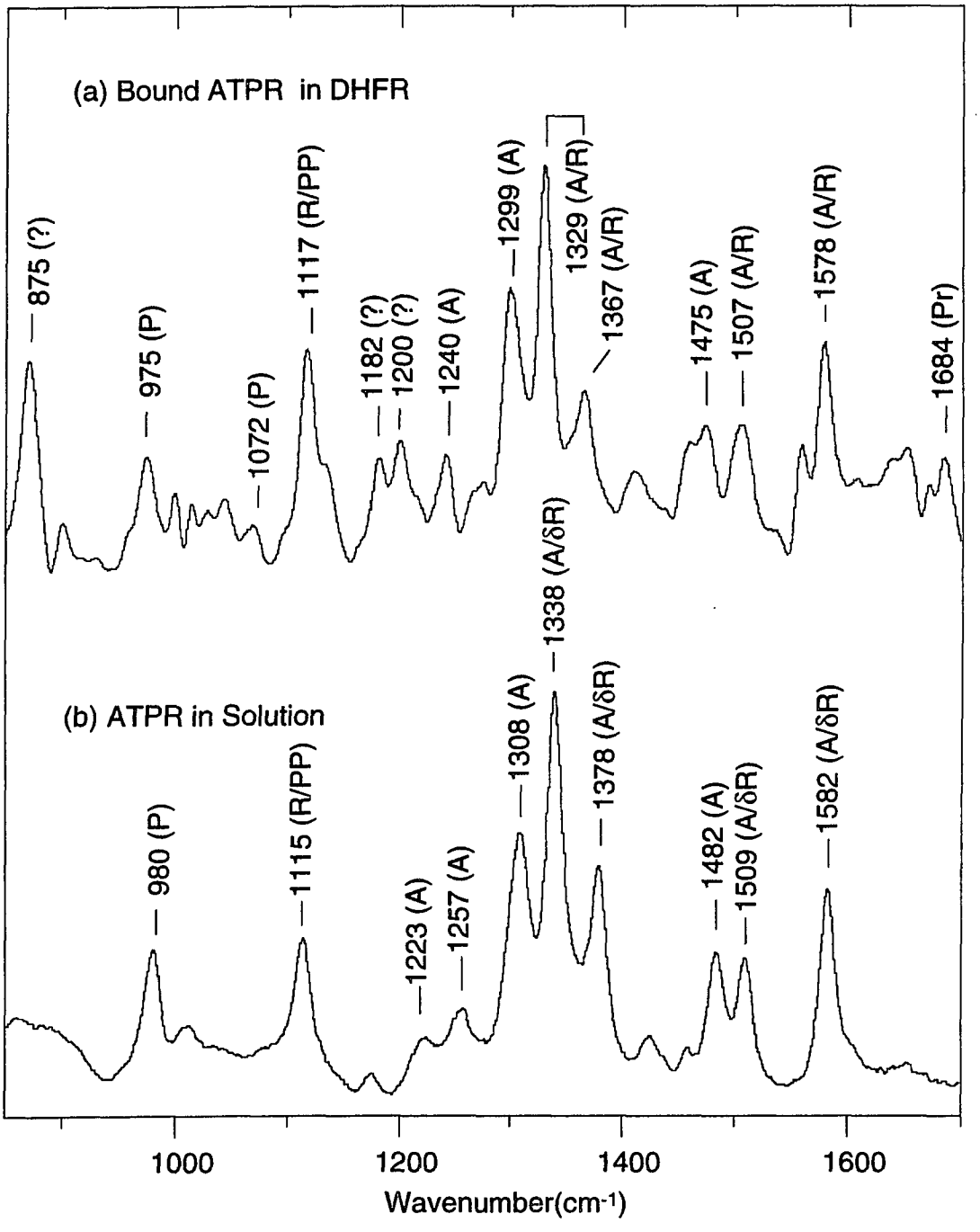

Figure 4.3 **(a)** Difference Raman spectrum of bound ATPR in DHFR at 4°C in 10 mM Tris and 0.5 M NaCl, pH 8.0 (Molar ratio in mM, DHFR:ATPR = 5:4.5) and **(b)** Raman spectrum of ATPR in solution at 4°C, pH 7.5 (100 mM). See text and Figure 4.1 for the labelling scheme. Laser excitation: 514.5 nm, 150 mW.

Chapter 5

Tautomerization of Folate and Biopterin Bound to DHFR

— Implication of the Oxidized Pterin Activation

5.1 Introduction to the Pterin Reduction

The primary reaction catalyzed by DHFR is the NADPH-dependent reduction of 7,8-dihydrofolate (DHF) to tetrahydrofolate (THF). Some DHFRs, notably those derived from vertebrate sources, will slowly reduce folate and biopterin also (Kisliuk, 1984). The rate of folate reduction by *E. coli* DHFR is about one-thousandth that of DHF reduction (Baccanari et al., 1975). The hydride ion from C4 of the nicotinamide ring is transferred to C7 of the pteridine ring of folate while it is transferred to C6 of DHF (see the review by Kraut & Matthews, 1987). The mechanism generally proposed for pterin reduction is the preprotonation mechanism, in which protonation of N8 precedes the hydride transfer to C7 and protonation of N5 precedes the hydride transfer to C6 (Huennekens & Scrimgeour, 1964). The latter is supported by the elevation of the pK_a of N5 of DHF bound to *E. coli* DHFR ternary complex with $NADP^+$ as determined by our Raman spectroscopic studies (Chapter 6), but there is no sign of the protonation of N8 of folate from numerous NMR studies (Cheung et al., 1993; Cheung et al., 1992; Selinsky et al., 1990). Moreover, the X-ray crystal structure of the ternary complex of *E. coli* DHFR•$NADP^+$•folate provides no indication of a direct path for proton transfer from either enzyme side chains or bound water molecules (Bystroff et al., 1990). In fact, the crystal structure shows

that the environment of folate's N8 is generally hydrophobic except the backbone carbonyl of Ile-5, which is 3.5 Å away to N8. An alternative mechanism involving O4-protonation of folate has been proposed on the basis of theoretical studies (Gready, 1985b). The O4 of folate is easily accessible to the bulk solvent and its protonated form could be stabilized by the ionized carboxyl side chain that is conserved in all DHFRs.

Since the vibrational frequency of C=O stretching mode is very sensitive the environment of carbonyl oxygen, a protonation of O4 of folate would certainly result in a large shift of the C4=O stretching frequency. In an attempt to learn more about how the enzyme interacts with the pterin ring, we have measured the Raman spectra of biopterin and folate bound in ternary complexes of wild-type *E. coli* DHFR with $NADP^+$ and the Asp-27 to serine (D27S) mutant with $NADP^+$. Since biopterin has the same pterin ring as folate but doesn't have the p-aminobenzoyl-L-glutamate group which often complicates the Raman spectrum, the band assignments of the pteridine ring modes are much easier with biopterin than with folate. Most importantly, biopterin is likely bound to the enzyme the same way as folate (McTigue et al., 1992). We will interpret the data mostly based on the spectra of biopterin except that bound to D27S complex where folate is pretty much bound but biopterin is probably not.

5.2 Raman Spectra of Folate and Biopterin

Figure 5.1a shows the Raman difference spectrum for bound biopterin in wild-type DHFR ternary complex at pH 7.0 by subtracting the spectrum of DHFR•$NADP^+$ binary complex from that of DHFR•$NADP^+$•biopterin ternary complex, and Figure 5.1b and 5.1c show the spectra for bound folate obtained similarly in wt DHFR and mutant D27S ternary complex with $NADP^+$ at pH 7.0,

respectively. The difference spectra for folate bound to wild-type DHFR ternary complex with $NADP^+$ have essentially no pH dependence in the range of 6 - 9.

For comparison and band assignments, the spectra of biopterin in solution at pH 5.2 and 12.0 are shown in Figure 5.2a and 5.2b. Biopterin in aqueous solution has two pK_a's at 2.43 and 7.7 (Viscontini & Mohlmann, 1959). The first is the deprotonation-protonation of N1. The second represents the deprotonation of N3 with the concomitant formation of the enolate form of the ring. Thus, the solution spectra at pH 5.2 (Figure 5.2a) and pH 12.0 (2b) are characteristic of biopterin's neutral and anionic forms. The high frequency band at 1700 cm^{-1} in Figure 5.2a is assigned to the C=O stretch mode of the keto form from its characteristic position and intensity. This band shifts down 20 cm^{-1} to 1680 cm^{-1} for biopterin in D_2O due to a small contribution from the N3-H in-plane bending vibration. A band at the same frequency with similar intensity is found for biopterin in DMSO (dimethyl sulfoxide; data not shown). These results imply that biopterin in the neutral form in aqueous solution adopts the keto tautomer, in agreement with earlier UV absorption results (Brown & Facobsen, 1961) and theoretical calculations (Uchimaru et al., 1989). At higher pH values in Figure 5.2b, the Raman spectrum of anionic biopterin is very different from that of the neutral form. The keto C=O stretch is absent as expected from the formation of the enolate form. Importantly for this study, the pteridine ring modes at 1307 and 1373 cm^{-1} at low pH are replaced by two strong bands at 1320 and 1343 cm^{-1} in the spectrum at high pH. The 1320 cm^{-1} band shifts down 4 cm^{-1} for [5-^{15}N]-biopterin while there is no shift for the 1343 cm^{-1} band (data not shown), indicating that the 1320 cm^{-1} band is from the ring stretching mode and the 1343 cm^{-1} band probably has large contribution from the stretching mode of C4-O^- single bond. Because biopterin's anionic form and enol form are structurally alike, and the long-wavelength absorption band of the enolate at 363 nm (ε=6600

$M^{-1}cm^{-1}$; Blakley, 1969) is very similar to strong absorption band at 358 nm of 2-amino-4-methoxy-pteridine (ε=6500 $M^{-1}cm^{-1}$; Pfleiderer et al., 1960), a model for the enol form of pteridine, it is likely that the 1320 and 1343 cm^{-1} bands from the pteridine ring are similar for the enol and enolate forms. We will use the presence of these bands in the spectrum of bound biopterin as markers for the formation of the enol forms of the pteridine ring. With this in hand, most of the features of the bound spectrum of Figure 5.1a may be understood.

The spectra of folate and biopterin bound in the ternary complex of DHFR with $NADP^+$ were found to contain virtually identical features in the region from 1630-1730 cm^{-1} (Figure 5.1b). For example, the 1653, 1678 and 1693 cm^{-1} peaks of Figure 5.1a lie at 1650, 1678, and 1694 cm^{-1}, respectively, in the bound folate spectrum, indicating that the pteridine rings of both biopterin and folate are indeed similarly bound. Thus, although the following assignments are based on the spectrum of bound biopterin, they apply to folate as well.

The negative band at 1668 cm^{-1} and the positive band at 1678 cm^{-1} almost certainly arise from perturbation of the protein amide I band (peptide backbone C=O stretch) due to disruption of certain backbone carbonyl stretches when biopterin binds to form the ternary complex. Such positive negative pairs have been observed in the same spectral position and with the same intensity levels in our previous work (e.g. Deng et al., 1989c). By comparing the relative intensity of the positive negative pair in the difference spectrum with that of the amide I spectrum of the apo-protein, we can calculate that on balance the change of approximately two polypeptide C=O stretches from 1668 cm^{-1} in the binary complex to 1678 cm^{-1} in the ternary complex would account for the observed 1668-1678 cm^{-1} couple.

The two bands at 1693 and 1653 cm^{-1} are assigned to the keto C=O stretch of the pteridine ring. There is no other normal modes which are candidates for

these bands. Moreover, both bands undergo a downshift in their positions in experiments in D_2O that are quite similar to that of biopterin's keto stretch in aqueous solution (the 1693 cm^{-1} band shifts to around 1675 cm^{-1} while the 1653 cm^{-1} moves to 1643 cm^{-1}; data not shown). Both bands are downshifted from the solution counterpart at 1700 cm^{-1} (Figure 5.2a) and are narrowed. There are a number of precedents whereby keto or carbonyl containing substrates undergo downward shifts in frequency, and band narrowing, when binding to their enzymes (Belasco & Knowles, 1980; Belasco & Knowles, 1983; Deng et al., 1989b; Kurz & Drysdale, 1987). This is generally the result of the response of the keto C=O stretch to the presence of nearby proton donors. A portion of the electrons in the C=O bond is pulled towards the donor, which decreases the force constant of the C=O bond by mixing more polar $^{+}C\text{-}O^{-}$ character into the double bond, and hence lowers the C=O stretch. In fact, linear (Badger-Bauer) relationships between the enthalpy of a hydrogen bond and the shift in the C=O frequency have been established for a number of keto and carbonyl containing compounds (Thijs & Zeegers-Huyskens, 1984). The presence of two keto stretches in the bound biopterin data of Figure 5.2a implies two populations of the pteridine ring in the ternary complex, one having a moderately polarized keto group, the 1693 cm^{-1} form which is similar to that in neutral solution, and the other having a more polarized group, the 1653 cm^{-1} form which is probably due to electrostatic interaction with the side chain of Asp-27 or partial protonation of O4. In fact, the 1653 cm^{-1} form, while very strongly polarized, is not without precedent. For example, the C=O group of acetone, whose C=O stretch almost certainly shifts less per unit of perturbant than does that of biopterin because of π electrons in the pteridine ring (Gready, 1985b), shifts from 1699 cm^{-1} in H_2O, to 1689 cm^{-1} in 37% HCl, to 1670 cm^{-1} in 70% $HClO_4$ and to 1663 cm^{-1} in 95% H_2SO_4 as a result of partial protonation of the carbonyl oxygen (data not shown).

From 1450 - 1600 cm^{-1}, the bands in the spectrum of bound biopterin (Figure 5.1a) generally shift down from that in solution at pH 5.2 (Figure 5.2a), and their relative intensities also change. These bands are generally associated with ring stretching mode with large contribution from pyrazine portion because they shift down 3 - 7 cm^{-1} with [5-^{15}N]biopterin.

From 1270-1450 cm^{-1}, the spectrum of bound biopterin also differs remarkably from that of neutral biopterin in aqueous solution. The new band at 1403 cm^{-1} in the bound data probably arises from the same species as that of 1653 cm^{-1} band, because their intensities seem to have the same pH dependence for biopterin in DHFR binary complexes (data not shown). A similar band at 1402 cm^{-1} is shown in the spectrum of bound folate (Figure 5.1b). The shoulder at 1320 cm^{-1} and the band at 1341 cm^{-1} look very similar to the bands at 1320 and 1343 cm^{-1} in the spectrum of biopterin in solution at pH 12 (Figure 5.2b). These bands can not be from free enolate due to the fact that they are present with similar intensities at pH 6.1 and 5.4 in the bound biopterin spectrum (data not shown). Moreover, the concentration of the enolate in aqueous solution is negligible at these low pH's. Thus, the bands at 1320 and 1341 cm^{-1} in the bound spectrum can be assigned to the enol form of biopterin bound to DHFR. Similar bands may be present in the spectrum of bound folate, but the strong peaks from folate's *p*-aminobenzoyl-*L*-glutamate portion make them difficult to identify.

The spectrum of bound folate in D27S ternary complex (Figure 5.1c) is quite unlike that bound to wild type protein complex (Figure 5.1b). It also differs quite a lot from that of folate in neutral aqueous solution, in particular, the 1703 cm^{-1} band appears in the solution spectrum of folate with same concentration as a broad band around 1690 cm^{-1} due to formation of folate dimer (Kisliuk, 1984), indicating that folate was mostly bound by the mutant enzyme under the experimental conditions (the concentrations of folate and DHFR•$NADP^+$ were 3.5 mM

and 4 mM, respectively). We assign the band at 1703 cm^{-1} to the carbonyl C=O stretch, similar to that of biopterin at neutral pH (Figure 5.2a). The lack of polarization of C4=O bond of folate bound to the mutant is expected, because the polarization and enolization of folate bound to wild-type DHFR almost certainly result from the interactions with the carboxyl side chain of Asp-27, and its replacement by serine greatly weakens this interaction (Howell et al., 1986). This result indicates that folate exists as a single keto tautomer when bound to the mutant D27S ternary complex with $NADP^+$.

5.3 Activation of Folate by DHFR

We have found that bound biopterin and folate in wild type DHFR ternary complex with $NADP^+$ exist as a mixture of enol form and two keto forms (with pteridine ring's carbonyl stretches at 1693 and 1653 cm^{-1}), but bound folate in mutant D27S ternary complex with $NADP^+$ exists only as one keto form.

Similar results have been reported for folate bound to *L. casei* DHFR by ^{13}C NMR studies (Birdsall et al., 1989; Cheung et al., 1993). These authors have found that there are three interconverting conformations of the *L. casei* DHFR•folate•$NADP^+$ complex: Forms I, IIa and IIb, with form I and IIa in N1 protonated enolic form and in an orientation similar to bound MTX, and form IIb, the catalytically active conformation, in the 4-keto form with N1 unprotonated and in an orientation with pterin ring flipped 180° relative to the other two forms. However, NMR studies on folate bound to *E. coli* DHFR have suggested that folate binds in a single conformation form on the basis that only single set of chemical shifts have been observed (Cheung et al., 1992; Falzone et al., 1990; Huang et al., 1991). Since the characteristic time scale for Raman scattering is 10^{-13} s, which is much faster than the NMR time scale of 10^{-3} s, it is

possible that the three species observed by Raman spectroscopy are interconverting too quickly for NMR spectroscopy to distinguish.

Figure 5.3 shows how the interconversion among the three species could be achieved in the enzyme active site with the help of the carboxyl side chain of Asp-27. The highly polarized keto forms (a, b and c) have a charge separation which is stablized by the ionized carboxyl side chain of Asp-27 and the bound structural water; the enolate form is due to an abstraction of the proton on N3 by the carboxyl group. The presence of the highly polarized C4=O bond of biopterin or folate bound to *E. coli* DHFR provides strong support for the O4-protonation mechanism of folate reduction which has been proposed on the basis of theoretical studies (Gready, 1985b). X-ray crystallography shows that N8 of folate is bound in a quite hydrophobic environment while O4 is easily accessible to the bulk solvent (Bystroff et al., 1990), making the protonation of O4 more achievable by the enzyme than the protonation of N8. The partial negative charge on O4 could easily abstract a proton from the bulk solvent through the bound structure waters to form O4-protonated pterin. Although the theroretical calculation shows that the O4-protonated pterin is energetically less favorable than the N8-protonated one by 16 kcal/mol, this energy difference will diminish if the interaction with the carboxyl side chain in the active site is taken into account. As shown in Figure 5.3, the carboxyl group of Asp-27 forms salt bridge with the O4-protonated pterin (e, h and i). A partial positive charge can develop on C7 by resonance (g, Figure 5.3), facilitating hydride transfer from C4 of nicotinamide ring. The slow rate of folate reduction compared with DHF reduction is probably due to much less positive charge residing on the pyrazine ring with O4-protonation of folate than with N5 protonation of DHF (Gready, 1985b).

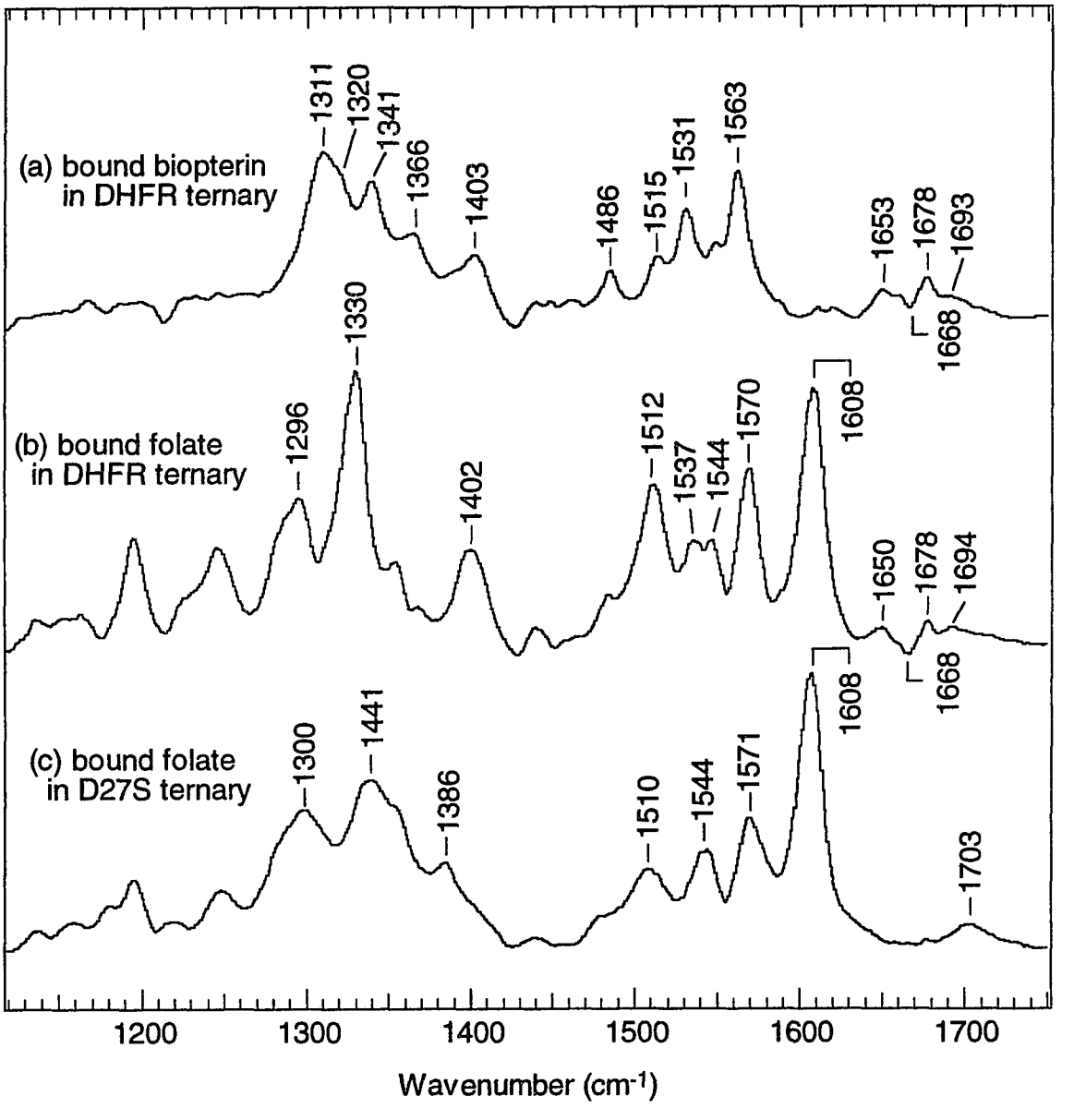

Figure 5.1 Raman spectra of (a) wt DHFR•$NADP^+$•biopterin minus DHFR•$NADP^+$; (b) wt DHFR•$NADP^+$•folate minus DHFR•$NADP^+$; and (c) mutant D27S•$NADP^+$•folate minus D27S•$NADP^+$. Experiments were done in 50 mM bis-tris propane buffer, pH 7.0. Protein concentrations were 3-4 mM. Laser excitation: 530.8 nm, 120 mW.

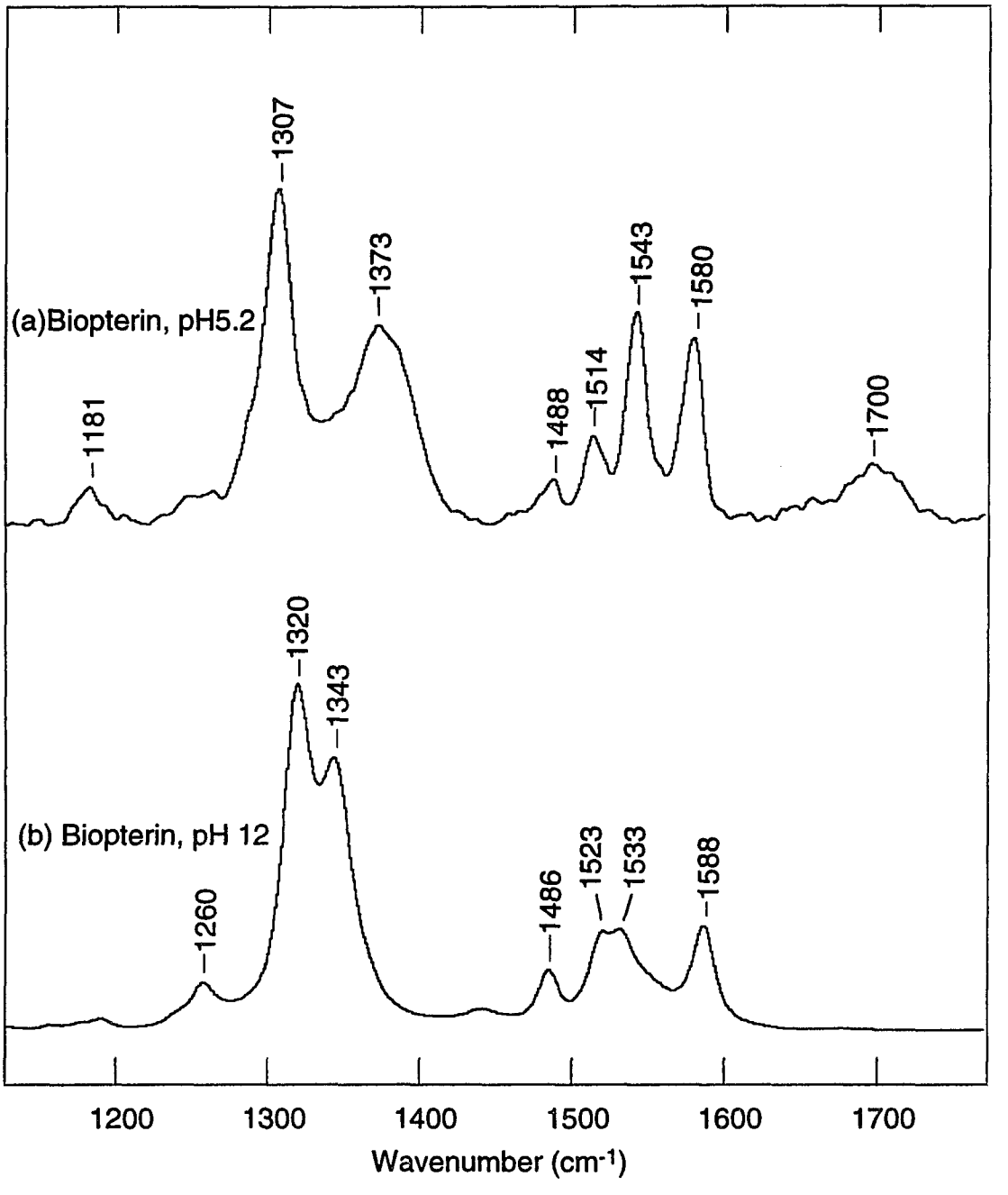

Figure 5.2 Raman spectra of biopterin in solution at (a) pH 5.2 (keto form) and (b) pH 12 (enolate form). Laser excitation: 530.8 nm, 150 mW.

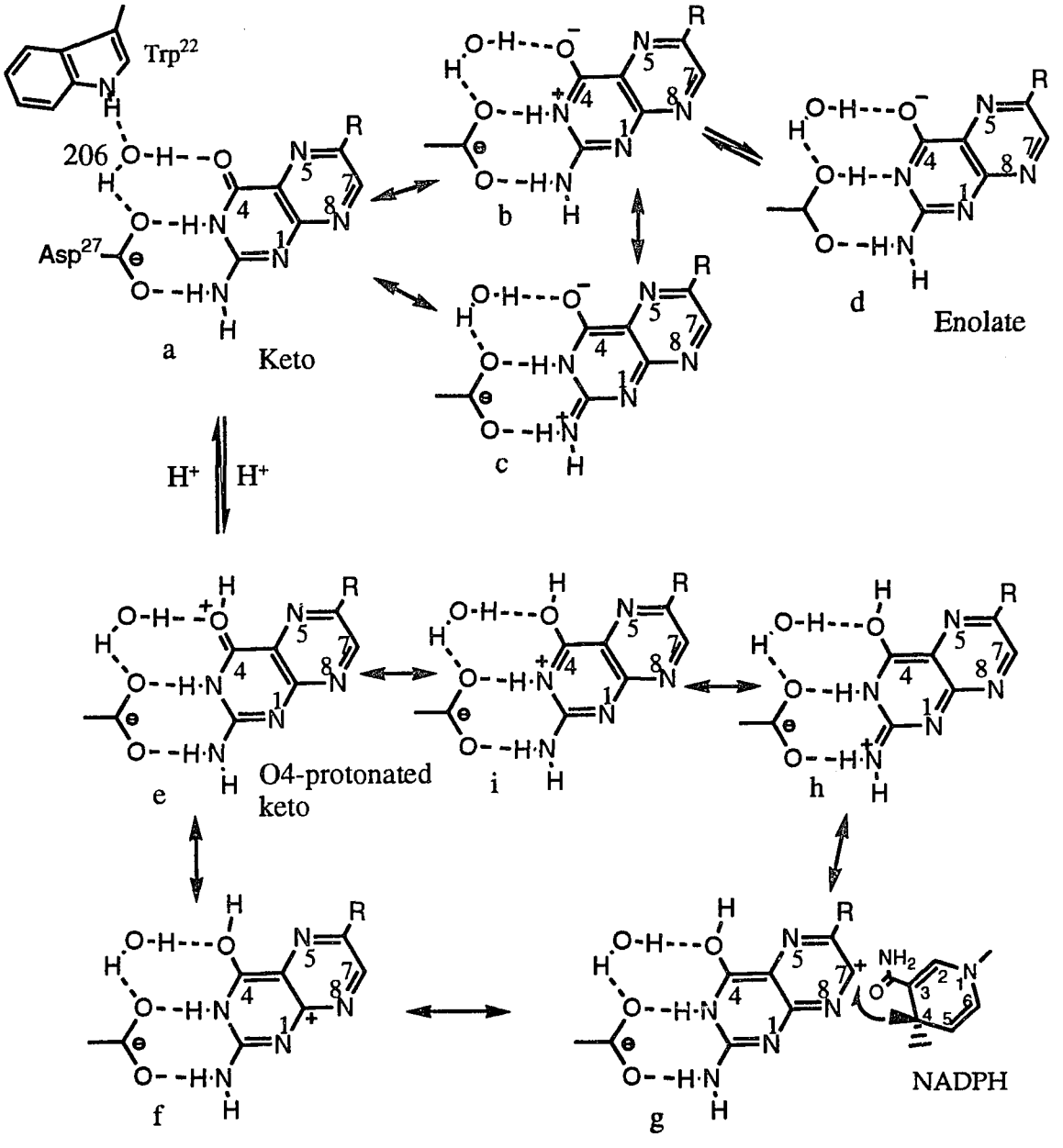

Figure 5.3 Enzyme catalyzed conversion of pterin from (a) keto form to (b) and (c) highly polarized keto form, and to (d) enolate form. The resonance forms of the O4-protonated keto (proposed in the Michaelis complex) are also shown (e, f, g, h, i). The C7-carbonium form (g) will facilitate hydride attack from C4 of nicotinamide ring.

Chapter 6

Protonation of DHF in DHFR•NADP+•DHF Ternary Complex

— Mechanistic Implication

A central issue concerning the catalytic mechanism of DHFR is how the enzyme accomplishes the protonation of N5 of DHF's pteridine ring. The solution pK_a of N5 is 2.6 (Maharaj et al., 1990) so that very little DHF is protonated at physiological pH. However, the rate of hydride transfer from NADPH to DHF in the presence of *E. coli* DHFR shows approximate Henderson-Hasselbalch dependence with a pK_a around 6.5 (Fierke et al., 1987; Morrison & Stone, 1988). These authors have suggested that a group at the active site of the enzyme with an pK_a of 6.5 is involved, presumably the strictly conserved carboxylic acid side chain (Asp-27 in *E. coli* DHFR), because it is the only ionizable protein group at the active site that is generally lined with hydrophobic side chains. However, X-ray crystallographic results show that its carboxyl group is hydrogen bonded, not to N5, but to the 2-amino group and to N3 of substrate's pteridine ring, and is more than 5 Å from N5 (Bystroff et al., 1990). Asp-27 therefore cannot form a direct interaction with N5 nor can it directly donate a proton. Instead, an indirect role has been proposed for Asp-27. In this view, a proton is transferred to N5 via two bound water molecules while the imino-keto tautamer isomerizes to the 4-hydroxyl form with the latter group participating in the proton relay system (Benkovic et al., 1988; Bystroff et al., 1990; Stone & Morrison, 1984; Uchimaru et al., 1989). In an attempt to find

evidence for or against this proposal, we carried out the Raman difference spectroscopy studies on dihydrofolate binding to *E. coli* DHFR.

6.1 DHF Bound to DHFR Ternary Complex with $NADP^+$

Figure 6.1a shows the difference spectrum between DHF bound in the ternary complex of DHFR with $NADP^+$ (the DHFR•$NADP^+$•DHF ternary complex) and the binary DHFR•$NADP^+$ complex at pH 6.1. Figure 6.1b is the same but at pH 7.4. There are three prominent bands in the spectrum at 1608, 1650, and 1675 cm^{-1}, and the intensity of the 1650, and 1675 cm^{-1} bands are clearly quite sensitive to pH in the range of 5.4 to 9.2 that we measured. The 1608 cm^{-1} band is assigned to a benzoyl ring mode of DHF. A band is found in similar locations of 1,4-disubstituted benzenes while it is absent in the spectra of H_2biopterin (see below), which has the pteridine ring structure of DHF but lacks its *p*-amino-benzoyl-*L*-glutamate group. Moreover, the 1608 cm^{-1} band is present in the spectra of methotrexate and folate (Ozaki et al., 1981; Saperstein et al., 1978); these molecules have substantially different electronic and vibrational spectra of the pteridine ring but contains the *p*-amino-benzoyl-*L*-glutamate group. As expected from this assignment, we observe little or no change in the intensity of the 1608 cm^{-1} band as a function of pH through 5-9. We therefore use this band as a reference in determining the intensities of the pH dependent bands.

The 1650 and the 1675 cm^{-1} bands can be assigned to the N5=C6 stretch of the pteridine ring of DHF for N5 unprotonated and protonated, respectively. The 1650 band shifts down 31 cm^{-1} to 1619 cm^{-1} for N5=^{13}C6 labeled DHF while the 1675 cm^{-1} shifts 32 cm^{-1} (Figure 6.1c). Moreover, the positions of these bands are close to solution models (see below). The mode for either form must be fairly

isolated to the N5=C6 group since the observed shifts on ^{13}C labeling are quite close to the predicted shift (36 cm^{-1}) for an isolated diatomic oscillator having the mass of a N=C molecule. In D_2O buffer, the 1675 cm^{-1} shifts down 14 cm^{-1} to 1661 cm^{-1} (data not shown) while the 1650 cm^{-1} is unaffected; the 14 cm^{-1} shift is typical of deuteration shifts found in the spectra of compounds containing a protonated -C=NH^+ group (see, e.g. Deng et al., 1993a).

6.2 H_2biopterin at Neutral and Low pH -- Solution Model for DHF

H_2biopterin is a good model for the pteridine ring of DHF because it contains the same pteridine ring as DHF and the pK_a of its N5 in solution is 2.6, which is the same as that of DHF, but it is much more stable and soluble than DHF at pH values below 4. Figure 6.2 shows the Raman spectra of H_2biopterin in solution below (panel a; pH 1.6) and above (panel b; pH 5) the pK_a. The 1635 cm^{-1} band is the unprotonated N5=C6 stretch while the 1671 cm^{-1} band is the protonated N5=C6 stretch. These assignments are confirmed by isotopic labeling studies on H_2biopterin. The 1671 cm^{-1} band shifts down to 1644 cm^{-1} for [5-^{15}N]H_2biopterin while the 1635 cm^{-1} band shifts to 1618 cm^{-1} (data not shown). It should be noted that the frequency of the unprotonated N5=C6 stretch of H_2biopterin in solution at 1635 cm^{-1} shifts down 6 cm^{-1} upon binding to the enzyme, which is the same for that of DHF (shifts down from 1656 cm^{-1} in solution to 1650 cm^{-1} upon binding), while the shift for the protonated stretch upon binding is not available because H_2biopterin is not protonated in DHFR•$NADP^+$•H_2biopterin ternary complex and the solubility of DHF at low pH is too low to allow Raman spectrum of reasonable quality be taken.

6.3 Determination of pK_a of N5 of DHF Bound to DHFR•$NADP^+$

From the above data, it is clear that the pK_a of DHF's N5 nitrogen is very altered in the ternary DHFR•$NADP^+$•DHF complex from its value in solution. Taking the intensities (I) of the 1650 and 1675 cm^{-1} bands as proportional to the concentrations of the neutral and protonated species, respectively, and that (I_{ref}) of the 1608 cm^{-1} band as an internal reference, a concentration profile of the neutral and protonated species as a function of pH can be determined. The result of intensity deconvolution for the two bands is plotted in Figure 6.3. The pK_a's were determined from Eq. 1 or 2, as appropriate, using nonlinear least-squares techniques:

$$I/I_{ref} = \frac{C}{1 + [H]/K_A} \qquad (1)$$

$$I/I_{ref} = \frac{C}{1 + K_A/[H]} \qquad (2)$$

where C represents the maximum relative intensity and K_A the acid dissociation constant. A pK_a for N5 was found to be 6.5 (±0.1) using the intensity profile for the 1675 cm^{-1} band and 6.4 (±0.1) from the 1650 cm^{-1} band. This is almost 4 pH units higher than its solution pK_a of 2.6.

It was found that the results described above pertain only to 'freshly' prepared samples. While DHF bound to *E. coli* DHFR in a binary complex was quite stable in the pH range measured, DHF bound in the ternary complex with $NADP^+$ showed substantial changes of its Raman spectrum with time. At pH values below 6.5, the intensity of the 1675 cm^{-1} band began to decrease after about one hour from preparation; on the other hand at pH values above 6.5, the

intensity of the 1675 cm^{-1} band steadily increased, accompanied by a concomitant intensity decrease of the 1650 cm^{-1} band. The ultraviolet absorption spectrum of dihydrofolate bound to enzyme ternary complex with $NADP^+$ showed a slow progressive change over 2 hr at 20°C and pH 5.8, with an increase in the 350-500 nm region and a decrease in the 280-350 nm region. This seems to be due to a chemical change in the pteridine since it was not reversed by raising the pH to 8.0. It probably reflects slow dismutation of dihydrofolate to folate and tetrahydrofolate and non-enzymatic destruction of the latter (Blakley & Cocco, 1984). The rate of this change was too slow to interfere with spectral measurements on the initial complex.

6.4 pK_a of DHF Bound to Other *E. coli* DHFR Complexes

Figure 6.4 shows Raman difference experiments on various protein-DHF complexes at pH 6.1. Figure 6.4a shows the difference spectrum of DHF bound to DHFR as a binary complex; Figure 6.4b shows the spectrum of DHF bound as a ternary complex with the NADPH analog H_2NADPH; Figure 6.3c shows the spectrum of bound DHF to the D27S mutant protein of DHFR in a ternary complex with $NADP^+$. In all of these cases, there is no evidence of the 1675 cm^{-1} band, characteristic of the protonated form of N5 that is found in the ternary DHFR•$NADP^+$•DHF complex. From a close examination of the maximum possible value of signal at 1675 cm^{-1} in these spectra and in the spectrum of Figure 6.1a, it can be determined that the pK_a of N5 of DHF bound in these complexes is less than 4.0, assuming simple Henderson-Hasselbalch behavior.

6.5 pK_a of DHF Bound to human DHFR•H_2NADPH

Since the pK_a of DHF's N5 bound to *E. coli* DHFR•$NADP^+$ is elevated to 6.5, it would be interesting to compare the pK_a of DHF bound to DHFR from other sources, particularly the human enzyme which is the target of cancer chemotherapy with methotrexate. The binding of folate to human DHFR (hDHFR) is similar to that to *E. coli* DHFR as revealed by X-ray crystallography (Davies et al., 1990), so similar protonation of DHF bound to hDHFR complexes might be obtained. Due to the back reaction between $NADP^+$ and DHF, the ternary complex of hDHFR•$NADP^+$•DHF is unstable, and a pK_a determination is very difficult. It has been found, however, that the pH dependent change of the UV absorption spectrum of the ternary complex of hDHFR•H_2NADPH•DHF has a pKa of 6.5 (R. L. Blakley, unpublished results). This ternary complex is stable enough to allow Raman difference spectra be taken. Figure 6.5 shows the difference spectra between the ternary complex of hDHFR•H_2NADPH•DHF and the binary complex of hDHFR•H_2NADPH at pH 6.5, 5.7, 5.1 and 4.7. The 1673 cm^{-1} band appears at pH below 6, and it shifts down to 1643 cm^{-1} with [6-^{13}C]DHF as that of DHF bound to *E. coli* DHFR•$NADP^+$, indicating that a portion of DHF is also protonated at N5 in the ternary complex of hDHFR•H_2NADPH•DHF. The relative intensity of 1673 cm^{-1} band (to 1607 cm^{-1} band) is relatively low compared with that of DHF bound to *E. coli* DHFR ternary complex with $NADP^+$, and is even lower at pH 4.6 than that at pH 5.4, suggesting that some of the protonated DHF is probably decayed as in *E. coli* DHFR ternary complex with $NADP^+$ at acidic pH. It may similarly dismutate to tetrahydrofolate and then be destroyed by the presence of some trace amount of NADPH or $NADP^+$ as impurities of H_2NADPH, or by H_2NADPH itself. Since there is little protonated DHF in the ternary complex at pH 6.5 by the lack of 1675

cm^{-1} band, the pK_a of DHF's N5 as estimated from the Raman data in Figure 6.5 is probably around 5, which is still about 2 pH units higher than that in solution. The discrepancy between this pKa value and that of 6.5 obtained from UV absorption spectroscopy might be caused by the dismutation of DHF as indicated above, as the end products of the destructed folate compound may complicate the UV absorption spectra.

6.6 Mechanism of DHF Protonation in DHFR Catalytic Pathway

The reduction of DHF to tetrahydrofolate involves the protonation of N5 of the pteridine ring. Indeed, the hydride transfer from NADPH to DHF as catalyzed by *E. coli* DHFR is pH dependent, pK_a = 6.5 (Fierke et al., 1987 Morrison & Stone, 1988). Thus, it has been a puzzle for some time as to how this is accomplished on the enzyme since, under physiological conditions, the amount of protonated N5, assuming a pK_a of 2.6, is very small. Most discussion of this issue has centered on the role of Asp-27 in *E. coli* DHFR, the only ionizable residue in the active site. It has been proposed that this residue donates a proton to N5 via groups of the pteridine ring and/or a series of structural water molecules even though its normal pK_a is around 4.

The results of this investigation suggest that most of this discussion has been misleading. We have determined that the pK_a of N5 of the pteridine ring of DHF in the ternary DHFR•$NADP^+$•DHF (freshly prepared) complex is 6.5. This is remarkable since, in solution, the pK_a of N5 is 2.6. Thus, the pK_a of N5 is raised about four units in this complex. It seems reasonable to suppose that N5 has a pK_a of 6.5 in the biologically relevant DHFR•NADPH•DHF ternary complex as well, given all the evidence pointing to a kinetic determinant with this pK_a along the pathway of enzymic catalysis of DHF to THF and the evident

need for protonation of N5 at physiological pH values. Moreover, there appears to be no significant structure difference in ternary complexes of E. coli DHFR associated with the oxidization state of the cofactor, as observed by X-ray crystallography (M. R. Sawaya and J. Kraut, unpublished data). This amounts to assuming that DHFR•NADP$^+$•DHF is an appropriate model of the Michaelis complex of the substrates with DHFR. Thus, our results solve a puzzle of how DHFR brings about protonation of N5 along the catalytic pathway. It does this by substantially raising its pK_a in the Michaelis complex. Two questions are raised by our observations. How does the enzyme raise the pK_a value by four units, and how is the proton delivered to N5, and particularly what is the role of Asp-27?

In general, there are many precedents for protein substantially altering the pK_a's of various groups, in particular raising the pKa values of a -C=N- group. For example, the linkage between the retinal chromophore of visual pigments and bacteriorhodopsin is via this moiety. In these cases, the nitrogen pK_a of solution models lie at about 6.5. However, the pK_a of the -C=N- moiety in bacteriorhodopsin is 13.5 (Druckmann et al., 1982) and in excess of 17 in the bovine visual pigment protein (Steinberg et al., 1993). In these cases, it is believed that the protonated structure is stabilized by the formation of hydrogen bonds between the protein and the -C=NH$^+$- group. The identity of the protein group that is involved in the hydrogen bond in both protein systems is almost certainly a carboxylate group, probably via a structural water molecule in a hydrogen bond network. It is thus interesting to note that recent X-ray structural studies place a structural water molecule at the active site of DHFR in close proximity to N5 (McTigue et al., 1992; J. Kraut et al., unpublished observations on the E. coli enzyme), and this comparison between the retinal containing pigments and DHFR suggests a role for the carboxyl group of Asp-27 as the

anion anchor, stabilizing the N5 protonated form of H_2folate by forming hydrogen bond to N5 via structural water molecules (as well as direct hydrogen bonds to NA2 and N3 of the pyrimidine ring, which bears almost a half of positive charge when N5 is protonated; Gready, 1985b).

Asp-27 is clearly required to raise the pK_a of N5 to 6.5 since, in the Asp to Ser mutant (D27S), the pK_a of N5 in its ternary complex with DHF and $NADP^+$ is substantially less. While Asp-27 is often supposed to be the proton donor to N5, this is not the necessary, or even the simplest conclusion, in view of the present results. More likely the ambient solution acting via a bound water molecule close to N5 is the proton donor, if, as we suppose the pK_a of N5 is raised 4 units upon formation of the DHFR•NADPH•DHF ternary complex. In this case the only physical requirements are that a substantial amount of N5 is protonated at physiological pH and that N5 equilibrate with its proton donor at a faster rate than k_{cat}. This is not an unreasonable expectation for a group with pK_a 6.5. Moreover, recent spectroscopic evidence indicates that neither Asp-27 in the *E. coli* enzyme nor Glu-30 in the human enzyme titrate in the pH range 5 to 9, as would be expected if these were the groups responsible for the observed kinetic pK_a of 6.5. Measurements of the vibrational spectrum of folate bound to *E. coli* DHFR ternary complex with $NADP^+$, over the pH range 6-9, show no changes in bands associated with motions of pteridine ring moieties which are physically close to and interacting with Asp-27. These vibrations would be expected to change if Asp-27 changed its ionization state (Chen, Kraut, and Callender, unpublished data). Additionally, NMR studies (Blakley et al., 1993) show no effect on the NMR spectra of folate bound to human DHFR as a function of pH from 5 to 7. The simplest explanation of these data is that the conserved carboxylic acid side chain at the catalytic site is ionized throughout the pH range 5-9, since the normal solution pKa of a carboxylic acid group is around 4.

However , it may be difficult to definitively determine the mechanism by which the pK_a of N5 is raised in DHFR, at least for the E. coli enzyme. From our studies, it is clear that the pK_a of N5 is less than 4.0 in the binary complex DHFR•DHF and the ternary complexes DHFR•H_2NADPH•DHF and D27S•$NADP^+$•DHF, while the (E. coli) DHFR•$NADP^+$•DHF ternary complex itself is stable for only a couple of hours with regards to the pK_a of N5. Thus, it appears that the presumed elevation of N5's pK_a by DHFR in the catalytically competent DHFR•NADPH•DHF ternary complex results from a conjunction of just the right structural features. Crystallizing and stabilizing the correct DHFR•$NADP^+$•DHF complex as a model of the Michaelis complex for X-ray structure determination may be difficult and perhaps impossible because of its limited lifetime.

In conclusion, it appears that we must now replace one puzzle relating to how and from what source a proton is transferred to N5 of a bound substrate molecule with another puzzle relating to how the holoenzyme, i.e. DHFR•cofactor, manages to increase the pK_a of N5 by 4 units, and especially what role Asp-27 plays in this phenomenon. A reasonable conjecture would be that the local electrostatic field of the holoenzyme is responsible. Possible contributions to the formation of a correct set of electrostatics and electrostatic interactions could also include the polar carboxamide moiety of the coenzyme, which is in close proximity to N5, as well as the carboxyl of Asp-27.

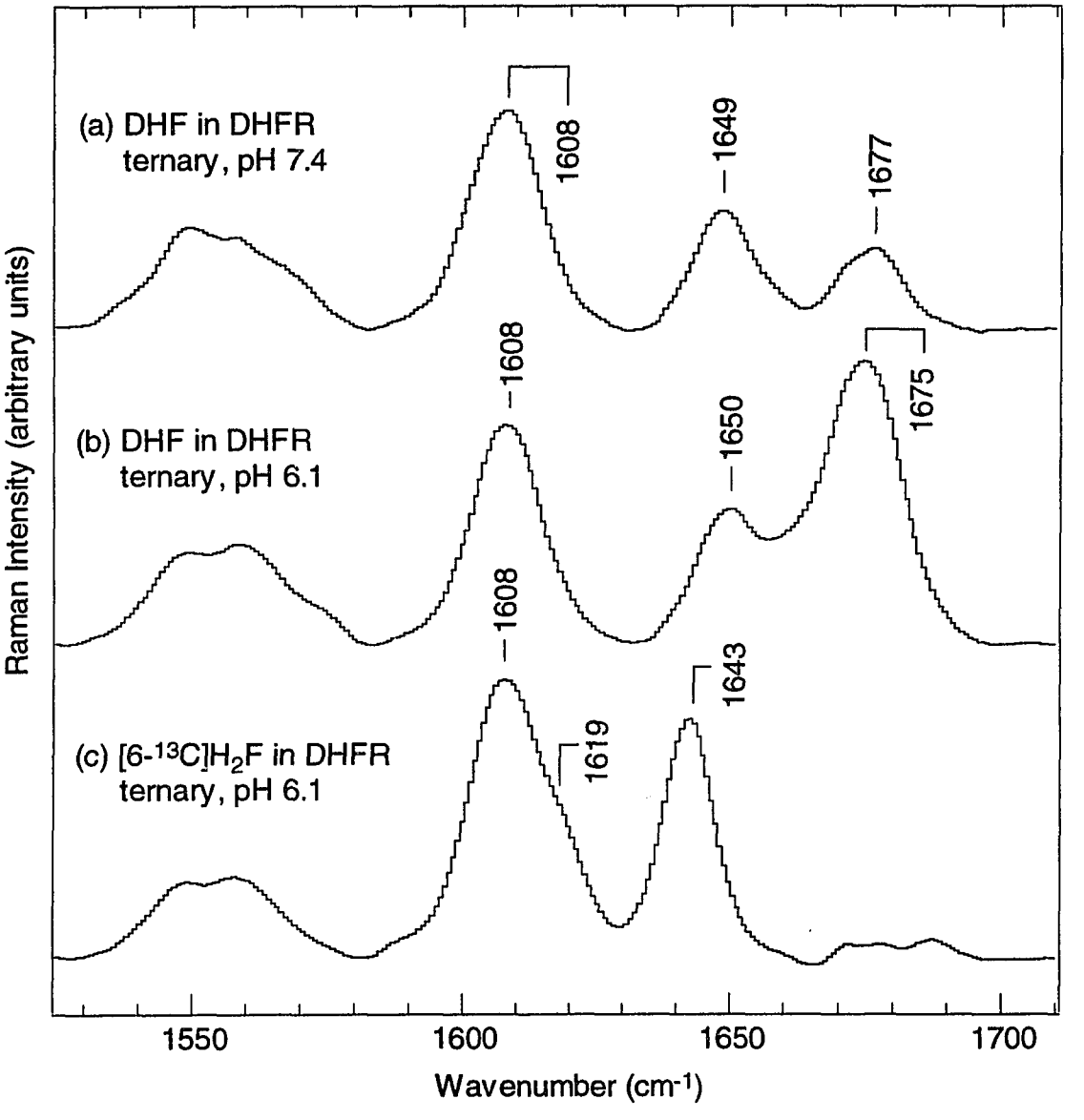

Figure 6.1 Difference Raman spectra of (a) DHF bound in the ternary complex of *E. coli* DHFR with $NADP^+$ in 20mM Tris buffer containing 0.5 M KCl, pH 7.4; (b) same as (a) but in 25 mM Bis-tris buffer containing 0.5 M KCl, pH 6.1; and (c) same as (b) but with [6-^{13}C]DHF. Enzyme concentrations were 3.4 mM. Laser excitation: 568.2 nm, 120 mW.

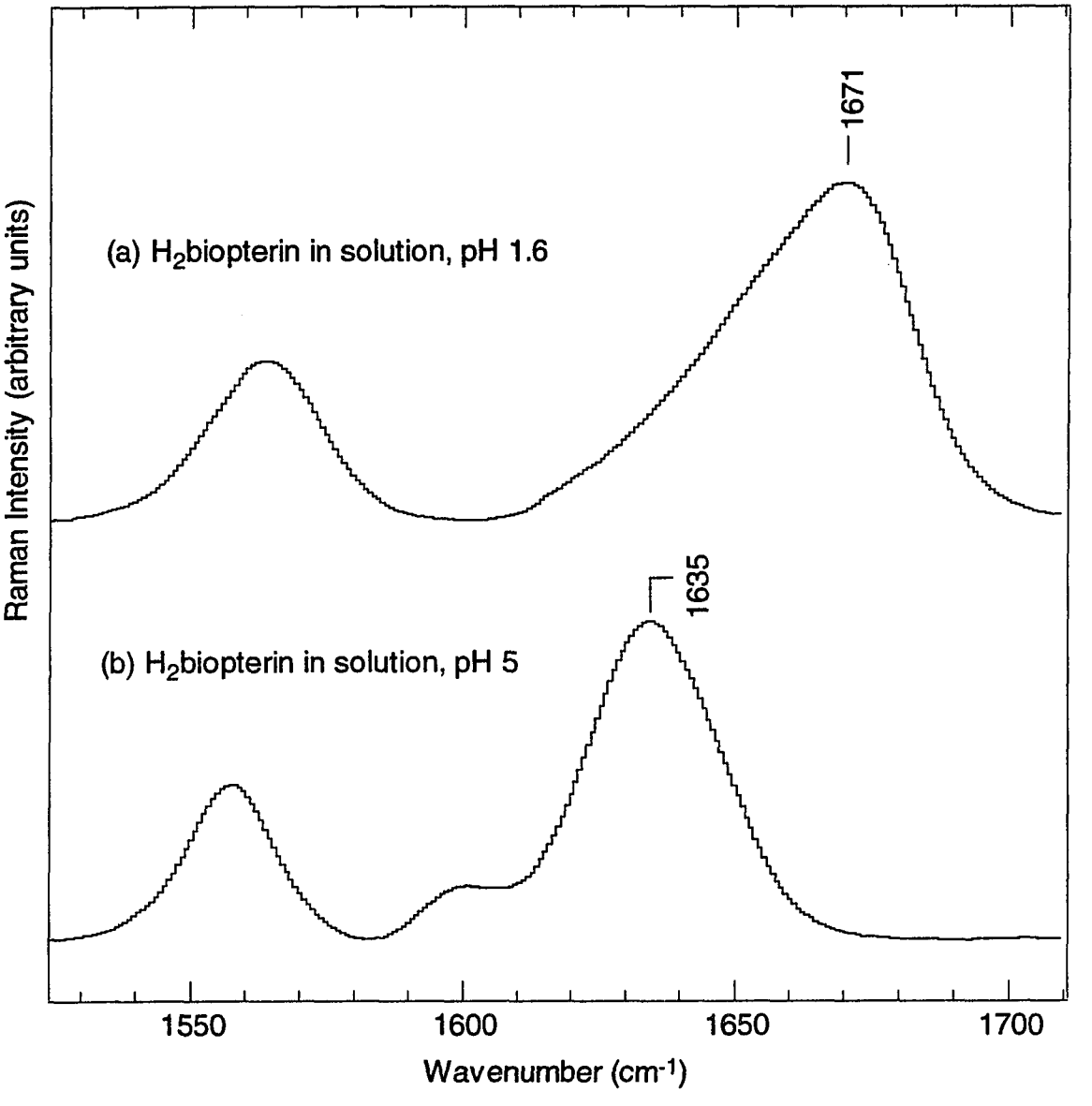

Figure 6.2 Raman spectra of H_2biopterin at 4°C in solution (7 mM) at (a) pH 1.6; and (b) pH 5.0.

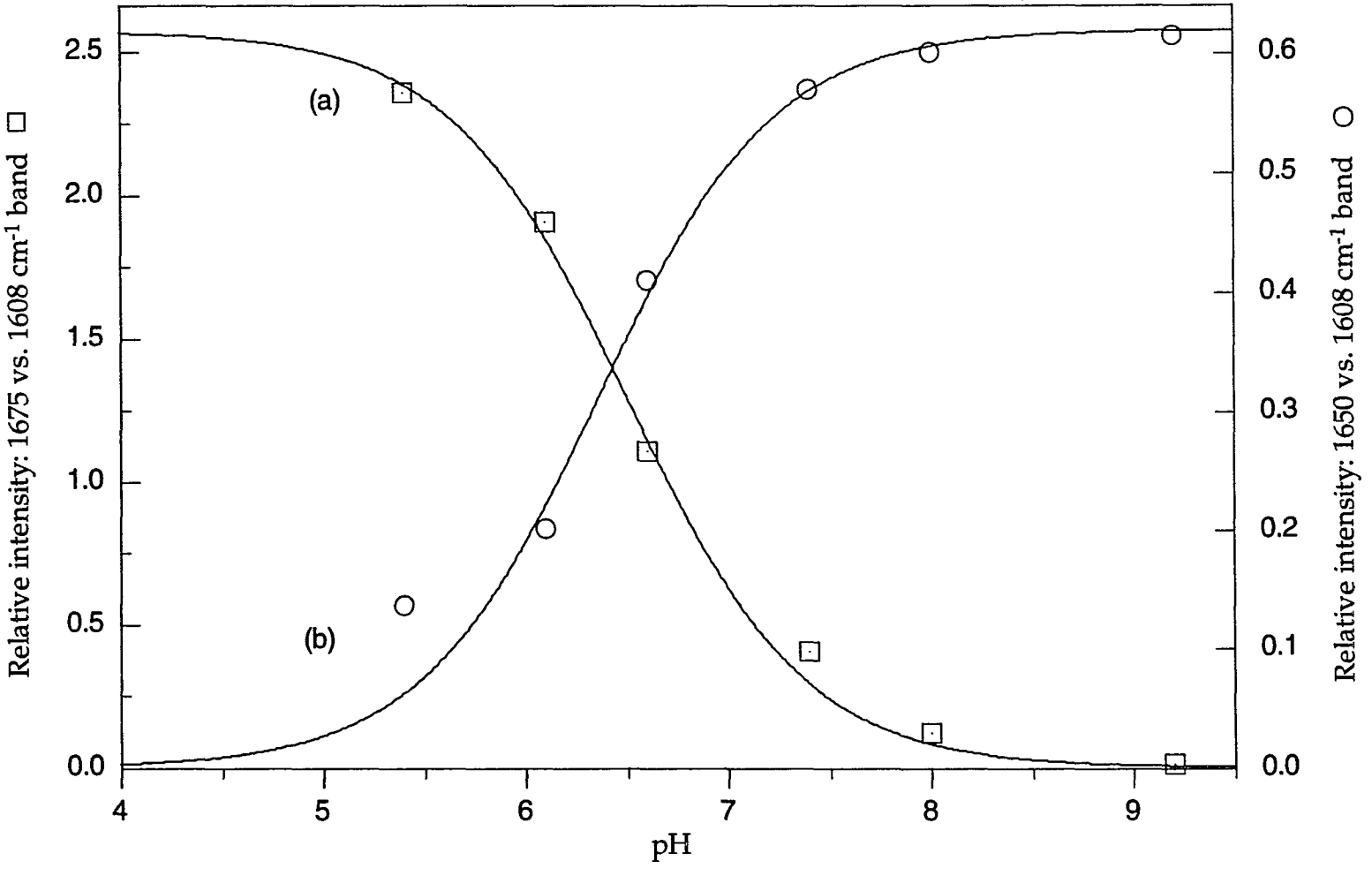

Figure 6.3 The pH dependence of the relative intensity (to 1608 cm^{-1} band) of peaks at 1675 cm^{-1} (square) and 1650 cm^{-1} (circle). The solid curves represent the best fits to Equations 1 or 2, as appropriate. The values found for the pKa's were: 6.5 (±0.1) using the 1675 cm^{-1} data and 6.4 (±0.1) for 1650 cm^{-1}.

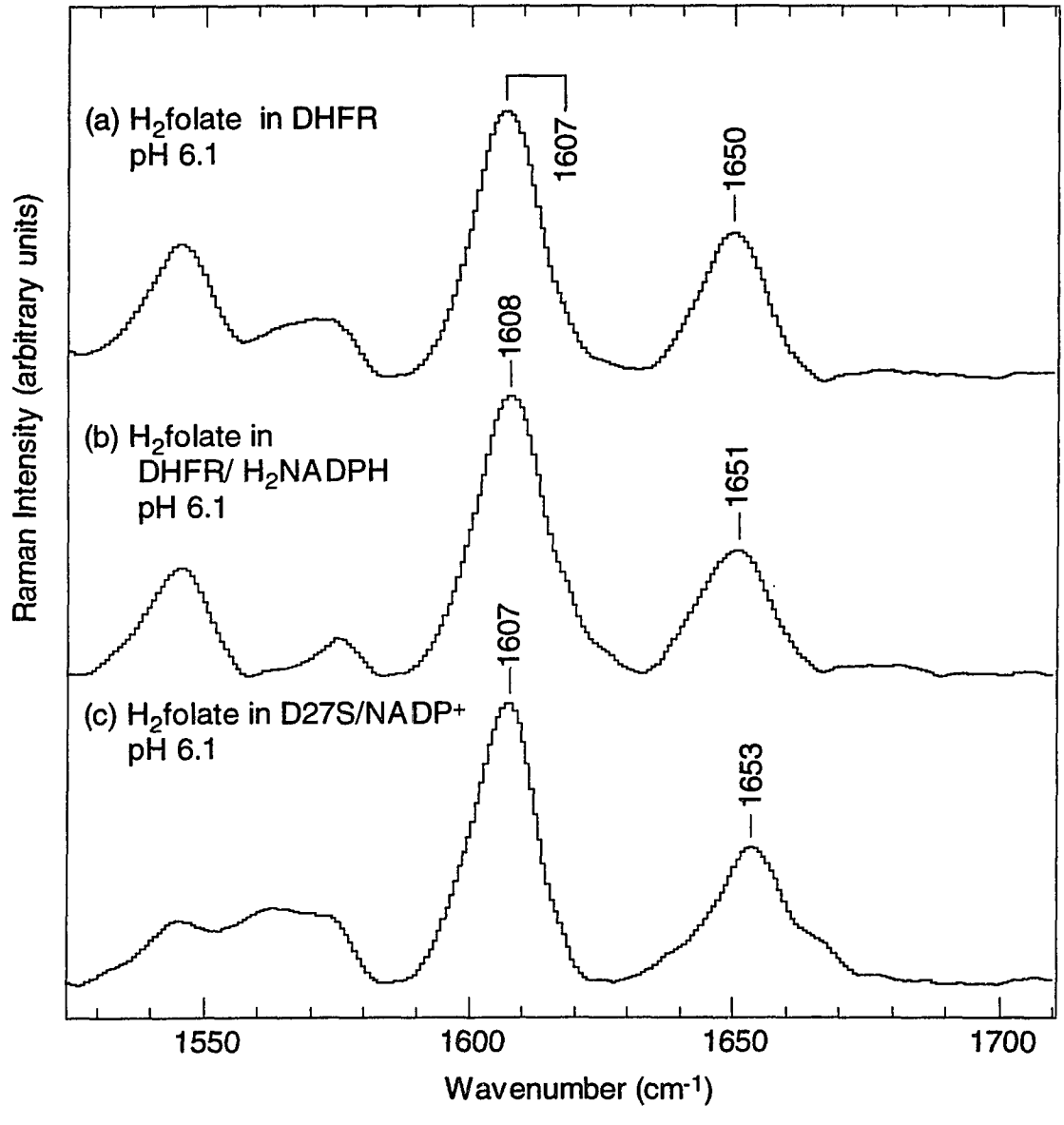

Figure 6.4 Difference Raman spectra of DHF bound in (a) the binary complex with DHFR (molar ratio DHFR:DHF = 3.4:2.5); (b) the ternary complex of DHFR with H_2NADPH (DHFR•H_2NADPH:DHF = 4.2:2.6); and (c) the ternary complex of mutant D27S with $NADP^+$(D27S•$NADP^+$:DHF = 3.5:2.6) at 4°C in 25 mM Bis-tris buffer containing 0.5 M KCl, pH 6.1.

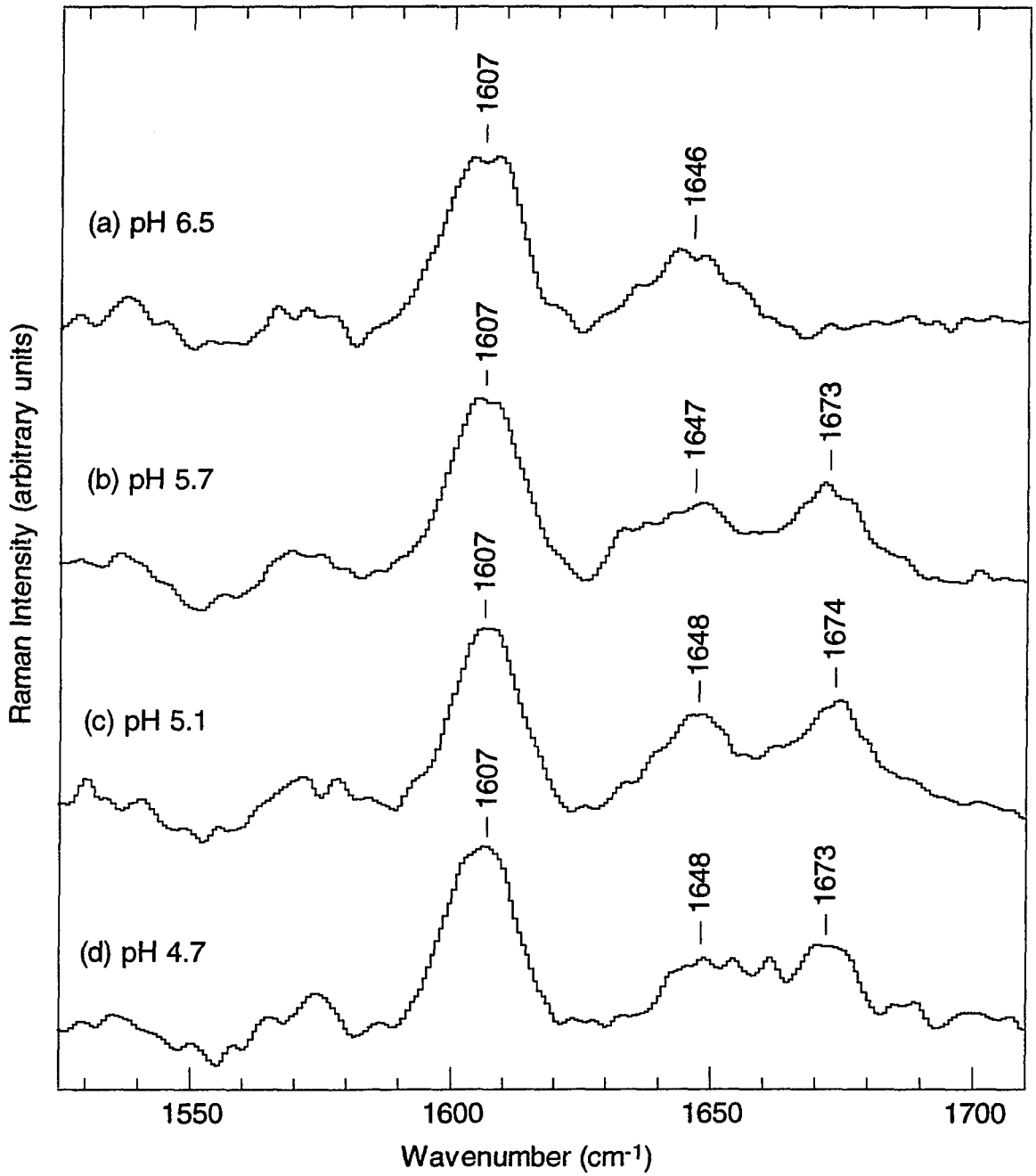

Figure 6.5 Difference Raman spectra of DHF bound in the ternary complexes of human DHFR with H_2NADPH at (a) pH 6.5; (b) pH 5.7; (c) pH 5.1; and (c) pH 4.7. Enzyme concentrations were 0.10 - 0.18 mM. Laser excitation: 568.2 nm, 120 mW.

Chapter 7

Reduction of MTX in DHFR•MTX•NADPH Ternary Complex

— Clinical Implication

7.1 The Clinical Use of MTX and Its Mechanism of Action

MTX is an antifolate that has been widely used in chemotherapy for many cancers, such as acute lymphocytic leukemia, non-Hodgkin's lymphoma, osteosarcoma, choriocarcinoma, head and neck cancer, ovarian cancer, and breast cancer (Jolivet et al., 1983). It has also been used in the treatment of various rheumatic diseases after primary therapy has failed(Korn & Dehoratius, 1989).

The primary mechanism of action of MTX for cancer chemotherapy is via inhibition of DHFR (Blakley, 1969), leading to depletion of intracellular pools of reduced folate. The most sensitive reactions to this depletion are thymidylate synthesis requiring N-5,10-methylene-THF and purine synthesis requiring N10-formyl-THF (Jolivet et al., 1983). The lack of either thymidylate or purine blocks DNA synthesis, stopping tumor growth.

Over the past two decades, the interaction of MTX with DHFR has been the subject of numerous and intensive investigations with various techniques, such as ultraviolet difference spectroscopy (Cocco et al., 1981; Gupta et al., 1977; Hood & Roberts, 1978; Poe et al., 1974; Stone & Morrison, 1983; Subramanian & Kaufman, 1978), Raman spectroscopy (Dwivedi et al., 1982; Ozaki et al., 1981; Saperstein et al., 1978), nuclear magnetic resonance studies (Cheung et al., 1992; Cocco et al., 1981; Cocco et al., 1983; Cocco et al., 1981; Huang et al., 1991), and X-

ray crystallography (Bolin et al., 1982; Matthews et al., 1978; Matthews et al., 1977). All these studies indicate that MTX is bound in the active site of DHFR with N1 protonated and forms ionic and hydrogen bond interactions with the carboxylate group of the active site aspartic or glutamic acid. Comparison of the structures for *E. coli* DHFR complexes with MTX and folate (Bystroff et al., 1990) shows that the pteridine ring of MTX is in a different orientation from that of folate, rotated roughly 165° about an axis approximately collinear with a line through N5 and NA2. A very interesting observation by Bystroff et al. is that the MTX binary complex fits quite well with a transition state conformation of the dihydrofolate•NADPH ternary complex modeled from the structure of the folate•NADPH ternary complex, which leads to the questioning of whether MTX might in some ways resemble a transition-state analog. To further explore this question, we carried out Raman spectroscopic studies on the ternary complex of *E. coli* DHFR•MTX•NADPH. To our surprise, we have found that NADPH and MTX reacts at the active site to give $NADP^+$ and 5,8-dihydro-MTX, and the latter probably converts back to MTX once dissociated from the enzyme active site.

7.2 Reduction of MTX by NADPH with DHFR

7.2.1 Identification of Reaction Products

Figure 7.1 shows the Raman difference spectra of DHFR•MTX•NADPH with DHFR•MTX excited with three different wavelengths. Figure 7.1a differs substantially from the spectrum of NADPH bound to DHFR binary complex under similar conditions (Figure 4.1a). The most prominent differences are the negative bands at 1364 and 1408 cm^{-1} and the new band at 1710 cm^{-1}, which are accompanied by the large intensity decrease of 1685 cm^{-1} band and the

appearance of a new band at 1031 cm^{-1}. Since the band at 1685 cm^{-1} is from the reduced nicotinamide ring while that at 1031 cm^{-1} is from the oxidized nicotinamide ring, data shown in Figure 7.1a strongly suggest that NADPH is oxidized to $NADP^+$ in the ternary complex rather than merely polarized by hydrogen bonding with protein backbone as previously suggested (Dwivedi et al., 1982). As a result of NADPH oxidation, MTX is almost certainly reduced. This is shown by the decrease of bands at 1364 and 1408 cm^{-1} (appearing as negative bands in Figure 7.1a) which are from the protonated pteridine ring of bound MTX (Ozaki et al., 1981; Saperstein et al., 1978) and the appearance of new band at 1710 cm^{-1}, which can be assigned to reduced MTX as argued below.

It is possible that the 1710 cm^{-1} band comes from the nicotinamide ring, such as C=O bond of the carboxamide or C=C bond of the ring, resulting from certain interactions with both the enzyme and the protonated pteridine ring of MTX. If that is the case, a frequency shift for the band would be expected with proper isotopic substitutions. However, both APADPH and [7-^{18}O]APADPH bound in DHFR ternary complex with MTX give a similar band at 1712 cm^{-1} (data not shown), indicating that C=O of the carboxamide group is unlikely to be the origin of 1710 cm^{-1} band. Similarly, [2,5,6-D]NADH, which has a band at 1656 cm^{-1} (shifting down from 1688 cm^{-1} for NADH) that is largely due to the C5=C6 stretch of the nicotinamide ring (Deng et al., 1992), produces the same band at 1710 cm^{-1} in the ternary complex of DHFR with MTX (data not shown), indicating that it is also unlikely that the band is from pyridine ring stretch.

Since the band at 1710 cm^{-1} is not from nicotinamide group, it must come from a product that is due to reduction by NADPH, i.e., a reduced pteridine ring. The unusual high frequency of the 1710 cm^{-1} band makes it unlikely to be due to the common 5,6-dihydro- or 7,8-dihydro-pteridine since the highest frequency for double bond is from C7=N8 or N5=C6 stretch and is usually below 1700 cm^{-1},

as shown by the N5=C6 stretch frequency for DHF bound to DHFR•NADP$^+$ at 1650 cm^{-1} with N5 neutral and 1675 cm^{-1} with N5 protonated. Could the pteridine ring be reduced differently to give the 1710 cm^{-1} band?

Figure 7.4 shows the relative positions of nicotinamide and pteridine rings in the X-ray crystal structure of *E. coli* DHFR•MTX•NADPH ternary complex (Mark Sawaya and Joseph Kraut, unpublished results). The distance between C4 of the nicotinamide ring and N5 of the pteridine ring is only 3.1Å, similar to the distance of 3.2 Å between C4 of nicotinamide ring and C6 of pteridine ring in the X-ray crystal structure of *E. coli* DHFR•NADP$^+$•folate ternary complex (Bystroff et al., 1990), suggesting possible hydride transfer from C4 to N5 of pteridine ring to give 5,8-dihydro-MTX shown below:

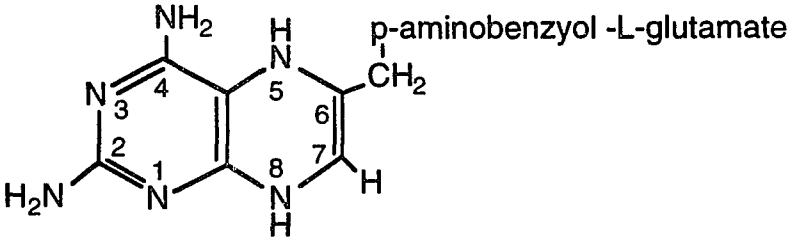

Similar hydride ion transfer was proposed previously for the dihydropteridine reductase catalyzed reduction of 7,8-dihydropterin to tetrahydropterin via 6,7-quinonoid dihydropterin intermediate (Gready, 1985a).

As can be seen from the structural formula, the C6=C7 double bond on the pyrazine ring is quite isolated form the π electron system on the pyrimidine ring, and its stretch could give the high frequency band at 1710 cm^{-1}. This is confirmed by the frequency shifts with [2,4a,6-^{13}C]MTX and various deuteration studies as well as calculated results using the AM1 method in the program AMPAC2.1 (Dewar et al., 1985), shown in Table 7.1. The 25 cm^{-1} down shift with [2,4a,6-^{13}C]MTX is quite close to the predicted shift of 30 cm^{-1} for C6=C7 bond stretch. Based on the calculation, the additional labeling with ^{13}C at C2 and C4a

has almost no effect on C6=C7 stretch frequency. The deuteration on either N5 when NADPH deuterated at C4-A-side ($NADPD_A$) is used or N8 when the experiment is carried out in D_2O generates 3 cm^{-1} down shift, which fits quite well with the calculated values. Consistent with these results is the shift of 6 cm^{-1} observed with $NADPD_A$ and in D_2O where both protons on N5 and N8 are deuterated. Since the band at 1710 cm^{-1} shifts down 3 cm^{-1} with NADPH deuterated at C4-A-side but not B-side, it is the A-side deuteron that is transferred to N5 of MTX. That the shift is observable in H_2O buffer indicates that the deuteron on N5 has little accessibility to the bulk solvent, in agreement with X-ray crystallographic findings (Bolin et al., 1982). In contrast, the proton on N8 of MTX is easily accessible to the solvent since the 1710 cm^{-1} band shifts down 3 cm^{-1} in D_2O.

Table 7.1 Shifts of the C6=C7 stretch of 5,8-dihydro-MTX at 1710 cm^{-1} in the ternary complex of DHFR•MTX•NADPH with various isotope substitutions.

Isotope labeling on reactants	Resulting labeling on pteridine	C6=C7 str. (cm^{-1})	Shift from 1710 cm^{-1}	
			Exp.	Calc.
none	none	1710	—	—
[2,4a,6-^{13}C]MTX	2,4a,6-^{13}C	1684	-26	-30
$NADPD_A$	5-D	1707	-3	-4
$NADPD_B$	none	1710	0	0
in D_2O	8-D	1707	-3	-2
$NADPD_A$, in D_2O	5,8-D	1704	-6	-6

7.2.2 Characterization of the MTX Reduction Reaction

Since the spectrum of 5,8-dihydro-MTX is not expected to contain bands at 1364 and 1408 cm^{-1} which are from protonated MTX bound to DHFR, its amount in the ternary complex can be estimated from the intensity of the negative band at 1364 cm^{-1} in the difference spectra (Figure 7.1) relative to that in the spectra of MTX bound to the enzyme binary complex (data not shown). As a result, about 41% of reduced MTX is present under the condition for Figure 7.1a, 33% for 7.1b, and less than 10% for 7.1c. On the other hand, using the band at 1329 cm^{-1} from adenine ring as internal reference (assuming adenine binding site is the same for NADPH and $NADP^+$), the percentage of $NADP^+$ can be estimated from the amplitude ratio of 1031 to 1330 cm^{-1} band, which is roughly 2.0 for $NADP^+$ bound to DHFR•MTX excited with 514.5 nm, 2.1 with 568.2 nm and 2.7 with 647.1 nm (data not shown). Thus, the amplitude of 1031 cm^{-1} band in Figure 7.1a represents about 60% of NADPH oxidation, 51% in 7.1b and only 14% in 7.1c.

Based on the above calculation of the amount of $NADP^+$ present, the remaining NADPH can also be obtained, which is about 40% under conditions for Figure 7.1a. However, the relative amplitude of 1685 cm^{-1} band (marker for NADPH) to 1329 cm band in Figure 7.1a is only 10% of that for NADPH bound in DHFR binary complex (Figure 4.1a), or one-fourth the amount expected. We believe this large discrepancy is caused by Raman hypochromism that is commonly observed in polynucleotides (Small & Peticolas, 1971; Tinoco, 1960; Tomlinson & Peticolas, 1970). In those studies, it was found that Raman intensities of some ring modes of the nucleotide bases decreased when they stacked together in the ordered structure of polynuleotides. Similar stacking is seen between nicotinamide ring of NADPH and pteridine ring of MTX in the ternary complex of *E. coli* DHFR•MTX•NADPH (Figure 7.2) where the closest

distance is 3.1 Å between the two rings. Since hypochromism is caused by a dipole-dipole interaction (Tinoco, 1960) which is between the reduced nicotinamide ring (absorption maximum at 345 nm) and the protonated pteridine ring (absorption maximum at 345 nm in DHFR binary complex), it may also result in an intensity decrease for the ring modes of MTX at 1364 and 1407 cm^{-1}, contributing to the negative bands in Figure 7.1. Thus, the actual amount of 5,8-dihydro-MTX could be less than that calculated. The discrepancy might be smaller in those for Figure 7.1b and 7.1c where the exciting wavelength is longer and the Raman hypochromism is likely pronounced (Tomlinson & Peticolas, 1970), as shown by the increasing relative intensity of 1685 cm band, which shows little hypochromism with 647.1 nm excitation (Figure 7.1c)

Since the amounts of $NADP^+$ and 5,8-dihydro-MTX decrease with increasing excitation laser wavelength, the reaction between NADPH and protonated MTX to form $NADP^+$ and 5,8-dihydro-MTX seems to be light driven. Based on the values estimated above, the forward equilibrium constant is close to 1 with 514.5 nm excitation, 0.5 with 568.2 nm but much less than 1 with 647.1 nm.

The reaction being light driven is further supported by the following observations. After measuring the difference spectrum with 647.1 nm excitation, the sample was measured with 514.5 nm excitation for one hour and a spectrum similar to that shown in Figure 7.1a was obtained. This sample was once again measured with 647.1 nm excitation and the difference spectrum changed only slightly from the previous 647.1 nm measurement excited with the same wavelength, with an increase of 1031 cm^{-1} band intensity from 14% to 20%. This is much less than that (60%) observed with 514.5 nm excitation, indicating that most of 5,8-dihydro-MTX and $NADP^+$ observed with 514.5 nm light reacted back to MTX and NADPH under red light.

7.2.3 UV-absorption Band for 5,8-dihydro-MTX

Figure 7.3 shows UV-Vis absorption difference spectra of NADPH and $NADP^+$ bound to DHFR•MTX. The most notable difference between the two spectra is the broad band at 422 nm for NADPH bound to DHFR•MTX, which is not shown by Poe et al. (1974). Since the 1710 cm^{-1} band assigned to 5,8-dihydro-MTX showed strong resonance Raman enhancement in the difference spectrum excited with 514.5 nm (Figure 7.1a) compared with that excited with 568.2 nm (Figure 7.1b) where the amounts of the reduced MTX for both spectra are close as indicated by the similar amount of $NADP^+$, the broad absorption band at 422 nm is very likely to be from the reduced MTX, which is a minor species in the ternary complex of DHFR•MTX•NADPH without light. The intensity of this band is about 4% of that for NADPH's absorption band at 340 nm. Assuming that 5,8-dihydro-pteridine and 1,4-dihydro-nicotinamide have similar extinction coefficients for their first absorption bands, the amount of reduced MTX would be near 4% of that of NADPH, or 4% of the total MTX amount. This value is consistent with the Raman intensity for the band at 1710 cm^{-1} (about 4% of that at 1685 cm^{-1}) in the difference spectrum excited with 647.1 nm (Figure 7.1c), where the preresonance enhancement is small.

7.3 Oxidation of 5,8-dihydro-MTX back to MTX in Solution

Figure 7.4 shows the time dependence of the peak amplitudes at 1031 cm^{-1} (marker band for $NADP^+$) and 1710 cm^{-1} (marker band for 5,8-dihydro-MTX) in the difference spectra between the ternary complex of DHFR•MTX•NADPH and the binary complex of DHFR•MTX at pH 8.1 with the excitation of 514.5 nm laser line (100 mW). The increase for 1031 cm^{-1} band is consistent with the decrease

for 1685 cm^{-1} marker band for NADPH (data not shown), indicating that NADPH was being constantly oxidized to $NADP^+$ under the experimental conditions. From the ratio of peak amplitude of the bands at 1031 cm^{-1} to that at 1329 cm^{-1}, the percentage of $NADP^+$ corresponding to the curve for 1031 cm^{-1} band in Figure 7.4 is estimated to be 50% at 2 minutes and 82% after 11 hours. Since NADPH in solution alone or bound to DHFR binary complex did not show detectable oxidation under the same experimental conditions, the oxidation of NADPH in the ternary complex of DHFR•MTX•NADPH must be accompanied by reduction of MTX. However, the amplitude of 1710 cm^{-1} band, expected to increase with that of $NADP^+$ as NADPH was oxidized and MTX was reduced, actually decreased with time (Figure 7.4a), indicating that the reduced MTX was decaying. Since the amplitude of the negative bands at 1364 cm^{-1} was decreasing with that of 1710 cm^{-1} band (data not shown), MTX is regained from the reduced one. This is further supported by the time course measurement of the difference spectrum between the ternary complex of DHFR•MTX•NADPH with three folds excess NADPH and the binary complex of DHFR•MTX, where an intensity decrease of 1688 cm^{-1} band and an increase of 1031 cm^{-1} band were observed but no change in 1710 cm^{-1} band or 1364 and 1407 cm^{-1} bands were detected, suggesting that the amount of MTX and 5,8-dihydro-MTX were constant despite that NADPH was being oxidized to $NADP^+$. Since there is one 5,8-dihydro-MTX formed for each oxidation of NADPH, the reduced MTX must somehow be oxidized back to MTX through another pathway to compensate for the amount of NADPH oxidized. This new pathway is likely to happen in aqueous solution when the reduced MTX dissociates from the enzyme active site. Here, it could quickly react with oxygen that is dissolved in solution or with certain group or groups on the enzyme (Scheme I, step b and c, b* and c*). As a result, the faster 5,8-dihydro-MTX dissociates from the enzyme, the faster it

decays, supported by the double exponential decay of the amplitude for 1710 cm^{-1} band that will be discussed below.

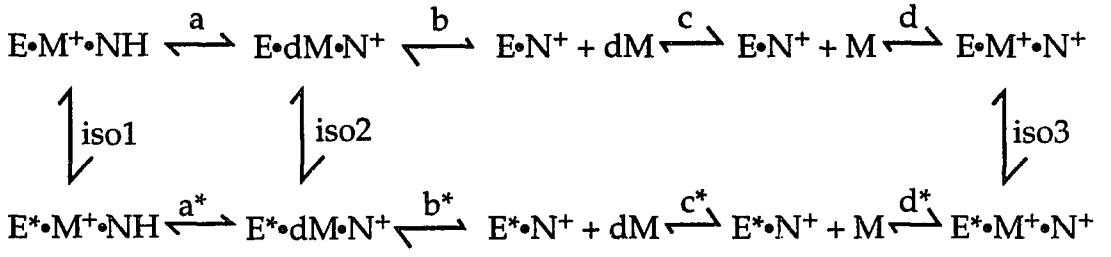

Scheme I. Reduction of MTX and the subsequent decay of 5,8-dihydro-MTX. E, *E. coli* DHFR; M, MTX; M^+, protonated MTX; dM, 5,8-dihydor-MTX; NH, NADPH; N^+, $NADP^+$. Steps iso1, iso2, and iso3: isomerization of the initial enzyme complexes E•inhibitor•coenzyme (major species in the firs 30 minutes after sample mixing) to the final tight binding complexes E*•inhibitor•coenzyme; Step a and a*: reduction of protonated MTX by NADPH to form 5,8-dihydro-MTX and $NADP^+$; Step b and b*: dissociation of 5,8-dihydro-MTX from the enzyme active site; Step c and c*: oxidation of 5,8-dihydro-MTX back to MTX in solution; Step d and d*: reassociation of MTX to the enzyme.

The solid lines in Figure 7.4 are best fit of the data to a double-exponential model

$$H(t) = \text{baseline} + A_1 e^{-k_1 t} + A_2 e^{-k_2 t} \qquad (7.1)$$

where H(t) is the peak height in the difference spectra at time t, A1 and A2 are the amplitude terms, and k1 and k2 are rate constants.

The time course for 1710 cm^{-1} band intensity (Figure 7.4a) shows a fast phase and a slow phase with rate constant of 0.057 (± 0.006) min^{-1} and 0.0087 (± 0.0003) min^{-1}, respectively. Since the intensity decrease of 1710 cm^{-1} band is due to decay of 5,8-dihydro-MTX back to MTX which happens in solution when the

reduced MTX dissociates from the enzyme, the double rates are probably caused by different dissociation rates of 5,8-dihydro-MTX from the enzyme due to isomerization of the initial enzyme ternary complex to the final tight-binding complex (Scheme I, step iso1 and iso2). Similar isomerization was observed from inhibition studies where it is shown that the initial ternary complex of DHFR•MTX•NADPH underwent conformational changes to a conformer with an inhibition constant ranging from several times to 400 times lower than the initial one depending on the source of DHFR and experimental conditions (Appleman et al., 1988a; Appleman et al., 1988b; Stone et al., 1984; Williams et al., 1979).

The increase of 1031 cm^{-1} band intensity (Figure 7.4b) also shows two phases with rate constants of 0.025 (±0.004) and 0.00079 (±0.00013) min^{-1}, respectively, which match quite well with those for the decrease of 1710 cm^{-1} band intensity, indicating that the increase of $NADP^+$ was driven by the depletion of the reduced MTX, as illustrated by Scheme I.

7.4 The MTX Reduction Pathway

All MTX bound to DHFR complexes that have been studied up to date are known to be protonated at N1 (Cocco et al., 1981; Cocco et al., 1983; Cocco et al., 1981; Ozaki et al., 1981; Saperstein et al., 1978; Subramanian & Kaufman, 1978). The carboxyl group at the active site of the enzyme forms hydrogen bonds with N1 and 2-amino group of MTX as indicated by X-ray crystal structures (Bolin et al., 1982; Cody et al., 1992). Since the carboxyl group is presumably in its anionic form, the interaction with N1 of MTX is ionic in nature.

The reduction of MTX to 5,8-dihydro-MTX involves a hydride transfer from C4 of nicotinamide ring to N5 of pteridine ring. A partial positive charge is likely to develop at N5 prior to hydride transfer, and could be achieved by

resonance of either the N1 protonated MTX or the N8 protonated MTX. Theoretical calculations on the model compound 2,4-diamino-6-hydroxymethyl-pteridine with the AM1 semiempirical method indicate that the N8 protonated pteridine is energetically less favorable by 8 kcal/mol than the N1 protonated one, but has 0.07 more positive charge on N5, which would facilitate the hydride transfer and result in the final product is 5,8-dihydro-MTX. The transformation of the N1 protonated MTX to N8 protonated MTX is likely promoted by the fixed water molecule (water 603 in Figure 7.2) that is often found in the crystal structure of MTX complexes, and is hydrogen bonded to both carboxyl oxygen and N8 of MTX (Bolin et al., 1982).

On the basis of the above conclusions, a reduction pathway of MTX to 5,8-dihydro-MTX can be constructed, shown in Figure 7.5. Bound MTX is initially protonated on N1, which is stabilized by ion-pair interaction with the charged carboxyl side chain of Asp-27 (panel a). The proton is then shuttled to N8 through the carboxyl side chain and a structure water molecule (panel b). The N8 protonated pteridine ring can develop a partial positive charge on N5 by resonance, invoking a hydride transfer from the reduced nicotinamide to N5 (panel c). The result is the formation of 5,8-dihydro-MTX and the oxidized nicotinamide (panel d).

Cheung et al. (1993) have reported that only one of the three inter-converting forms of folate (form IIb) bound in *L. casei* DHFR complexes has the pteridine ring turned over by 180° as compared to the DHFR•MTX complex while the other two (form I and IIa) have a pteridine orientation similar to that in the DHFR•MTX complex, and most surprisingly, they are also protonated at N1 and are in enolic form (mimicking 4-amino group). It would be interesting to investigate whether folate in form I and form IIa can be reduced in a similar fashion as MTX.

7.5 Clinical Implication of the Reactions Involving 5,8-dihydro-MTX

MTX has been used in the treatment of various cancers for many years, and its toxicity is generally well recognized (Jolivet et al., 1983) although it is not well understood. Several metabolites of MTX, such as 4-amino-10-methyl-pteroic acid, 7-hydroxymethotrexate and methotrexate polyglutamates have been reported (McGuire et al., 1984). They might be responsible for certain toxicity. For example, 7-hydroxymethotrexate or its polyglutamyl derivatives could play a direct role in hepatotoxicity (Fabre et al., 1984).

Our Raman spectroscopic studies have identified 5,8-dihydro-MTX in the ternary complex of *E. coli* DHFR•MTX•NADPH. Since the X-ray crystal structure of recombinant human DHFR ternary complex with NADPH and methotrexate-γ-tetrazole shows that the closest contact between cofactor and inhibitor is 3.1 Å between N5 of pteridine ring and C4 of the nicotinamide ring (Cody et al., 1992), similar to that in the crystal structure of *E. coli* DHFR•MTX•NADPH (Figure 7.2), 5,8-dihydro-MTX could also be formed in the ternary complex of human DHFR•MTX•NADPH, and thus could be a metabolite of MTX in human body. Because it is very unstable and reactive in solution, the reduced MTX could react with various substances in cells, and some of the products may be toxic to patients. This toxicity could be reduced if the patient avoids light exposure after MTX administration, for the formation of 5,8-dihydro-MTX is mostly light driven.

The molar ratio of NADPH and $NADP^+$ also affects the amount of 5,8-dihydro-MTX. By administering $NADP^+$ prior to or at the same time with MTX to the patients, the amount of 5,8-dihydro-MTX could be further reduced.

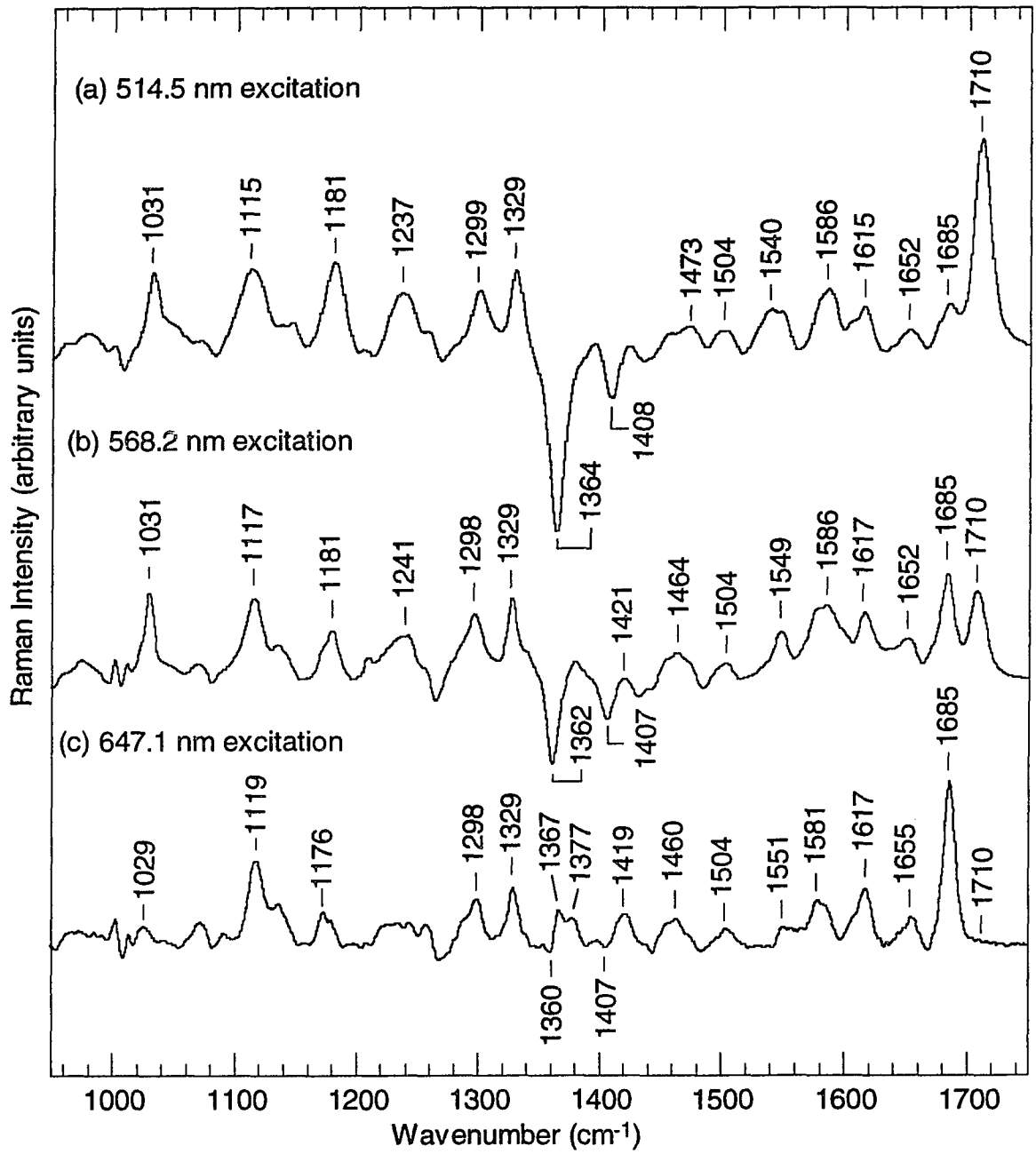

Figure 7.1 Raman difference spectra between the ternary complex of *E. coli* DHFR•MTX•NADPH (Molar ratio of 1:1:0.9) and the binary complex of DHFR•MTX (Molar ratio of 1:1) with excitation of (a) 514.5 nm; (b) 568.2 nm; and (c) 647.1 nm. Experiments were done at 4 °C in 10 mM Tris, 0.5 M KCl, pH 8. Enzyme concentrations were ~ 4 mM.

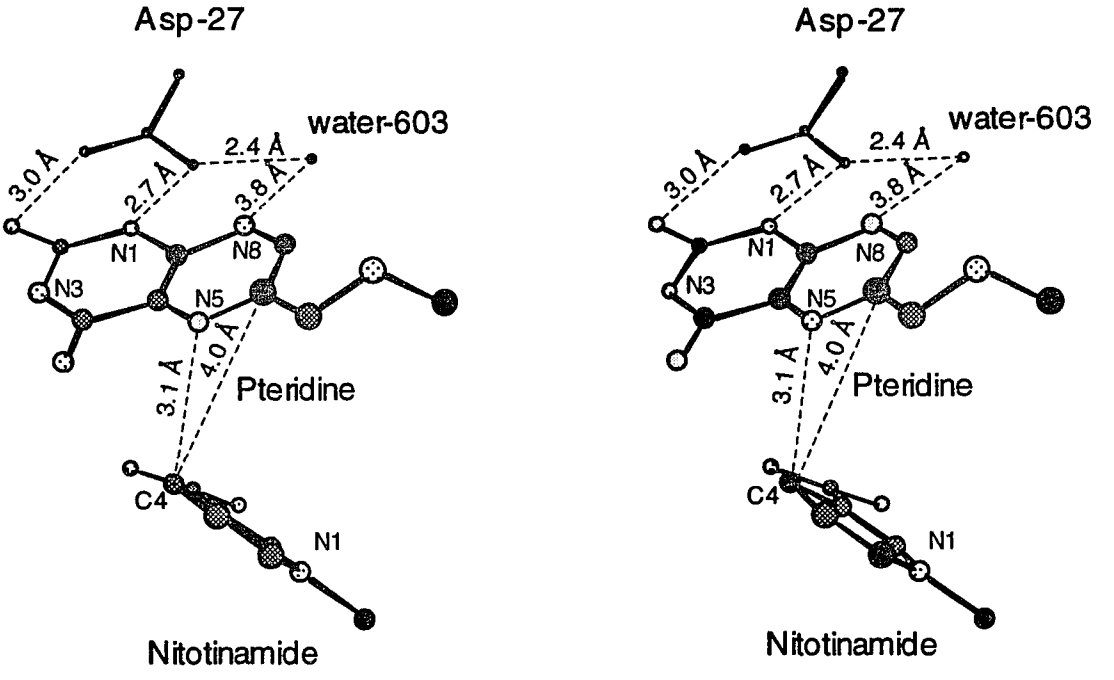

Figure 7.2 The relative positions of the pteridine and nicotinamide rings in the X-ray crystal structure of *E. coli* DHFR•MTX•NADPH ternary complex (obtained from Michael Sawaya and Joseph Kraut, unpublished results). The distances between interesting atoms are indicated.

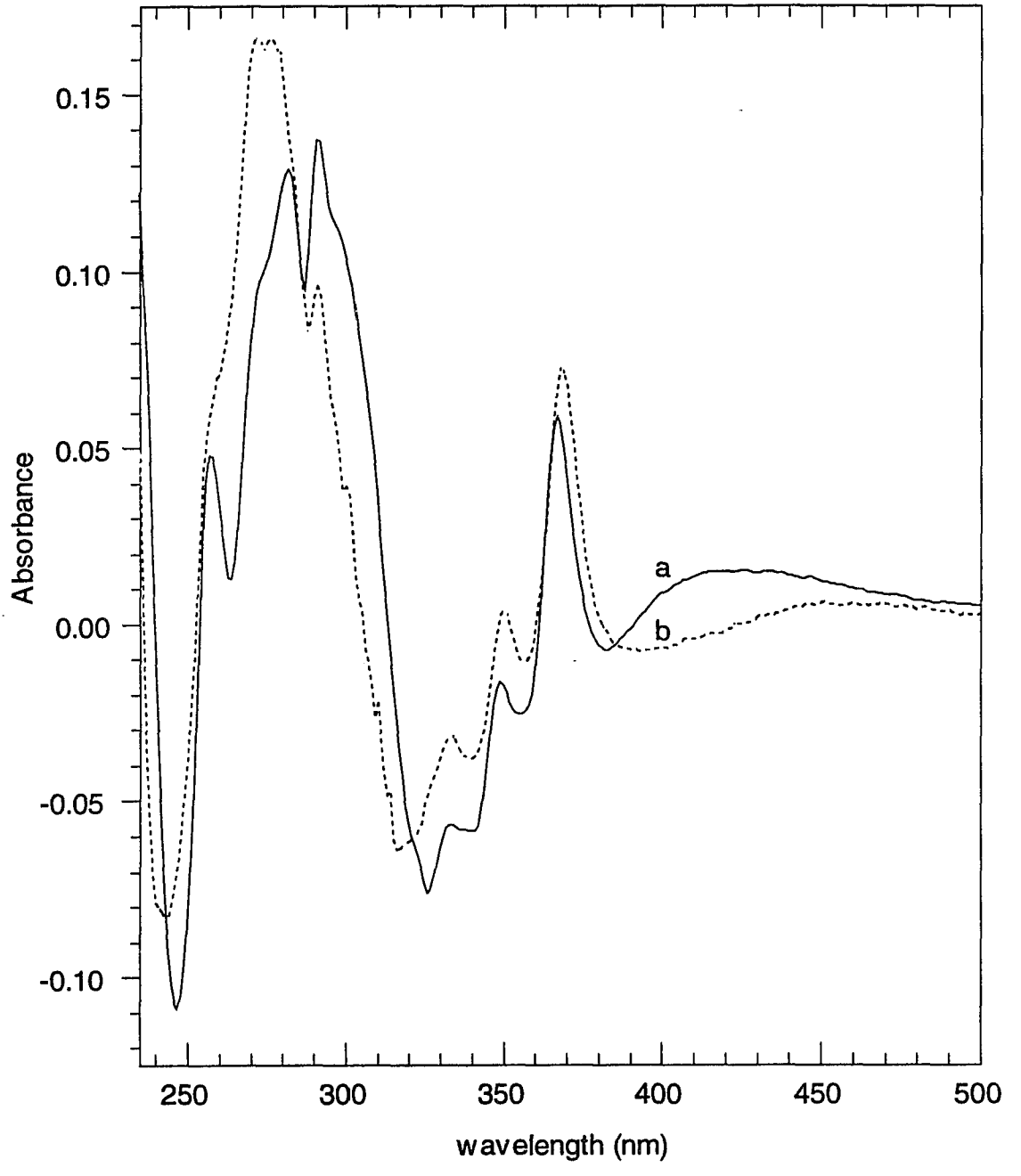

Figure 7.3 UV-Vis absorption difference spectra of (a) NADPH bound to DHFR•MTX (solid line) and (b) $NADP^+$ bound to DHFR•MTX (dashed line). The enzyme concentrations were 45 mM. The experiments were done at 10 °C in 10 mM Tris buffer containing 0.5 M KCl, pH 8.0.

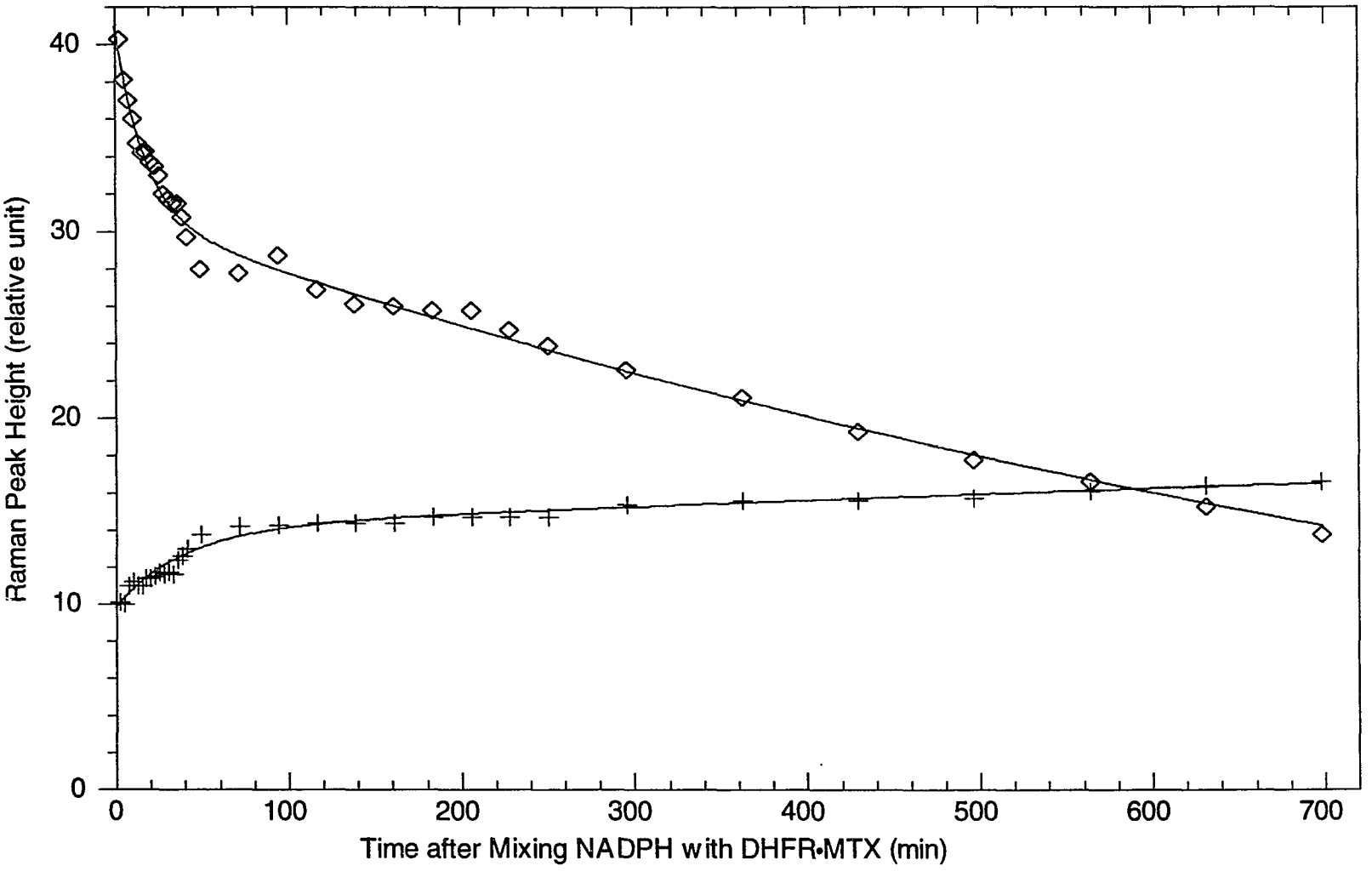

Figure 7.4 Time dependence of the peak amplitudes at (a) 1710 cm^{-1} (◊) and (b)1031 cm^{-1} (+). The solid lines are the least square best fits of the data to a double exponential model. The rate constants are 0.057 (± 0.006) and 0.0087 (± 0.0003) min^{-1} for the time course of 1710 cm^{-1} band, and 0.025 (±0.004) and 0.00079 (± 0.00013) min^{-1} for that of 1031 cm^{-1} band.

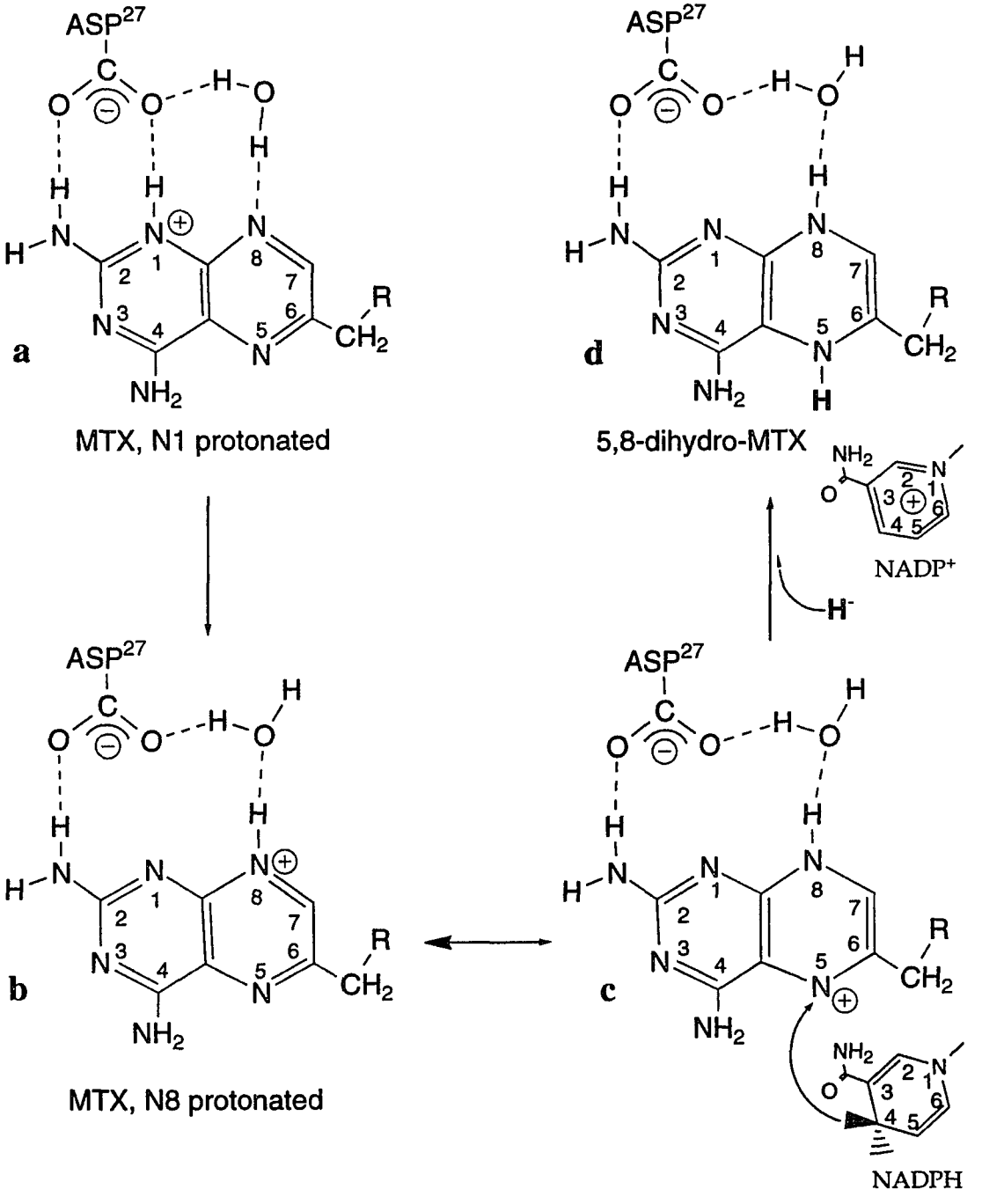

Figure 7.5 MTX reduction pathway. MTX bound to DHFR is initially protonated at N1 (a); the proton is shuttled to N8 via Asp-27 and a water molecule (b); the N8 protonated MTX can develop a resonance structure with partial positive charge on N5 (c); A hydride is transferrred from A side of 1,4-dihydronicotinamide ring of NADPH to N5 of the pteridine ring to form 5,8-dihydro-MTX (d).

Chapter 8

Difference Spectra of wild-type DHFR and mutant D27S

—— Role of Asp-27's Side Chain

8.1 Overview

The active site of all DHFRs contains an invariant carboxylic acid residue, aspartic acid in bacteria and glutamic acid in vertebrates, which is the only ionizable residue in the active site cavity. X-ray crystallographic data show that this carboxylic residue interacts directly with folates and antifolates but not with coenzymes NADPH or $NADP^+$ (Bolin et al., 1982; Bystroff et al., 1990). It has been proposed that DHFR catalyzes hydride transfer from NADPH to substrates by facilitating protonation of N-5 of dihydrofolate or N-8 of folate (Huennekens & Scrimgeour, 1964), presumably with the help of the carboxylic residue in the active site, as demonstrated by site-direct mutagenesis experiments in which Asp-27 of *E. coli* DHFR was changed to asparagine or serine (Howell et al., 1986). The activity (k_{cat}/K_m) of the Asn-27 mutant was found to be lower than that of the wild-type enzyme by a factor of 1000 at pH 7.0, while the activity-pH profiles indicated that the mutant DHFR rapidly turns over preprotonated substrate but not unprotonated substrate.

X-ray crystallographic results show that in the productive binding of substrate to DHFR, the Asp-27 side chain is hydrogen bonded to the 2-amino group and to N-3 of the substrate but is more than 5 Å away from N-5. Thus Asp-27 cannot be a direct proton donor to substrates, and an indirect role has

been proposed (Bystroff et al., 1990; Morrison & Stone, 1988; Uchimaru et al., 1989). An essential step of most versions of this theory is that bound pterin substrates are converted from the imino-keto tautomer to the 4-hydroxyl tautomer and that the 4-hydroxyl group becomes part of a proton relay system for proton donation to the substrate. Particularly, in the mechanism proposed by Bystroff et al. (1990), the carboxylic acid side chain promotes enolization of the pyrimidine ring by relaying a proton from N-3 to O-4 via a fixed water, and another temporary bound water H-bonded to both O-4 and N-5 promoted the protonation of N-5 with concomitant return of the substrate to the keto form. An interesting feature in this mechanism is that the Asp-27 side chain is protonated during the entire process, implying that the pK_a of Asp-27 is at neutral pH. However, recent NMR studies show that there is no ionization change in the active site carboxyl group in the enzyme-folate binary complex throughout the accessible pH range (Blakley et al., 1993). Furthermore, we have shown by Raman spectroscopy that the pK_a of 6.5 observed in the ternary complex of DHFR•H_2folate•$NADP^+$ is due to N5 of H_2folate (Chen et al., 1994, see also Chapter 6). Could the pK_a of Asp-27 in the apo enzyme be at neutral pH and decrease to normal value of 4 upon substrate binding? We measured the difference Raman spectra between wild type and D27S mutant in an attempt to answer this question.

8.2 Spectra of *wt* DHFR minus *mutant* D27S and of model compounds

The carboxylic acid group of aspartate's side chain has a characteristic C=O stretch band at 1705-1740 cm^{-1} when protonated, and a symmetric CO_2^- ($\frac{1}{2}^-O\cdots C\cdots O\frac{1}{2}^-$, bond-and-a-half) stretch band at 1360-1450 cm^{-1} when ionized (Daimay et al., 1991). The Raman intensity of C=O stretch at 1738 cm^{-1} for the

protonated carboxyl group of Asparagine at pH 2 is about one and half times the intensity of the C=O stretch band at 1672 cm^{-1} for the side chain amide group which is similar to protein Amide I band, while the intensity of the CO_2^- stretch at 1420 cm^{-1} at pH 10 is about 4 times. If the carboxyl group of Asp-27 has pK_a of 6.5, it would be mostly protonated at pH 5.6 while all the other carboxyl groups are mostly ionized, and the difference Raman spectrum between wild-type DHFR and mutant D27S at pH 5.6 would contain a C=O stretch band at 1705-1740 cm^{-1} with an intensity about 1% of that of protein amide I band since *E. coli* DHFR has 159 amino acid residues. If Asp-27 has a normal pK_a of 4, a CO_2^- stretch band at 1360-1450 cm^{-1} with an intensity about 2.5% of that of protein amide I band would be expected. The difference spectrometer used in our studies is capable of detecting signal changes as small as 0.1% of the protein Amide I band. Therefore, in principle, we should be able to distinguish whether the side chain of Asp-27 is protonated or ionized.

Figure 8.1a shows the difference Raman spectrum between wild-type DHFR and mutant D27S at pH 5.6, scaled to the percentage of protein Amide I band. There is no sizable band in 1705-1740 cm^{-1} region that can be attributed to C=O stretch of protonated carboxyl group, which appears at 1716 cm^{-1} in the difference spectrum of Aspartate and Serine at pH 2 (Figure 8.2a). Instead, a band at 1436 cm^{-1} has an intensity about 2% of protein Amide I band and is very likely due to the symmetric CO_2^- stretch, indicating that the side chain of Asp-27 is mostly ionized at pH 5.6, in agreement with recent NMR finding that Glu-30 carboxyl group of hDHFR is fully ionized at all accessible pH values above 5.2 (Blakley et al., 1993). This band is more than 10 cm^{-1} higher than that at 1422 cm^{-1} in the difference Raman spectrum of Aspartate and Serine at pH 7.7 (Figure 8.2b), probably due to different conformation adapted by the side chain in the enzyme active site. Since this band arises from appreciable mixing between the

C_β-C_γ stretching and the CO_2^- symmetric stretching vibrations (Spinner, 1964), a strain on the side chain of Asp-27 exerted by nearby groups could cause the increase of the vibrational frequency.

The difference Raman spectrum between wild-type DHFR and mutant D27S at higher pH is much more complicated. Figure 8.2b shows the difference spectrum at pH 8. Several bands have intensity of 3-5% of the protein Amide I band and the CO_2^- symmetric stretching band is probably masked by the strong negative band at 1421 cm^{-1}, which is due to environment change of tryptophan's indole ring as shown below.

The indole ring of tryptophan has N-H bending vibration at 1435 cm^{-1} and ring stretch mode at 1551 cm^{-1} in solution (Lord & Yu, 1970), which shift down when the solvent becomes more hydrophobic. This is shown by the derivative bands at 1420 and 1437 cm^{-1}, and 1550 and 1558 cm^{-1} in Figure 8.1d, the difference spectrum between tryptophol in water (polar solvent) and in chloroform (hydrophobic solvent) (tryptophol has the same indole ring as tryptophan):

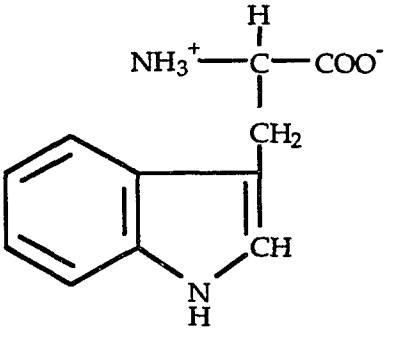

Tryptophan

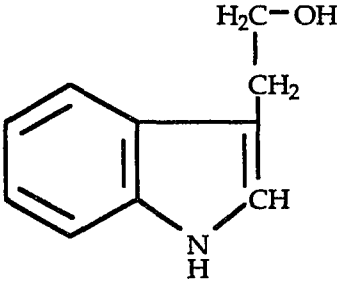

Tryptophol

Thus, the pair of derivative bands at 1421 and 1435 cm^{-1} and another pair at 1542 and 1553 cm^{-1} in Figure 8.1b, which are almost gone at pH 5.6 (Figure 8.1a),

probably result from different environments of a tryptophan residue, hydrophilic in wild-type DHFR and hydrophobic in D27S. It is reasonable to suppose that this residue is Trp-22 whose N_ε proton is hydrogen bonded to Asp-27 through a structure water in the X-ray determined crystal structure of the wild-type DHFR complexes (Bolin et al., 1982; Bystroff et al., 1990). This hydrogen bond is almost certainly missing in the mutant D27S, resulting in a somewhat more hydrophobic environments for Trp-22 at the active site.

Another derivative set of bands at 1661 and 1671 cm^{-1} in Figure 8.1a and 8.1b can be assigned to perturbation to the protein backbone carbonyl. From the relative intensity, one can estimate that there are 3 - 4 carbonyl affected by the mutation at pH 8 while only one or two at pH 5.6.

Figure 8.1c shows the difference spectrum between the wild-type DHFR and mutant D27S in 6 M urea, pH 8 where the proteins are unfolded (Touchette et al., 1986) and the perturbation of residue-27 substitution on other part of the protein is minimal. The 1398 cm^{-1} band, again about 2% of protein amide I band, is assigned to the symmmetric CO_2^- stretch. The 24 cm^{-1} down shift from that in solution, as opposed to 15 cm^{-1} up shift in the folded active site, is probably due to protein unfolding which allows the Asp-27 side chain to adopt a relaxed position, making full contact with the solvent. The 1586 cm^{-1} band is probably the remnants of a strong urea band that is incompletely subtracted.

While the protonation of Asp-27 side chain is not observed at pH above 5.6, the relative amplitude of the derivative bands at 1542 and 1553 cm^{-1} does have a pH dependent profile, shown in Figure 8.3. A pK_a of 6.3 (±0.1) was found by fitting the relative amplitude of the derivative bands to the protein band at 1450 cm^{-1} (A/A_{1450}) to the following equation using nonlinear least-squares techniques:

$$A/A_{1450} = \frac{C}{1 + K_A/[H]} \qquad (8.1)$$

where C represent the maximum amplitude and K_A is acid dissociation constants.

8.3 Role of Asp-27's side chain in DHFR Catalysis

pK_a of the active site carboxyl group. It has been widely assumed that protonation of only one group on DHFR is responsible for the pH-dependence of kinetic parameters and that this group is the active site acidic group (Fierke et al., 1987; Morrison & Stone, 1988; Stone & Morrison, 1983). Our direct measurement on the pK_a of Asp-27 does not provide evidence to support this view.

The Aspartate side chain normally has a pK_a in the range of 3.7 to 4.7. In order to assign the calculated pK_a value ranging from 5.6 (Murphy & Benkovic, 1989) to 8.4 (Adams et al., 1989), it must be assumed that the micro environment of this side chain is very different from that of bulk solvent, presumably in a very hydrophobic environment. However, a close examination of recent X-ray crystal structures reveals that the active site of DHFR is quite polar and a number of water molecules are present and hydrogen bonded to the carboxyl group and to other water molecules that form a hydrogen bond network extending to external solvent (Bystroff, 1990; McTigue, 1992). Moreover, in the absent of ligands, the active site conformation changes only slightly from that of the binary or ternary complexes and is pretty much filled with water molecules (Bystroff, 1991), making the carboxyl group of Asp-27 having an highly elevated pK_a unreasonable. Stone and Morrison (1983) found a pK_a of 6.65 from the pH-dependence of the apparent dissociation constants for methotrexate binding the

E. coli DHFR. In an attempt to find the identity of the ionizable group or groups responsible for this pK_a, they tried the same experiment in the presence of 2-methoxylethanol (25%, v/v) and obtained a pK_a of 5.81. Should the ionizable group be the side chain of Asp-27, the pK_a would increase in the presence of organic solvent (Tipton & Dixon, 1979). Therefore, the carboxyl group at the active site is more likely to be fully ionized at all accessible pH values. This being so, then what is responsible for the pK_a around 6.3 observed by various methods?

Much of the relevant published data does not exclude the possibility that ionization of more than one group either on the protein or on the substrate is involved in the pH dependence effect of various kinetic parameters. From our Raman spectroscopic results and other published data, there are at least two groups that could be responsible for the observed pK_a. One is N5 of H_2folate, which has a pK_a of 6.5 in the ternary complex of DHFR•$NADP^+$•H_2folate (Chen et al., 1994) and it is also very likely to be responsible for the similar pK_a determined from the rate of hydride transfer from NADPH to H_2folate (Fierke et al., 1987). Another is a group or groups on the enzyme, which is responsible for the pK_a of 6.3 obtained here for the apo enzyme and the pK_a of 6.65 obtained from the pH-dependence of the apparent dissociation constants for methotrexate binding the E. coli DHFR (Stone & Morrison, 1983). The group or groups exert their effects to the enzyme active site probably by triggering a conformational change that has subtle influence on the active site. This pH-dependent conformational change might disrupt the hydrogen bond network in the active site near Trp-22 at low pH, making this residue's micro environment similar to that in the mutant D27S and thus the derivative bands due to Trp side chain in the Raman difference spectra of the wt and mutant enzymes decrease with decreasing pH (Figure 8.1a, 8.1b and 8.3). This conformational change could be caused by

certain ionizable group or groups which have long range effects on the enzyme's active site, possibly a histidine residue. For example, a mutation more than 20 Å away from the active site raises the apparent pK_a from 6.5 in the wild type to 7.5 and 8.4 in the mutant of H45Q and R44L, respectively, while a triple mutant (H45R, W47Y, and I50F) has no effect on the pK_a of its binary complex with NADPH (6.4), but raises the pK_a of the ternary complex with NADPH and H_2folate (N5) to 7.3 (Adams et al., 1989).

Function of Asp-27's side chain in catalysis. During reduction of H_2folate to H_4folate, a hydride from C4 of reduced nicotinamide ring of NADPH is transferred to C6 and a proton is added to N5. Where does the proton come from? Several proposed mechanisms implying that the proton comes from the protonated carboxyl group of Asp-27 through O-4 and several structural waters (Bystroff et al., 1990; Morrison & Stone, 1988; Uchimaru et al., 1989) are probably untrue in view that the side chain of Asp-27 is ionized in all accessible pH. However, this carboxyl group must somehow help this protonation as revealed by mutagenesis (Howell et al., 1986). It probably does this by maintaining a hydrogen bond network in the active site extending to the bulk solvent, which keeps the active site open in the absence of ligands and assists the proton relay to N5 of H_2folate in the proper ternary complex such as the productive ternary complex of DHFR•H_2folate•NADPH and dead-end DHFR•H_2folate•$NADP^+$.

Another important role played by the ionized carboxyl side chain is to stabilize the protonated substrate, supported by the increase of the pK_a of H_2folate's N-5 to 6.5 in the presence of $NADP^+$ and wild-type DHFR but not the mutant D27S. However, it probably does not contribute to transition state stabilization. In fact, the Asp-27 side chain, in the ionized state, might have negative effect on the formation of a transition state once the substrate is already protonated as shown by kinetic studies on the mutants D27N and D27S. Here, it

was found that if the mutant enzymes were presented with totally protonated H_2folate, their activity would actually somewhat exceed that of the wild-type enzyme toward unprotonated dihydrofolate (Howell et al., 1986). The same study also shows that the k_{cat} of D27S almost reaches that of wild-type enzyme at pH 5. The reason for this phenomenon is that the negative charge on carboxyl group tends to delocalize the positive charge on pyrazine moiety toward the pyrimidine moiety, resulting in a decrease of the carbonium character of C6 and thus a decrease in the rate of hydride transfer. At physiological pH, maintaining a sufficient amount of protonated H_2folate is far more important in contributing to k_{cat} than the somewhat decrease of hydride transfer rate, so k_{cat} for the wild-type enzyme is several orders higher than that of either D27N or D27S at neutral pH.

Aside from the functions described above, the carboxyl group of Asp-27 may help precisely position the substrate relative to coenzyme for maximal hydride transfer rate, as shown from the studies of a mutant with Asp replaced by Glu, where despite the crystal structure of this mutant D27E·MTX complex is virtually identical to that of wt DHFR·MTX, the hydride transfer rate constant for D27E is 1.7 times lower at pH 5.0 and 3.4 times lower at pH 7.3 (David et al., 1992).

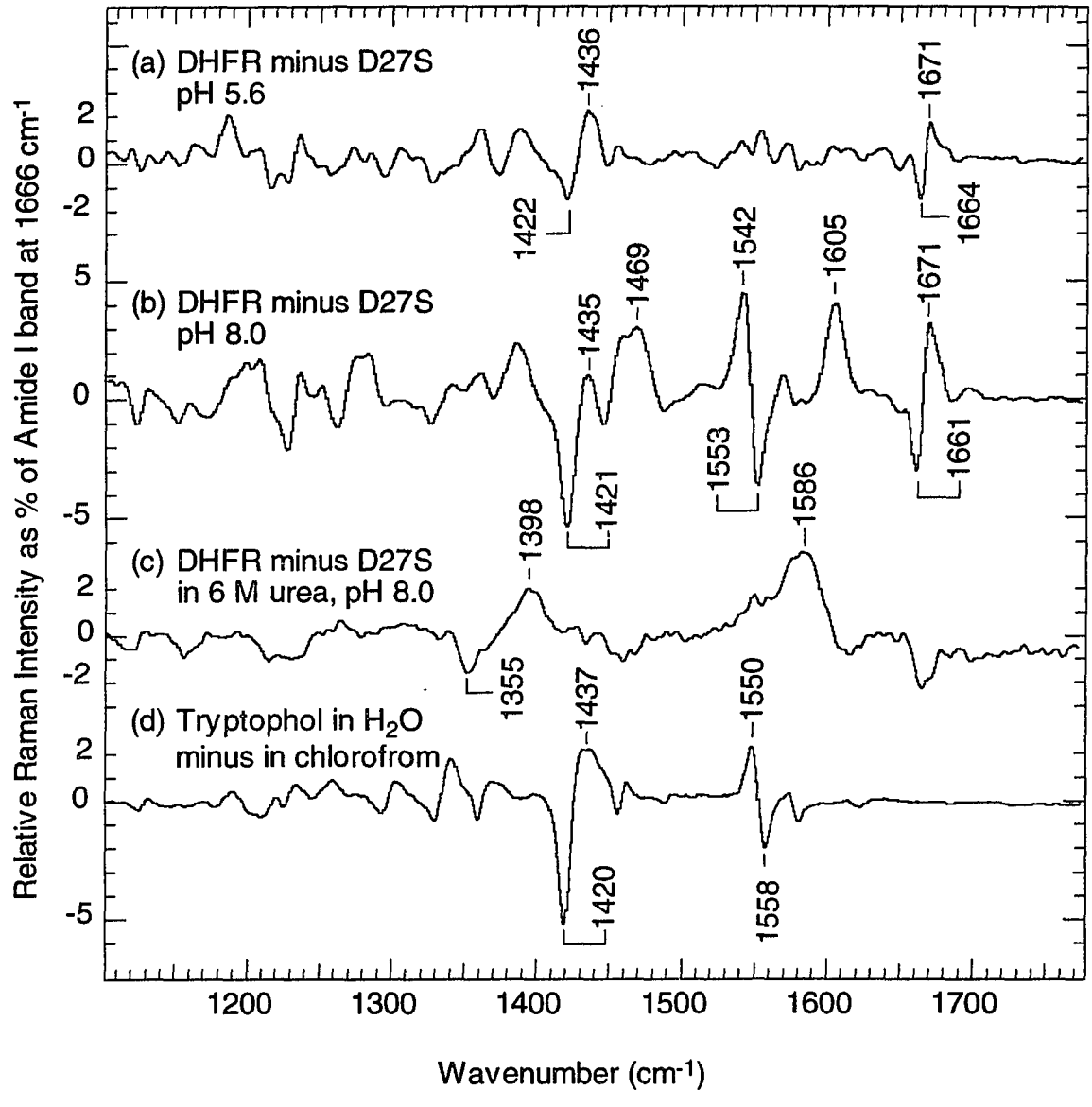

Figure 8.1 Raman difference spectra between *wt* DHFR and *mutant* D27S in (a) 25 mM Mes and 0.3 M KCl, pH 5.6; (b) 10 mM Tris and 0.5 M KCl, pH 8.0; (c) 10 mM Tris and 6 M urea, pH 8.0. Protein concentrations were 3-4 mM. (d) Raman spectrum of tryptophol in H_2O minus that in chloroform (solvent spectra were subtracted out).

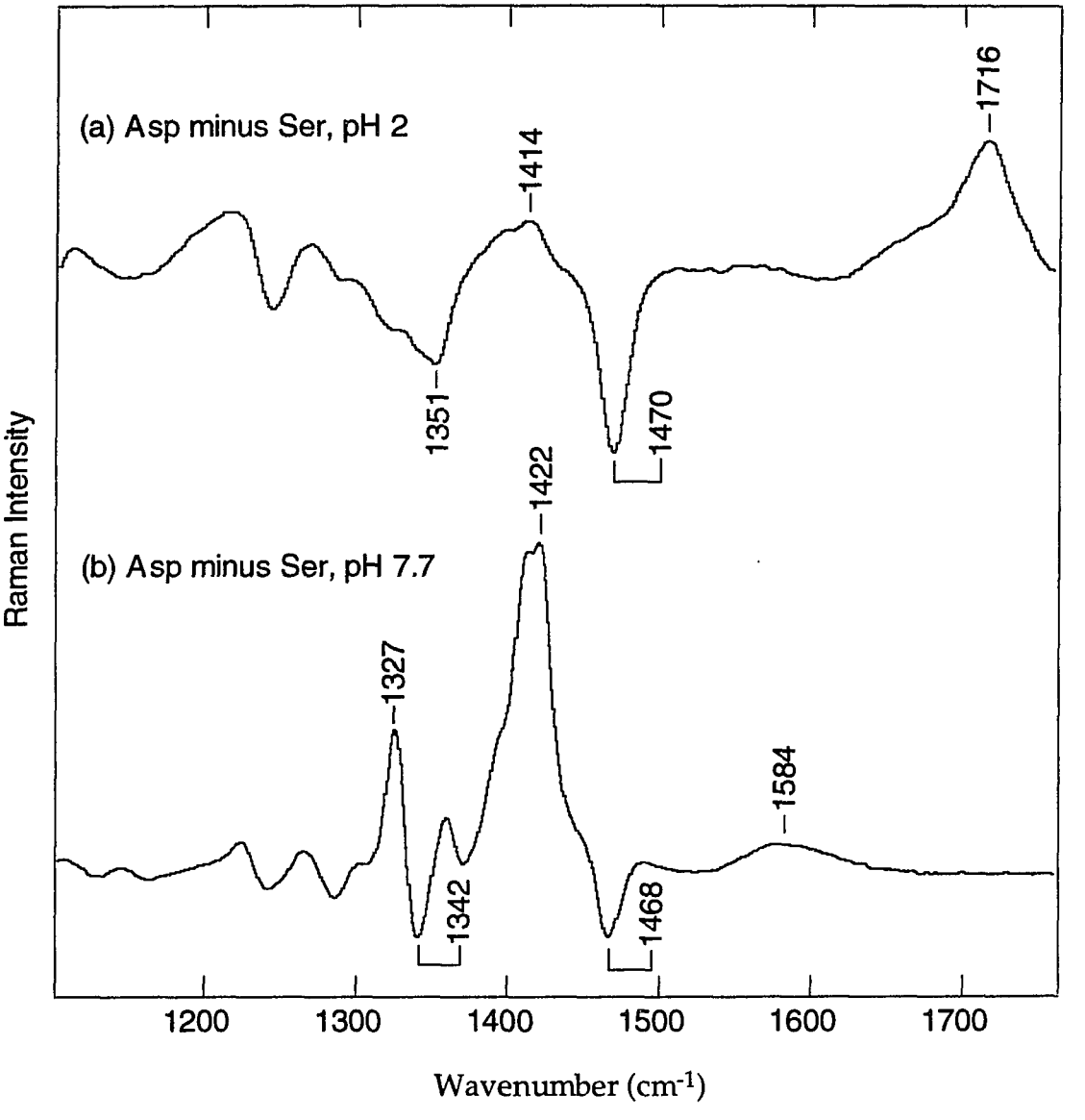

Figure 8.2 Raman spectra of Aspartate minus Serine (about 100 mM) at (a) pH 2.0; (b) pH 7.7.

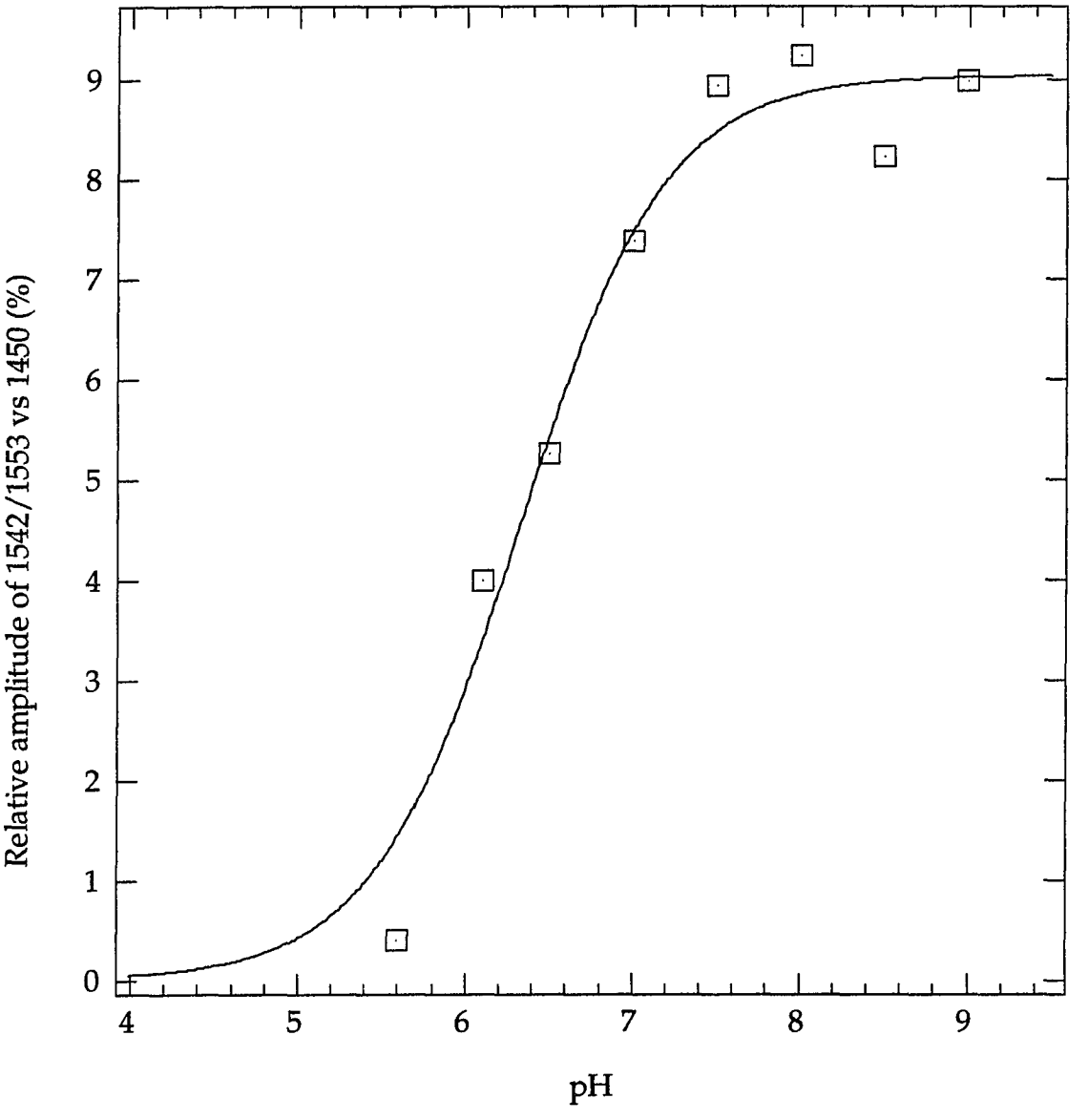

Figure 8.3 The pH dependence of the relative amplitude of the derivative bands at 1542 and 1553 cm^{-1} (to protein band at 1450 cm^{-1}). The solid line represents the best fit of data points to a titration curve with amplitude and pK_a as the only parameters. The value found for pK_a was 6.3 (±0.1).

Chapter 9

A Study of C4-D Stretch of NADPH bound to DHFR

— Implication for Nicotinamide Ring Activation

9.1 Pyridine Nucleotide Cofactors in Enzyme Catalysis

Dihydrofolate reductase is one of several hundred known pyridine nucleotide-dependent oxidoreductases that catalyze the transfer of a hydride ion to or from the C4 of nicotinamide ring. For all these enzymes, the nicotinamide binds in a cleft in the interior of the proteins, with one side of the ring interacting with residues of the coenzyme binding domain while the other side facing the active side and interacting with substrates or inhibitors (Westheimer, 1987). Thus, the oxidation-reduction reactions are stereospecific with respect to substrate as well as coenzyme. Based on the side of the hydrogen from the nicotinamide ring being transferred (see the structural formula below), the dehydrogenases are divided into two classes:

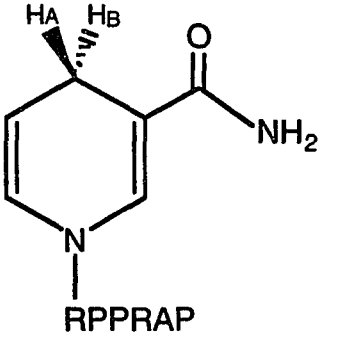

Nicotinamide ring

those transferring the *pro*-R (A-side) hydrogen are called A-specific enzymes, and those transferring the *pro*-S (B-side) hydrogen are B-specific enzymes (You et al., 1978).

DHFR is an A-specific enzyme and catalyzes the transfer of the A-side hydrogen of NADPH to *si* face of either dihydropteridine ring at C6 or pteridine ring at C7 (see review by Kraut & Matthews, 1987). The activation of the pterin ring of DHF is quite well understood, and generally involves protonation of N5 preceding hydride transfer to C6 (Bystroff et al., 1990; Gready, 1985b; Morrison & Stone, 1988; Uchimaru et al., 1989; see also Chapter 6). In contrast, the activation of NADPH by DHFR is less understood. An attempt to understand this issue has been made by Filman et al. (1982) based on the high resolution crystal structure of the ternary complex of *L. casei* DHFR with NADPH and MTX. They have proposed that the three protein oxygen atoms of THR 45, ILE 13 and ALA 97 that are close to C2, C4 and C6 and in the plane of the nicotinamide ring form C-H···O hydrogen bonds and stabilize the nicotinamide ring intermediates during catalysis. A similar geometry occurs in the crystal structure of *E. coli* DHFR ternary complex with $NADP^+$ and folate (Bystroff et al., 1990). However, recent studies with $CHARM_m$ molecular dynamics simulations do not find support for this view (Almarsson & Bruice, 1993).

The activation of NAD(P)H should have some effects on the C4–H bond of the nicotinamide ring, especially the reacting side, which serves as an internal coordinate for hydride transfer. If NAD(P)H is destabilized in terms of the redox system, the C4–H bond should become more hydride-like (more easily transferred), and if it is stabilized, the bond should become more acidic (less easily transferred as a hydride). Thus, monitoring the C4–H bond could provide some information on the nature of the interaction of the nicotinamide ring with the enzyme and substrates or inhibitors. The C4–H bond of NAD(P)H can be

studied by vibrational spectroscopy with deuteration at either the *pro*-R or *pro*-S C4 position, which lowers the frequency of the now C4–D stretch to near 2100 cm^{-1}. The C4–D stretch frequency of $NAD(P)^+$ is near 2300 cm^{-1}. These bands are in a vibrationally silent spectral region apart from some low-intensity water overtone bands, so they are easily identified. Moreover, deuteration lowers the frequency of the C4–D stretch so that the mode is substantially uncoupled from all other vibrational modes and is, therefore, quite localized to the C4–D group. This considerably simplifies analysis of the results. The method has been applied to the studies of NADH bound to lactate and malate dehydrogenases and some normal mode calculations have also been carried out to interpret the data (Deng et al., 1992; Deng et al., 1992). We have used similar approach to the studies of NADPH and $NADP^+$ bound to *E. coli* DHFR binary complex and ternary complex with MTX. The results are interpreted with some modeling studies based on the highly refined X-ray crystal structures. The implication to the activation of nicotinamide ring is discussed.

9.2 Raman Spectra of Deuterium-labeled NADPH and $NADP^+$

Figure 9.1 shows the Raman difference spectra in the 1900 - 2400 cm^{-1} region between the *pro*-R deuterated NADPH ($NADPD_A$) and NADPH or the *pro*-S deuterated NADPH ($NADPD_B$) and NADPH in the aqueous environment (panel a and b), bound to E. coli DHFR binary complex (panel c and d), and bound to DHFR ternary complex with MTX (panel e and f).

The 2116 cm^{-1} band for $NADPD_A$ and the 2119 cm^{-1} band for $NADPD_B$ in solution are assigned to the C4–D stretch of the dihydronicotinamide ring (Deng et al., 1992). The broadness of the bands are indicative of multiple conformations adopted by the ring. The slight difference between the two stretch frequencies

are probably caused by the stacking of the nicotinamide ring (B-side) with the adenine ring in aqueous solution (Oppenheimer, 1987). It was suggested that the slightly higher frequency for the C4–D stretch of $NADPD_B$ results from the nicotinamide ring puckering toward A-side (Zheng, 1991). We will show that this is not necessary the reason, since the close contact of the B-side hydrogen with adenine ring could also cause the upshift.

The C4–D stretch frequency changes upon binding to DHFR (Figure 9.1c and d) are similar to those upon binding to lactate dehydrogenase (LDH) and malate dehydrogenase (MDH) with essentially no change for A-side and substantial upshift for B-side (23 cm^{-1} in LDH, 30 cm^{-1} in MDH and 44 cm^{-1} in DHFR). Deng et al. (1992) have attributed these changes in LDH and MDH mostly as the result of two conformational changes of the nicotinamide ring that occur when NAD(P)H forms a binary complex with the enzyme: the rotation of the amide group from a solution syn conformation (with carbonyl oxygen close to C2) to a bound anti conformation (with carbonyl oxygen close to C4) in situ and the adoption of a "half-boat" of the dihydronicotinamide ring of NADH when bound to the enzyme from an essentially planar solution structure. The rotation of the amide group is well supported by the X-ray crystal structures of enzyme complexes with NAD(P)(H) (Almarsson & Bruice, 1993, see also Table 9.1), but the ring puckering to form boat or half-boat conformation, proposed for the transition-state structure (Wu & Houk, 1987), still lacks sound experimental foundation (Glasfeld et al., 1988). Some of the deformations of the nicotinamide rings from X-ray structures of enzyme bound NAD(P)H as registered in the Brookhaven database (release of 1992, Brookhaven National Laboratory) are shown in Table 9.1, where α_C and α_N are the bending angles of C4 and N1 relative to the average plane of C2, C3, C5 and C6 of the nicotinamide ring, and positive values represent the bending of C4 and N1 toward the *re*-face of ring (A-

side). As can be seen from this table, there is no apparent tendency for the nicotinamide ring to pucker appreciably toward A-side.

Table 9.1 Some structural Parameters for NAD(P) Cofactors in Protein Data Bank Entries of Dehydrogenases Enzymes

PDB code (cofactors), resolution (Å)	ref	χ_{am} (degree)	α_C (degree)	α_N (degree)	Atoms near C4 along C4-H_B bond except stated otherwise
?dfr (NADPH),2.5	a	161.3	0.0	0.0	2.96 Å to OH of Tyr100; 3.12 Å to N5 of MTX (along C4-H_A)
8dfr (NADPH),1.7	b	-179.8	-2.5	8.1	3.38 Å to OH of Tyr121
3dfr (NADPH),1.7	c	-175.6	1.0	3.9	4.71 Å to $C_{\eta 2}$ of Phe103; 3.25 Å to carbonyl O of Ala97 (close to the ring plane)
1ldm (NADH),2.1	d	173.6	-7.3	4.1	3.81 Å to $C_{\gamma 2}$ of Ile249
3ldh (NADH),3.0	e	-177.3	6.1	-5.2	3.20 Å to C_η of Lys250
4mdh (NAD^+),2.5	f	161.7	0.0	-1.1	3.68 Å to C_β of Ala245

[a]*E. coli* DHFR ternary complex with MTX: Mark Sawaya and Joseph Kraut, unpublished results; [b]Chicken liver DHFR binary complex: Davies et al., 1989; [c]*L. casei* DHFR ternary complex with MTX: Filman et al., 1982; [d]Dogfish muscle LDH ternary complex with oxamate: Abad-Zapatero et al., 1987 (revised 1990); [e]Dogfish muscle LDH ternary complex with pyruvate: White et al., 1976 (revised 1991); [f]Porcine heart MDH: Birktoft et al., 1989 (revised 1992).

An alternative explanation for the C4–D stretch frequency of the B-side of the nicotinamide ring to shift up is that the upshift is a result of the repulsion between the electron clouds of the B-side deuteron and the atoms having closer than van der Waals contact with C4 (Table 9.1) which is caused by the strong hydrogen bonds between the amide group and protein residues (see Chapter 5). For example, the distance between the hydroxyl oxygen of Tyr100 and C4 of nicotinamide ring is only 2.9 Å while normal van der Waals contact is 3.4 Å.

Some evidence supporting this view from vibrational calculations and model compound studies will be present in next section.

When the nicotinamide ring is bound to the DHFR ternary complex with MTX, the C4–D stretch band of the nicotinamide ring split into two distinct bands (Figure 9.1e and 9.1f), with one band shifting up 4 - 5 cm^{-1} and the other shifting up 37 - 46 cm^{-1}, and the relative intensities of the two bands are complementary for the A- and B-side, suggesting that the nicotinamide ring adopts two conformations in the ternary complex with somewhat different environments. One conformation has C4-D stretch frequencies at 2119 cm^{-1} for $NADPD_A$ and 2155 cm^{-1} for $NADPD_B$, probably with C4 close to the hydroxyl oxygen of Tyr-100 similar to that in the binary complex (resulting higher C-D stretch for B-side); the other has C4-D stretch frequencies at 2163 cm^{-1} for $NADPD_A$ and 2123 cm^{-1} for $NADPD_B$, probably with C4 less close to the hydroxyl oxygen of Tyr-100 but close to N5 of MTX (resulting higher C-D stretch frequency for A-side). It is a little puzzling that only one conformation was observed in NMR studies with isotopic labeling on MTX (Cheung et al., 1992; Falzone et al., 1991; Huang et al., 1991). One possible conjecture is that the two conformations that we detected by Raman spectroscopy are close and interconverting too rapidly for NMR to distinguish. Indeed, as we will see from the results of model compound simulation in the next section (Figure 9.3), a change of 0.1 to 0.2 Å in the nicotinamide ring position could produce the observed C4–D stretch frequency shift of 44 cm^{-1} when the distance of the nearby atom to C4 is already around 3.1 Å observed in X-ray crystal structure (Mark Sawaya and Joseph Kraut, unpublished results).

We also measured the C4–D stretch of [4-D]$NADP^+$ bound to DHFR, shown in Figure 9.2. The C4–D stretch band at 2300 cm^{-1} is essentially the same in the binary complex (Figure 9.2b) as in solution (Figure 9.2a), indicating that the

nicotinamide ring is probably not bound or not tightly bound, in agreement with the crystallographic and NMR findings that this ring is loosely bound in the DHFR binary complexes (Bystroff et al., 1990; Cayley et al., 1980). This band shifts up 19 cm^{-1} when $NADP^+$ bound in the DHFR ternary complex with MTX, and also becomes sharper than that in the binary complex, indicating that the nicotinamide ring is tightly bound in the ternary complex, with accessible conformations significantly reduced. Once again, the upshift is probably caused by the close contact of C4 of the nicotinamide ring with protein residues or the inhibitors as discussed below.

9.3 Model Studies and Vibrational Analysis

N-Methyl-1,4-dihydronicotinamide is used as the model compound for the normal mode analysis of the C4–D stretching vibrations of either A- or B-side deuterated NADPH. The AM1 method, implemented in the QCPE program AMPAC2.1 (Dewar et al., 1985), was used to optimize the geometry of the molecules and then to calculate their vibrational normal modes.

A quite complete normal mode analysis assessing the effects of various factors on the C4–D stretch frequency was previously reported (Deng et al., 1992). These factors include the interactions between the nicotinamide ring nitrogen and the ribose oxygen, the torsional angle of the amide arm, puckering of the ring, and the external charge or dipole modeled by a formaldehyde. It has been suggested that the rotation of the amide group to an anti position with respect to C2 and the ring puckering toward A-side of C4 are mostly responsible for the frequency upshifts of C4–D stretches of $NADD_B$ upon binding to LDH and MDH, and the dipole interactions contribute the additional upshift of C4–D stretch of $NADPD_B$ upon binding *E. coli* DHFR.

We have extended the model compound study by examining the effects to C4-D stretch frequency by nearby atoms that are closer to C4 than normal van der Waals distance, which are often found in X-ray crystal structures (see Table 9.1). These interactions have been modeled by moving the carbon of ethane or formaldehyde, or the oxygen of formaldehyde or 4-methyl phenol along one of the C4–H bond (the change is smaller if not along C4-H bond). The nicotinamide ring was fixed at a planar position and the ethane, formaldehyde and 4-methyl phenol were fixed in the orientations as shown in the inset in Figure 9.3. The calculated C–D stretch frequencies as a function of the distance between the C4 and the appropriate atoms are shown in Figure 9.3. The perturbation on the C4-D stretch frequency of the other side is less than 3 cm^{-1} when the approaching atoms are not closer to 3 Å to C4 (data not shown). Initially, they all shift down as the distance decreases due to van der Waals attraction between the deuteron and the approaching atoms. When the atoms are getting closer to deuteron than the van der Waals contact distance (roughly 4.2 Å from C4 to ethane carbon, 3.7Å to formaldehyde carbon with C=O bond perpendicular to C4–D bond, and 3.7 Å to the oxygen of formaldehyde or 4-methyl phenol), electron clouds between the deuteron and the approaching atoms begin overlap and electron-electron repulsion becomes dominant. This van der Waals repulsion leads to the C4–D bond length to decrease (Figure 9.4) and the frequency to shift up. The corresponding change in the heat of formation is small. It is less than 5 kcal/mol when the distance of C4 to either the carbon or the oxygen of formaldehyde is less than 3 Å (Figure 9.4).

Compared to other factors, such as ring puckering, the van der Waals repulsion between the hydrogen on C4 and the nearby atoms have much stronger effects on the C4-D stretch frequency. It may be responsible for most of the upshift observed C4-D of NAD(P)D bound enzymes. For example, the

observed distance between C4 of nicotinamide ring and the oxygen of Tyr100 side chain in the X-ray crystal structures of *E. coli* DHFR complexes is 2.9 - 3.0 Å, and roughly along C4-H_B bond (Bystroff et al., 1990;Mark Sawaya and Joseph Kraut, unpublished results). This short contact would cause more than 100 cm^{-1} upshift for the B-side C4–D stretch from the calculation (Figure 9.3). However, only 44 cm^{-1} shift is observed for $NADPD_B$ bound in DHFR binary complex and 36 cm^{-1} in the ternary complex with MTX (Figure 9.1). This discrepancy may result from an overestimation of the interactions by the AM1 method, or a difference in the distance between the enzyme in crystalline state and in situ, or some inaccuracy in the X-ray structural determination.

A calculation for C4–D stretch frequencies of nicotinamide ring in a complex with N1-protonated 2,4-diamino-pteridine and ionized carboxyl group in a fixed geometry taken from the X-ray crystal structure of *E. coli* DHFR ternary complex with MTX and NADPH (Figure 7.2) has also been performed. The C4-D stretch frequency of $NADPD_A$ shifts up 67 cm^{-1}, which is comparable with the observed 46 cm^{-1} upshift. The 2163 cm^{-1} band of $NADPD_B$ in the binary complex shifts down to 2155 cm^{-1} in the ternary complex, and this may be due to a protein conformation change which slightly increases the distance between C4 of the nicotinamide ring and the oxygen of the Tyr100 side chain.

Some normal mode calculations were also performed for the oxidized nicotinamide ring. When the formaldehyde oxygen approaching C4 along C4-D bond, the C–D stretch frequency initially shifts down, by 40 cm^{-1} at 3.4 Å, then increases as the two get closer (Figure 9.5). The frequency shifts upto 30 cm^{-1} at 3.1 Å, 78 cm^{-1} at 3.0 Å. Thus the 19 cm^{-1} upshift of the C4–D stretch frequency of [4-D]$NADP^+$ bound in the DHFR ternary complex with MTX is also likely caused by close contact with protein residues or the inhibitor.

9.4 Implication for the nicotinamide ring activation by DHFR

The most striking features of enzyme catalyzed reactions, compared with the uncatalyzed or the non-enzyme catalyzed chemical reactions, are the specificity and the rate acceleration, which are generally achieved by non-covalent interactions of the enzyme active site with the substrate and/or coenzyme (Palmer, 1985). The currently favored mechanism of catalysis is substrate transition-state stabilization or strain ground state caused by the interactions with the enzyme. X-ray determined crystal structures of the DHFR ternary complexes with coenzyme and substrate or inhibitors clearly show the existence of such a strain (Bystroff et al., 1990; Cody et al., 1992; Filman et al., 1982; McTigue et al., 1992; McTigue et al., 1993). On the basis of the crystallographically observed *E. coli* DHFR•folate•$NADP^+$ ternary complex, Bystroff et al. (1990) built a model transition-state ternary complex for DHFR•DHF•NADPH, in which the reacting atoms, C4 of nicotinamide group and C6 of pteridine group, were brought from the observed distance of 3.2 Å in the crystal structure to a theoretically predicted distance of 2.6Å for hydride transfer (Wu & Houk, 1987) with a change in the geometry at C6 of the dihydropteridine ring from planar-trigonal in ground state to pyramidal and slight puckering C4 of nicotinamide ring toward the substrate. This arrangement relieves many of the unfavorable short contacts among DHFR, DHF and NADPH, in agreement with the transition-state theory. In modeling this transition state complex, Bystroff et al. found that an enzyme conformation approaching that seen in the MTX binary complex fits the transition state quite well, suggesting that MTX might in some ways resemble a transition-state analog. This is supported by our observations that MTX is slowly reduced by NADPH in *E. coli* DHFR ternary complex, and the reaction can be driven forward by excitation of light (Chapter 7). The substrate

conformation of the ternary complex as observed by X-ray crystallography or our C–D stretch measurement is probably strained in such a way as to approaching the transition-state.

Two C4–D stretch bands are observed for either $NADPD_A$ or $NADPD_B$ bound in the ternary complex of DHFR with MTX. Since the effects of close contacts of C4 with nearby atoms on C4–D stretch frequency are much greater than that of nicotinamide ring puckering, we suggest that the higher frequency bands are caused by strained close contact between C4 and nearby atoms along either A-side or B-side C4-D bond. The observation of two C4–D stretch bands suggests that the nicotinamide ring adopts two conformations in the ternary complex with slight changes in the contact distance between C4 of the ring and its nearby atoms. These two conformations may result from protein conformational changes involving movements of active site residues and inhibitors or by some slight change in the nicotinamide including ring puckering and ring rotation. The conformation with higher C4–D stretch frequency band of $NADPD_A$ corresponds to a conformation with closer contact between C4 the nicotinamide ring and N5 of MTX, which increases the strain in the reactants and facilitates the hydride transfer. The existence of two slightly different conformations may have their advantage: as the two conformations interconverts with C4 of the nicotinamide ring moving against the pteridine ring, there is more chance that the two rings reach the hydride transfer position than the single strained conformation.

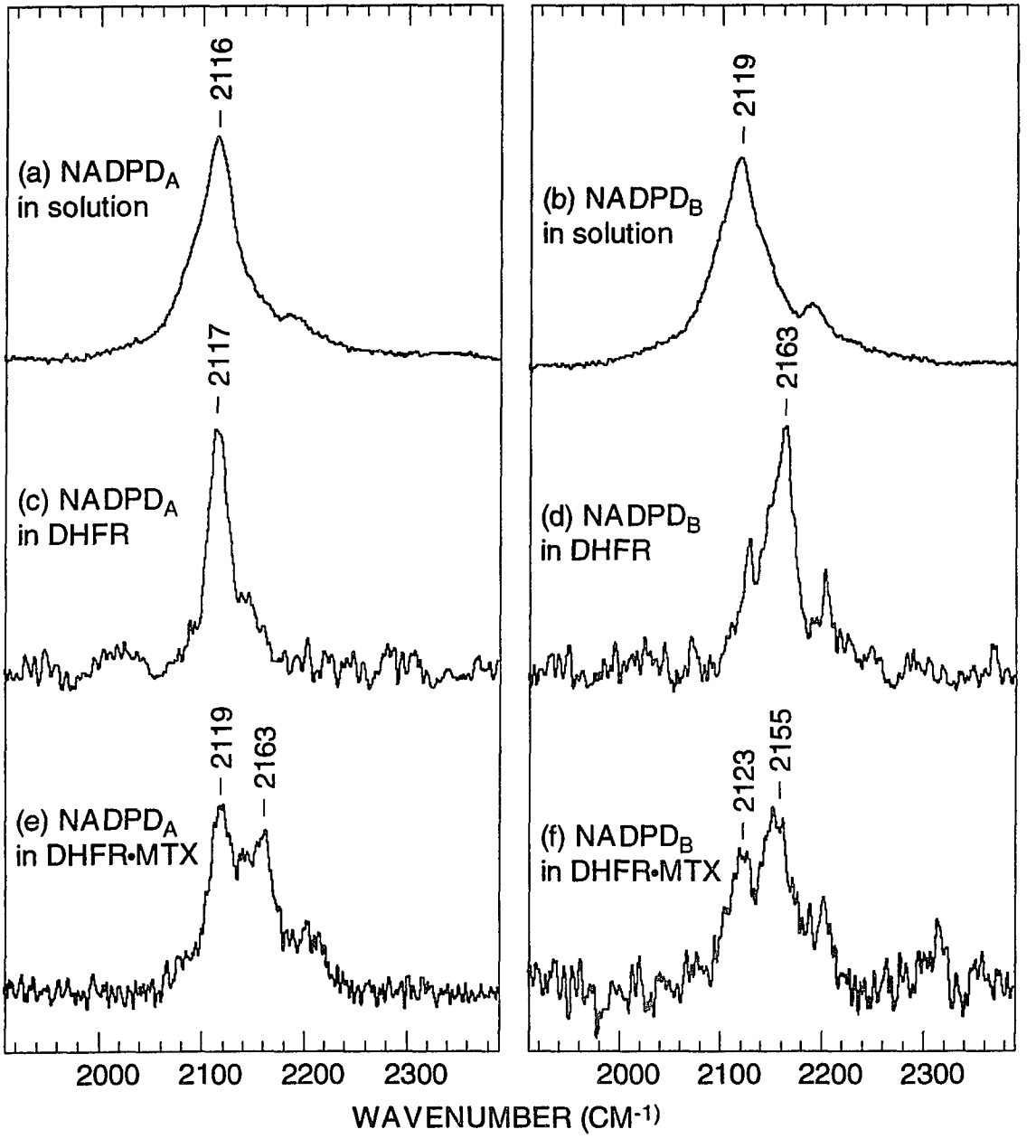

Figure 9.1 Raman difference spectra of (a) and (b) $NADPD_A$ and $NADPD_B$ in aqueous solution; (c) and (d) $NADPD_A$ and $NADPD_B$ bound to DHFR binary complex; (e) and (f) $NADPD_A$ and $NADPD_B$ bound to DHFR ternary complex with MTX. All spectra were obtained by subtracting the correspoding NADPH spectra under the same conditions. Enzyme concentrations were about 4 mM. Laser excitation: for c and d, 568.2 nm, 120 mW; for the rest, 647.1 nm, 120 mW.

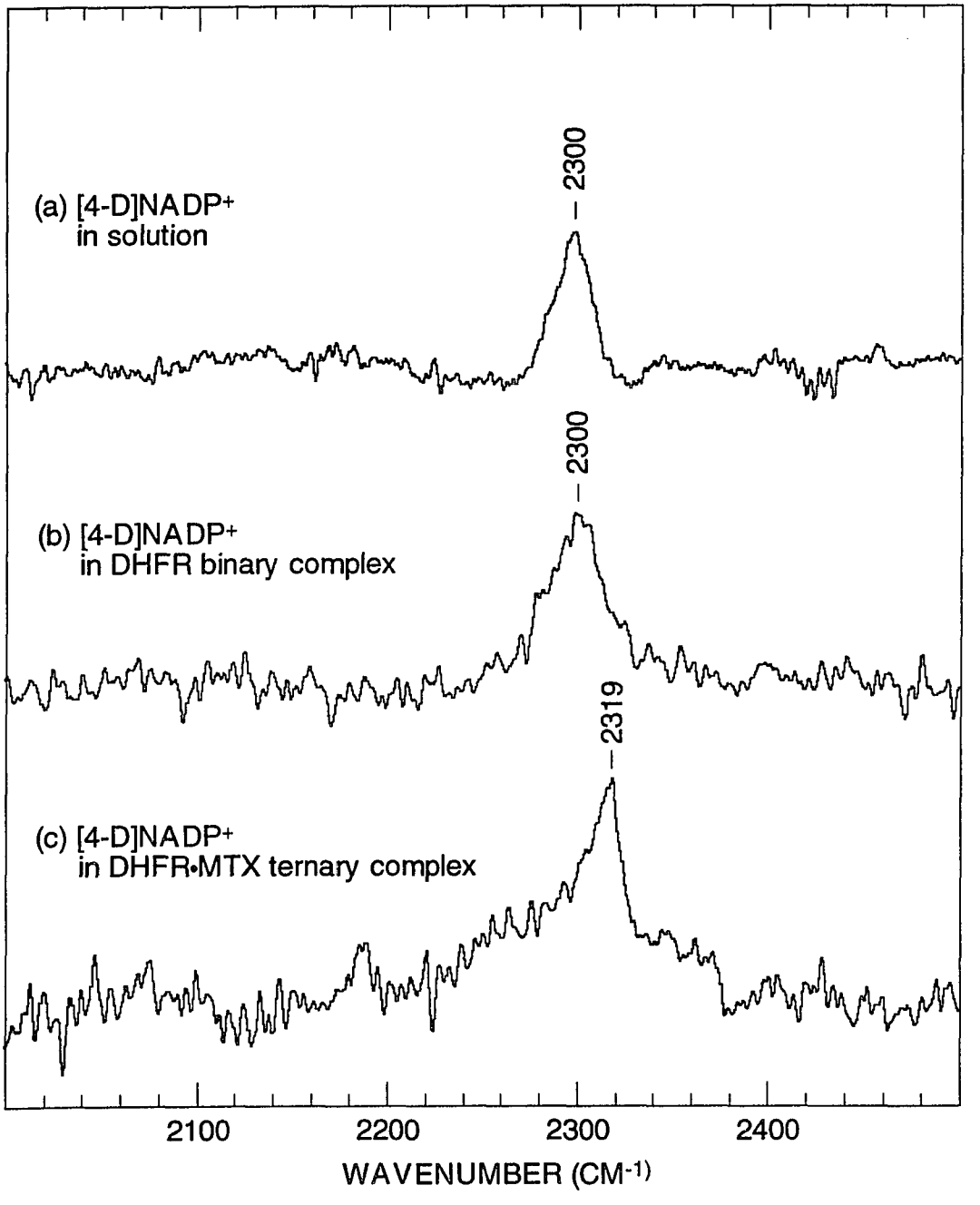

Figure 9.2 Raman difference spectra [4-D]NADP+ (a) in aqueous solution; (b) bound to DHFR binary complex; (c) bound to DHFR ternary complex with MTX. All spectra were obtained by subtracting the correspoding NADP+ spectra under the same conditions. Enzyme concentrations were about 4 mM. Laser excitation: 568.2 nm, 120 mW.

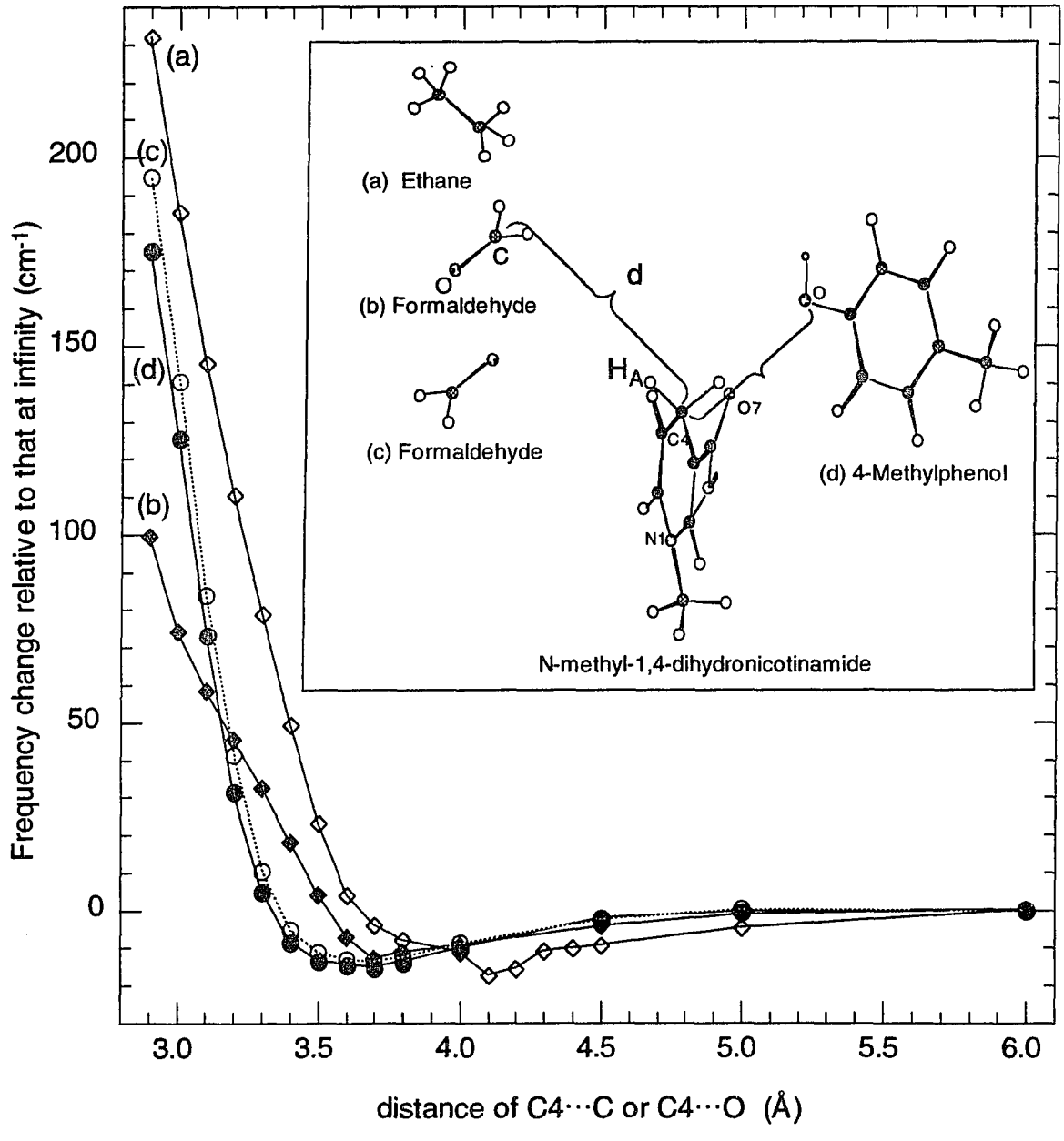

Figure 9.3 Am1 calculated C4–D stretch frequency of N-methyl-1,4-dihydronicotinamide with (a) the carbon atom of an ethane approaching C4 (open diamond); (b) the carbon atom of a formaldehyde approaching C4 (solid diamond); (c) the oxygen atom of a formaldehyde approaching C4 (open circle); and (d) the oxygen atom of 4-methylphenol approaching C4 (solid circle). They all approach C4 along one of the C4–D bonds with orientations shown in the inset.

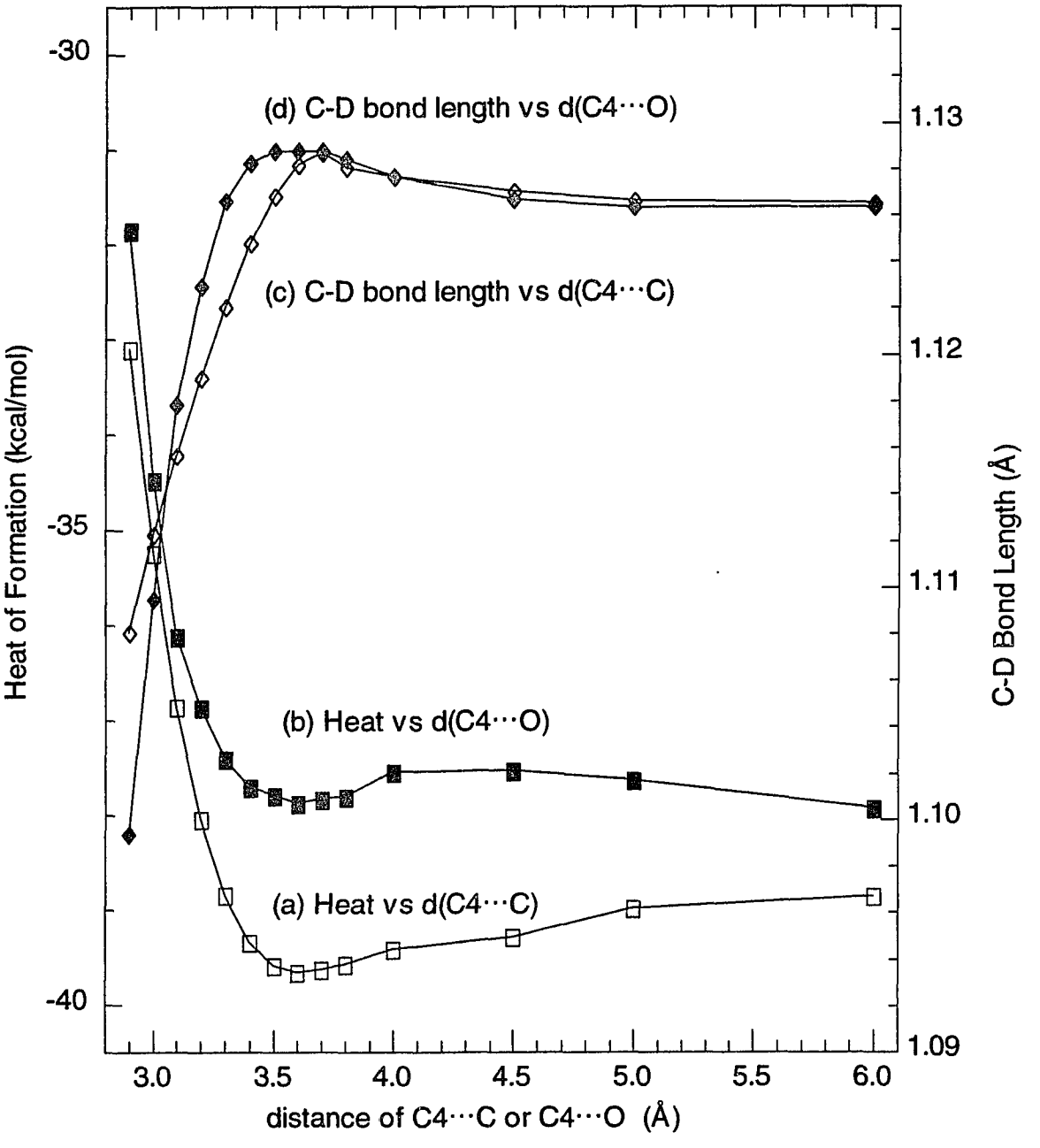

Figure 9.4 Am1 calculated heat of formation of the N-methyl-1,4-dihydronicotinamide/formaldehyde system with C4 close to (a) the carbon (open square) and (b) the oxygen (solid square) of the formaldehyde; and the C4-D bond length of the nicotinamide ring with C4 close to (c) the carbon (open diamond) and (d) the oxygen (solid diamond) of the formaldehyde.

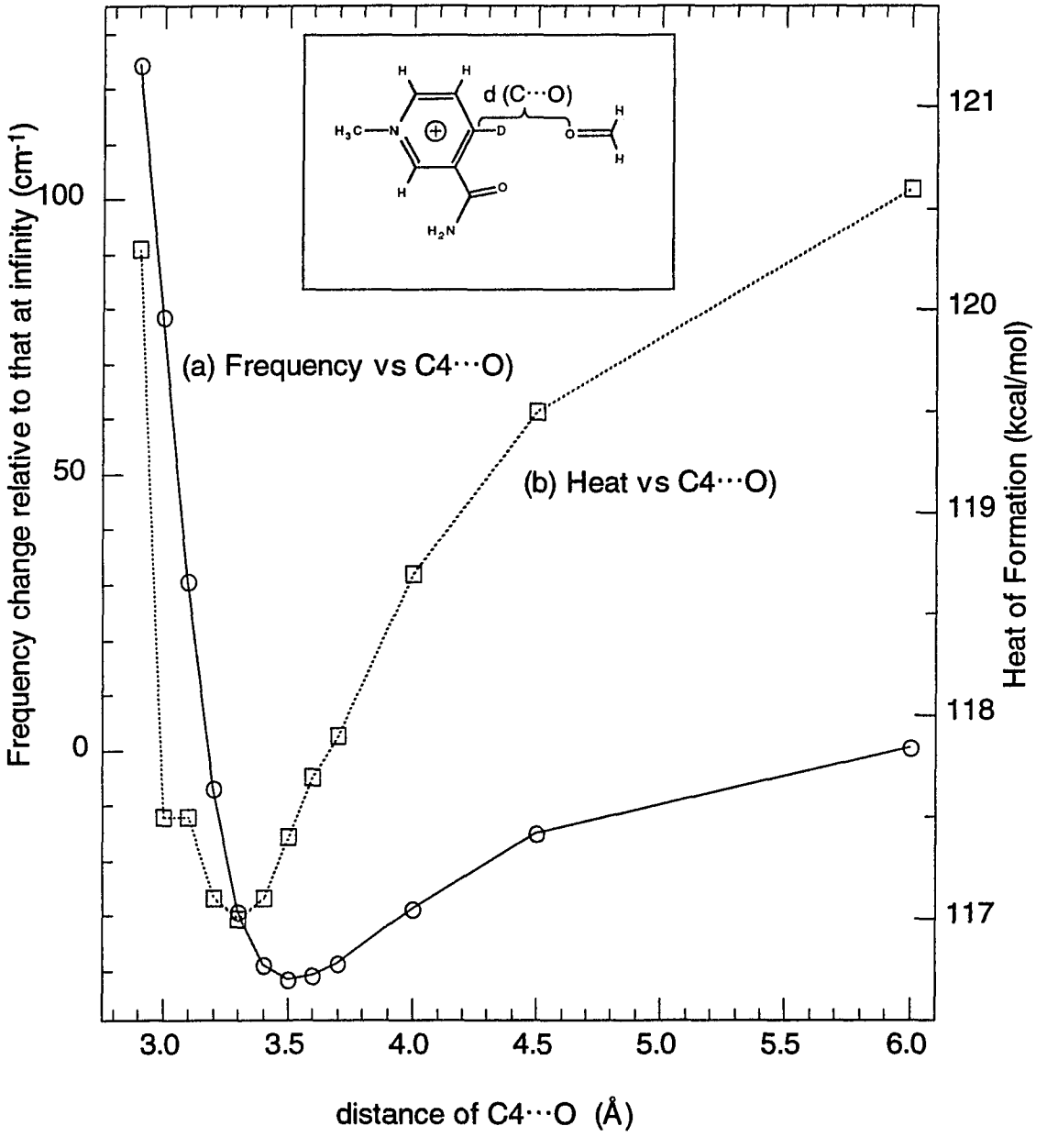

Figure 9.5 Am1 calculated (a) the C4–D stretch frequency (circle) and (b) heat of formation (square) of the N-methyl-nicotinamide (oxidized)/formaldehyde system with C4 close to the oxygen of the formaldehyde (inset).

REFERENCES

Abad-Zapatero, C., Griffith, J. P., Sussman, J. L. , & Rossmann, M. G. (1987) *J. Mol. Biol.* **198,** 445.

Adams, J., Johnson, K., Matthews, R. , & Benkovic, S. J. (1989) *Biochemistry.* **28,** 6611-6618.

Almarsson, O. , & Bruice, T. C. (1993) *J. Am. Chem.Soc.* **115,** 2125-2138.

Appleman, J. R., Howell, E. E., Kraut, J., Kuhl, M. , & Blakley, R. L. (1988a) *J. Biol. Chem.* **263,** 9187-9198.

Appleman, J. R., Prendergast, N. J., Delcamp, T. J., Freisheim, J. H. , & Blakley, R. L. (1988b) *J. Biol. Chem.* **263,** 10304-10313.

Baccanari, D., Phillips, A., Smith, S., Sinski, D. , & Burchall, J. (1975) *Biochemistry.* **14,** 5267.

Belasco, J. G. , & Knowles, J. R. (1980) *Biochemistry.* **19,** 472-477.

Belasco, J. G. , & Knowles, J. R. (1983) *Biochemistry.* **22,** 122-129.

Bellamy, L. J. (1975) *Advances in Infrared Group Frequencies.* Chapman and Hall, London.

Benkovic, S. J., Fierke, C. A. , & Naylor, A. M. (1988) *Science.* **239,** 1105-1110.

Biellmann, J.-F. , & Jung, M. J. (1971) *Eur. J. Biochem.* **19,** 130-134.

Birdsall, B., Feeney, J., Tendler, S. J. B., Hammond, S. J. , & Roberts, G. C. K. (1989) *Biochemistry.* **28,** 2297-2305.

Birktoft, J. J., Rhodes, G. , & Banaszak, L., J. (1989) *Biochem.* **28,** 6065-6081.

Blakley (1969) *the Biochemistry of Folic Acid and Related Pteridines.* North-Holland, Amsterdam.

Blakley, R. L., Appleman, J. R., Freisheim, J. H. , & Jablonsky, M. J. (1993) *Archives of Biochemistry and Biophysics.* **306,** 501-509.

Blakley, R. L. , & Cocco, L. (1984) *Biochemistry.* **23,** 2377-2383.

Bolin, J. T., Filman, D. J., Matthews, D. A., Hamlin, R. C. , & Kraut, J. (1982) *J. Biol. Chem.* **257,** 13650-13662.

Brown, D. J. , & Facobsen, N. W. (1961) *J. Chem. Soc.* 4413-4420.

Bystroff, C., Oatley, S. J. , & Kraut, J. (1990) *Biochem.* **29,** 3263-3277.

Callender, R. , & Deng, H. (1994) *Ann. Rev. Biophys. Biomol. Struct.* **23,** 215-245.

Cayley, P. J., Feeney, J. , & Kimber, B. J. (1980) *Int. J. Biol. Macromal.* **2,** 251-255.

Chen, D., Yue, K. T., Martin, C., Rhee, K. W., Sloan, D. , & Callender, R. (1987) *Biochemistry.* **26,** 4776-4784.

Chen, Y.-Q., Kraut, J., Blakley, R. L. , & Callender, R. (1994) *Biochemistry.* **33,** 7021-7026.

Cheung, H. T. A., Birdall, B., Frenkiel, T. A., Chau, D. D. , & Feeney, J. (1993) *Biochem.* **32,** 6846-6854.

Cheung, H. T. A., Birdsall, B. , & Feeney, J. (1992) *FEBS Letters.* **312,** 147,151.

Cocco, L., Groff, J. P., Temple, C., Jr., Montgomery, J. A., London, R. E., Matwiyoff, N. A. , & Blakley, R. L. (1981) *Biochemistry.* **20,** 3972-3978.

Cocco, L., Roth, B., Temple, C., Jr., Montgomery, J. A., London, R. E., Matwiyoff, N. A. , & Blakley, R. L. (1983) *Arch. Biochem. Biophys.* **226,** 567-577.

Cocco, L., Temple, C., Jr., Montgomery, J. A., London, R. E. , & Blakley, R. L. (1981) *Biochem. Biophys. Res. commun.* **100,** 413-419.

Cody, v., Luft, J. R., Ciszak, E., Kalman, T. I. , & Freisheim, J. H. (1992) *Anti-Cancer Drug Design.* **7,** 483-491.

Daimay, L.-V., Colthup, N. B., Fateley, W. G. , & Grasselli, J. G. (1991) *The Handbook of Infrared and Raman Characteristic Frequencies of Organic Molecules.* Academic Press, San Diego.

David, C. L., Howell, E. E., Farnum, M. F., Villafranca, J. E., Oatley, S. J. , & Kraut, J. (1992) *Biochemistry.* **31,**

Davies, J. F., Delcamp, T. J., Predergast, N. J., Ashford, V. A., Freisheim, J. H. , & Kraut, J. (1990) *Biochemistry.* **29,** 9467-9479.

Davies, J. F., Matthews, D. A., Oatley, S. J., Kaufman, B. T., Xuong, N. , & Kraut, J. (1989) *to be published.*

Deng, H., Burgner, J. , & Callender, R. (1991) *Biochemistry.* **30,** 8804-8811.

Deng, H., Burgner, J. , & Callender, R. (1992) *J. Am. Chem. Soc.* **114,** 7997-8003.

Deng, H., Goldberg, J. M., Kirsch, J. F. , & Callender, R. (1993a) *J. Am. Chem. Soc.* **115,** 8869-8870.

Deng, H., Ray, W. J., Burgner, J. W. , & Callender, R. (1993b) *Biochemistry.* **32,** 12984-12992.

Deng, H., Zheng, J., Burgner, J. , & Callender, R. (1989a) *J. Phys. Chem.* **93,** 4710-4713.

Deng, H., Zheng, J., Burgner, J. , & Callender, R. (1989b) *Proc. Nat'l. Acad. Sci. (USA).* **86,** 4484-4488.

Deng, H., Zheng, J., Burgner, J., Sloan, D. , & Callender, R. (1989c) *Biochemistry.* **28,** 1525-1533.

Deng, H., Zheng, J., Sloan, D., Burgner, J. , & Callender, R. (1992) *Biochem.* **31,** 5085-5092.

Dewar, M. J. S., Zoebisch, E. G., Healy, E. F. , & Stewart, J. J. P. (1985) *J. Am. Chem. Soc.* **107,** 3902-3910.

Druckmann, S., Ottolenghi, M., Pande, A., Pande, J. , & Callender, R. (1982) *Biochem.* **21,** 4953-4959.

Dwivedi, C. M., Plante, L. T., Kisliuk, R. L., Pastore, E. J., Verma, S. P. , & Wallach, D. F. H. (1982) *Archives of Biochem. and Biophys.* **213,** 338-340.

Fabre, G., Fabre, I., Matherly, L. H., Cano, J.-P. , & Goldman, I. d. (1984) *J. Biol. Chem.* **259,** 5066-5072.

Falzone, C. J., Benkovic, S. J. , & Wright, P. E. (1990) *Biochemistry.* **29,** 9667-9677.

Falzone, C. J., Wright, P. E. , & Benkovic, S. J. (1991) *Biochemistry.* **30,** 2184-2191.

Feeney, J., Birdsall, B., Roberts, G. C. K. , & Burgen, A. S. V. (1975) *Nature.* **257,** 564-566.

Fierke, C. A., Johnson, K. A. , & Benkovic, S. J. (1987) *Biochemistry.* **26,** 4085-4092.

Filman, D. J., Bolin, J. T., Matthews, D. A. , & Kraut, J. (1982) *J. Biol. chem.* **257,** 13633-13672.

Fischer, P., Fleckenstein, J. , & Hones, J. (1988) *Photochem. Photobiol.* **47,** 193-199.

Futterman, S. (1957) *J. Biol. Chem.* **228,** 1031-1038.

Glasfeld, A., Zbinden, P., Dobler, M., Benner, S. A. , & Dunitz, J. D. (1988) *J. Am. Chem. Soc.* **110,** 5152-5157.

Gready, J. E. (1985a) *J. Am. Chem. Soc.* **107,** 6689-6695.

Gready, J. E. (1985b) *Biochemistry.* **24,** 4761-4766.

Greenberg, G. R. (1954) *Fed. Proc.* **13,** 745.

Gupta, S. V., Greenfield, N. J., Poe, M., Makulu, D. R., Williams, M. N., Moroson, B. A. , & Bertino, J. R. (1977) *Biochemistry.* **16,** 3073-3079.

Hitcings, G. H. , & Baccanari, D. P. (1984) in *Folate Antagonists as Therapeutic Agents,* (Sirotnak, F. M., Burchall, J. J., Ensminger, W. D. , & Montgomery, J. A., Ed.) 151-173, Academic Press, Orlando.

Hood, K. , & Roberts, G. C. K. (1978) *Biochem. J.* **171,** 357-366.

Howell, E. E., Villafranca, J. E., Warren, M. S., Oatley, S. J. , & Kraut, J. (1986) *Sci.* **231,** 1123-1128.

Huang, F.-Y., Yang, Q.-X. , & Huang, T.-h. (1991) *FEBS Letters.* **289,** 231-234.

Huennekens, F. M. , & Scrimgeour, K. G. (1964) in *Pteridine Chemistry,* (Pfliederer, W. , & Taylor, E. C., Ed.) 355-376, MacMillan, Oxford, England.

Joesten, M. , & Schaad, L. J. (1974) *Hydrogen Bonding.* Marcel Dekker, Inc., New York.

Jolivet, J., Cowan, K. H., Curt, G. A., Clendeninn, N. J. , & Chabner, B. A. (1983) *N. Engl. J. Med.* **309,** 1094-1104.

Kisliuk, R. L. (1984) in *Folate Antagonists as Therapeutic Agents,* (Sirotnak, F. M., Burchall, J. J., Ensminger, W. B. , & Montgomery, J. A., Ed.) 1-68, Academic Press, Orlando.

Korn, S. , & Dehoratius, R. J. (1989) *American Family Physician.* **40,** 243-246.

Kraut, J. , & Matthews, D. A. (1987) in *Biological Macromolecules and Assemblies: Active Sites of Enzymes,* (Jurnak, F. A. , & McPherson, A., Ed.) 1-72, John Wiley, New York.

Kurz, L. C. , & Drysdale, G. R. (1987) *Biochemistry.* **26,** 2623-2627.

Latajka, Z. , & Scheiner, S. (1990) *Chem. Phys. Letts.* **174,** 179-184.

Lord, R. C. , & Yu, N.-T. (1970) *J. Mol. Biol.* **50,** 509-524.

Maharaj, G., Selinsky, B. S., Appleman, J. R., Perlman, M., London, R. E. , & Blakley, R. L. (1990) *Biochemistry.* **29,** 4554-4560.

Margosiak, S. A., Appleman, J. R., Santi, D. V. , & Blakley, R. L. (1993) *Arch. Biochem. Biophys.* **305,** 499-508.

Mathews, C. , & van Holde, K. E. (1990) *Biochemistry*. The Benjamin/Cummings Publishing Company, Redwood City, CA.

Matthews, D. A., Alden, R. A., Bolin, J. T., Filman, D. J., Freer, S. T., Hamlin, R., Hol, W. G. J., Kisliuk, R. L., Pastore, E. J., Plante, L. T., Xuong, N. , & Kraut, J. (1978) *J. Biol. Chem.* **253,**

Matthews, D. A., Alden, R. A., Bolin, J. T., Freer, S. T., Hamlin, R., Xuong, N., Kraut, J., Poe, M., Williams, M. , & Hoogsteen, K. (1977) *Science.* **197,** 425-455.

McGuire, J. J., Hsieh, P. , & bertino, J. R. (1984) *Biochemical Pharmacology.* **33,** 1355-1361.

McTigue, M. A., Davies, J. F., II, Kaufman, B. T. , & Kraut, J. (1992) *biochem.* **31,** 7264-7273.

McTigue, M. A., Davies, J. F., II, Kaufman, B. T. , & Kraut, J. (1993) *Biochemistry.* **32,** 6855-6862.

Morrison, J. F. , & Stone, S. R. (1988) *Biochemistry.* **27,** 5499-5506.

Murphy, D. J. , & Benkovic, S. J. (1989) *Biochemistry.* **28,** 3025-3031.

Nishimura, Y. , & Tsuboi, M. (1986) *J. Molec. Struct.* **146,** 123-153.

Oppenheimer, N. J. (1987) in *Coenzymes and Cofactors,* (Dolphin, D., Avramovic, O. , & Poulson, R., Ed.) 185-230, John Wiley & Sons, New York.

Osborn, M. J. , & Huennekens, F. M. (1958) *J. Biol. Chem.* **233,** 969-974.

Ozaki, Y., King, R. W. , & Carey, P. R. (1981) *Biochem.* **20,** 3219-3225.

Palmer, T. (1985) *Understanding Enzymes.* Ellis Horwood Limited, Chichester.

Pfleiderer, W., Liedek, E., Lohrmann, R. , & Rukwied, M. (1960) *Chem. Ber.* **93,** 2015-2024.

Poe, M., Greenfield, N. J. , & Williams, M. N. (1974) *J. Biol. Chem.* **249,** 2710-2716.

Roth, B. , & Cheng, C. C. (1982) in *Progress in Medicinal Chemistry,* (Ellis, G. P. , & B., W. G., Ed.) 269-331, Elsevier Biomedical Press, Amsterdam.

San Pietro, A. (1955) *J. Biol. Chem.* **217,** 579-587.

Saperstein, D. D., Rein, A. J., Poe, M. , & Leahy, M. F. (1978) *J. Am. Chem. Soc.* **100,** 4296-4300.

Seeger, D. R., Cosulich, D. B., M., S. J. , & Hultquist, M. E. (1949) *J. Am. Chem. Soc.* **71,** 1753.

Selinsky, B. S., Perlman, M. E., London, R. E., Unkefer, C. J., Mitchell, J. , & Blakley, R. L. (1990) *Biochemistry.* **29,** 1290-1296.

Small, E. W. , & Peticolas, W. L. (1971) *Biopolymers.* **10,** 1377-1416.

Spinner, E. (1964) *J. Chem. Soc.* 4217.

Steinberg, G., Ottolenghi, M. , & Sheves, M. (1993) *Biophysical J.* **64,** 1499-1502.

Stone, S. R., Montgomery, J. A. , & Morrison, J. F. (1984) *biochem. Pharmac.* **33,** 175-179.

Stone, S. R. , & Morrison, J. F. (1983) *Biochim. Biophys. Acta.* **745,** 247-258.

Stone, S. R. , & Morrison, J. F. (1984) *Biochem.* **23,** 2753-2758.

Subramanian, S. , & Kaufman, B. T. (1978) *Proc. Natl. Acad. Sci. USA.* **75,** 3201-3205.

Thijs, R. , & Zeegers-Huyskens, T. (1984) *Spectrochemica Acta.* **40A,** 307-313.

Tinoco, I., Jr. (1960) *J. Am. Chem. Soc.* **84,** 4785-4790.

Tipton, K. F. , & Dixon, H. B. F. (1979) *Methods Enzymol.* **63,** 183-233.

Tomlinson, B. L. , & Peticolas, W. L. (1970) *J. Chem. Phys.* **52,** 2154-2156.

Touchette, N. A., Perry, K. M. , & Matthews, C. R. (1986) *Biochemistry.* **25,** 5445-5452.

Tsuboi, M., Nishimura, Y., Hirakawa, A. Y. , & Peticolas, W. L. (1987) in *Biological Application of Raman Spectroscopy,* (Spiro, T. G., Ed.) John Wiley & Sons,

Uchimaru, T., Tsuzuki, S., Tanabe, K., Benkovic, S. J., Furukawa, K. , & Taira, K. (1989) *Biochem. Biophys. Res. Commun.* **161,** 64-68.

Villafranca, J. E., Howell, E. E., Voet, D. H., Strobel, M. S., Ogden, R. C., Abelson, J. N. , & Kraut, J. (1983) *Science.* **222,** 782-788.

Viola, R. E., Cook, P. F. , & Cleland, W. W. (1979) *Anal. Biochem.* **96,** 334-340.

Viscontini, M. , & Mohlmann, E. (1959) *Helv. Chim. Acta.* **42,** 836.

Westheimer, F. H. (1987) in *Pyridine Nucleotide Coenzymes, Part A,* (Dolphin, D., Poulson, R. , & Avramovic, O., Ed.) 253-322, John Wiley & Sons, New York.

White, J. L., Hackert, M. L., Buehner, M., Adams, M. J., Ford, G. C., Lentz, P. J., Smiley, I. E., Steindel, S. J. , & Rossmann, M. G. (1976) *J. Mol. Biol.* **102,** 759-779.

Williams, J. W., Morrison, J. F. , & Duggleby, R. G. (1979) *Biochemistry.* **18,** 2567-2573.

Wu, Y.-D. , & Houk, K. N. (1987) *J. Am. Chem. Soc.* **109,** 2226-2227.

You, K.-S., Arnold, L. J. J., Allison, W. S. , & Kaplan, N. D. (1978) *Trends. Biochem. Sci.* **2,** 265.

Yue, K. T., Deng, H. , & Callender, R. (1989) *J. Raman Spec.* **20,** 541-546.

Yue, K. T., Martin, C. L., Chen, D., Nelson, P., Sloan, D. L. , & Callender, R. (1986) *Biochemistry.* **25,** 4941-4947.

Yue, K. T., Yang, J. P., Martin, C. L., Lee, S. K., Sloan, D. , & Callender, R. (1984) *Biochem. Biophys. Res. Comm.* **122,** 225-229.

Zakrzewski, S. F. , & Nichol, C. A. (1958) *Biochem. Biophys. Acta.* **27,** 425-426.

Zheng, J. (1991) Ph. D Dissertation.